UNIVERSITY OF CALIFORNIA

Santa Barbara

Advancing personalized medicine with electrochemical aptamer-based (EAB) sensors

A dissertation submitted in partial satisfaction of the

requirements for the degree Doctor of Philosophy

in Psychological & Brain Sciences

by

Nicole Ann Emmons

Committee in charge:

Professor Tod Kippin, Chair

Professor Kevin Plaxco

Professor Karen Szumlinski

Professor Ron Keiflin

December 2024

The dissertation of Nicole Ann Emmons is approved.

_____

Kevin Plaxco

_____

Ron Keiflin

_____

Karen Szumlinski

_____

Tod Kippin, Committee Chair

December 2024

Advancing personalized medicine with electrochemical aptamer-based (EAB) sensors

By

Nicole Ann Emmons

ACKNOWLEDGEMENTS

I would like to first thank my incredible mentor and principal investigator, Dr. Tod Kippin. Thank you for giving me a chance, recognizing my potential, and supporting me every step of the way. I could not have asked for a better mentor, boss, and friend to guide me through my graduate career.

I sincerely thank Dr. Kevin Plaxco for his constant insight and support. Thank you for challenging me and for always encouraging my intellectual curiosity.

I would like to thank my thesis committee for their incredible insight, thought-provoking questions, constant flexibility, and professional support throughout this process.

To Julian Gerson, my mentor, officiant, and cherished friend, I would not be where I am today if not for your guidance, patience, and support. Thank you for seeing my potential and teaching me the skills needed to succeed in this lab and beyond.

I would like to extend my sincerest gratitude to my family, who have always encouraged me to pursue my passions and have never wavered in their support. To my mom and dad, I could not have done this without your various forms of support. Mom, you have instilled in me your zest for life and your relentless drive, and I am so grateful to be your daughter. To my dad, thank you for always believing in me, even in moments when I did not believe in myself.

I thank all past and current members of the Kippin and Plaxco lab for always letting me distract them. I could not have made it through graduate school without you—you are an incredible team of scientists and even better friends. To Jenny, Lisa, and Kevin, thank you for being there through it all!

Finally, throughout my time in graduate school, I have been blessed to be a girlfriend, a fiancé, and now a wife to the most incredible person I have ever met. Thank you to my husband, Guillaume, for your patience, support, and love, and for always allowing me to gripe about whatever hiccups arose in my graduate journey. I cannot wait to see what our future holds.

VITA OF NICOLE ANN EMMONS

December 2024

EDUCATION

University of Santa Barbara, California *Santa Barbara, CA* (2020 – Current)

- Doctor of Philosophy; Psychological and Brain Sciences (Neuroscience and Behavior)
- Emphasis in Bioengineering
- GPA: 3.90

Reed College *Portland, OR* (2016 - 2020)

- Bachelor of Arts - May 2020
- *Major*: Psychology and Neuroscience; *Allied Field*: Computational Sciences

AWARDS AND HONOR

National Defense Science and Engineering Graduate Fellow (2021-2024)

Bioengineering; Office of Naval Research

Commendation for Excellence in Scholarship (2018-2020)

Reed College*, Portland, OR*

PROFESSIONAL EMPLOYMENT

University of Santa Barbara, California *Santa Barbara, CA* (2020 – Current)

Graduate Student Researcher and Teaching Assistant

PUBLICATIONS

Chamorro-Garcia, A.; Gerson, J.; Flatebo, C.; Fetter, L.; Downs, A. M.; **Emmons, N.**; Ennis, H. L.; Milosavić, N.; Yang, K.; Stojanovic, M.; Ricci, F.; Kippin, T. E.; Plaxco, K. W. Real-Time, Seconds-Resolved Measurements of Plasma Methotrexate In Situ in the

Living Body. *ACS Sens*. **2023**, *8* (1), 150–157. https://doi.org/10.1021/acssensors.2c01894.

Gerson, J.; Erdal, M. K.; McDonough, M. H.; Ploense, K. L.; Dauphin-Ducharme, P.; Honeywell, K. M.; Leung, K. K.; Arroyo-Curras, N.; Gibson, J. M.; **Emmons, N. A**.; Meiring, W.; Hespanha, J. P.; Plaxco, K. W.; Kippin, T. E. High-Precision Monitoring of and Feedback Control over Drug Concentrations in the Brains of Freely Moving Rats. *Science Advances.* **2023**, *9* (20), eadg3254. https://doi.org/10.1126/sciadv.adg3254.

Leung, K. K.; Gerson, J.; **Emmons, N**.; Roehrich, B.; Verrinder, E.; Fetter, L. C.; Kippin, T. E.; Plaxco, K. W. A Tight Squeeze: Geometric Effects on the Performance of Three-Electrode Electrochemical-Aptamer Based Sensors in Constrained, in Vivo Placements. *Analyst* **2023**, *148* (7), 1562–1569. https://doi.org/10.1039/D2AN02096C.

Leung, K. K.; Gerson, J.; **Emmons, N**.; Heemstra, J. M.; Kippin, T. E.; Plaxco, K. W. The Use of Xenonucleic Acids Significantly Reduces the In Vivo Drift of Electrochemical Aptamer-Based Sensors. *Angewandte Chemie.* **2024**. https://doi.org/10.1002/ange.202316678.

Alkhamis, O.; Canoura, J.; Wu, Y.; **Emmons**, **N. A**.; Wang, Y.; Honeywell, K. M.; Plaxco, K. W.; Kippin, T. E.; Xiao, Y. High-Affinity Aptamers for In Vitro and In Vivo Cocaine Sensing. *J. Am. Chem. Soc.* **2024**, 146 (5), 3230–3240. https://doi.org/10.1021/jacs.3c11350.

Chung, J.; Billante, A.; Flatebo, C.; K. Leung, K.; Gerson, J.; **Emmons, N**.; E. Kippin, T.; Sepunaru, L.; W. Plaxco, K. Effects of Storage Conditions on the Performance of an Electrochemical Aptamer-Based Sensor. *Sensors & Diagnostics.* **2024**. https://doi.org/10.1039/D4SD00066H.

Gerson, J., Erdal, M., Fetter, L., Leung, K., **Emmons, N.,** M., Kippin, T., Plaxco, K. A high-resolution view of the multicompartment pharmacokinetics of vancomycin achieved via simultaneous, seconds-resolved measurements in the plasma and interstitial fluid. [Submitted]

Emmons, N., McDonough, M., Gibson, J., Gerson, J., Leung, K., Plaxco, K., Kippin, T. Simultaneous, seconds-resolved intravenous and subcutaneous measurements of doxorubicin provide a quantitative picture of the relationship between plasma and ISF pharmacokinetics. [In process]

Emmons, N., Duman, Z., Erdal., M., Hespanha, J., Plaxco, K., Kippin, T. Feedback control over plasma drug concentrations achieves rapid and accurate control over solid-tissue drug concentrations. [In process]

Emmons, N., Sobieri, A., Heurta Sanchez, L.., Ostler., D., Plaxco, K., Kippin, T. Seconds-resolved studies of plasma cocaine pharmacokinetics in male and female rats. [In process]

ABSTRACT

Advancing personalized medicine with electrochemical aptamer-based (EAB) sensors

by

Nicole Ann Emmons

Personalized medicine, a rapidly evolving field of healthcare, aims to improve therapeutic outcomes by individualizing patient care. Therapeutic drug monitoring (TDM) presents a vast improvement to personalized medicine, enabling clinicians to optimize dosing regimens to improve therapeutic outcomes while minimizing toxicity. The state of the art of TDM is significantly limited by the current techniques employed to perform it. Existing technologies are limited by reliance on ex vivo quantification that generally results in single time point or low temporal resolution measurements and the inability to measure drug levels in different physiological compartments simultaneously. Electrochemical aptamer-based (EAB) sensors, a novel biosensing platform, present a powerful means of overcoming these limitations, providing seconds-resolved, cross-compartment measurements of drug distribution in real-time. Centered around the focus of advancing TDM, this work first utilizes EAB sensors to better elucidate drug transport from blood to solid tissue, with an ultimate goal of improving transport into the brain. Using doxorubicin as a testbed, I first demonstrate that EAB sensors can capture the distribution of chemotherapeutics from the bloodstream to the peripheral

subcutaneous tissue. I then utilize these measurements to perform high-precision feedback-controlled drug delivery over plasma drug levels. After careful evaluation of the permeation of drugs into tissue not separated by a physiological barrier, I then demonstrate the in-brain EAB platform can explore how pharmacological manipulations and drug encapsulation methods may improve drug permeation into the brain. Finally, this work utilizes individual, subject-specific measurements to suggest EAB sensors could be used to inform inter-patient pharmacokinetic variability. Collectively, this work argues that EAB sensors could significantly advance both our understanding of drug transport to the brain and peripheral tissues and revolutionize personalized medicine by enabling high-precision therapeutic drug monitoring.

TABLE OF CONTENTS

Chapter 1: Introduction

1.1 Overview

The ability to monitor drugs and other small molecule concentrations in the body in real-time would drastically improve our understanding of pharmacokinetics, which would better inform how we diagnose and treat disease. The advancement of personalized medicine relies on methods to quantify the individual relationship between dose and response (Chan & Ginsburg, 2011; Goetz & Schork, 2018). Thus, our ability to individualize patient care and advance therapeutic efficacy is significantly limited by the techniques with which we quantify drug distribution. The ability to measure drugs in real-time and with high temporal resolution would be advantageous for two primary reasons, both of which are significantly advanced by the research outlined in this work. First, seconds-resolved measurements of drug distribution in the body would enable clinicians to optimize therapeutic outcomes by improving the permeation of therapeutics in their intended sites of action. Second, these measurements could detect individual differences in pharmacokinetics to minimize variably in drug exposure, increasing therapeutic efficacy while minimizing toxicity. Both advancements would improve our understanding of drug transport through and elimination from the body and advance high-precision, individualized medicine.

Comprehensively, this thesis posits that state-of-the-art biosensing techniques, specifically electrochemical aptamer-based (EAB) sensors, would significantly advance both our understanding of pharmacokinetics and our ability to perform truly personalized medicine. Personalized medicine is a healthcare field that prioritizes the customization of patient care to improve therapeutic outcomes (Chan & Ginsburg, 2011; Goetz & Schork, 2018). Therapeutic drug monitoring (TDM) is a foundational component of personalized medicine, and its advancement would greatly improve the methods by which we treat and

diagnose disease. TDM is a clinical practice achieved most often by single time point measurements during the lifetime of specific drug administrations to maintain therapeutic concentrations in the bloodstream (Kang & Lee, 2009). These measurements are, at times, performed at sequential intervals to provide more insight into the drug's distribution and elimination in plasma. The goal of this practice is to individualize therapeutic dosing regimens to optimize clinical benefit while potentially decreasing adverse side effects associated with overdose. Achieving the "state of the art" of TDM is currently limited by numerous factors related to the drawbacks of conventional sampling techniques.

Although blood sampling is ubiquitous in TDM, the ability to quantify drug concentration at the site of action of specific drugs would provide a significant advancement in the state of the art. How drugs are transported from the blood into the solid tissues that are, most often, their sites of action, is poorly understood. Drug transport into the brain, for example, is limited by the blood-brain barrier, a critical neuroprotective defense mechanism that excludes the passage of harmful substances while permitting the passage of essential molecules and nutrients (Goldstein & Betz, 1986). This same selectivity restricts the passage of many therapeutic drugs aimed at targeting neurological abnormalities or specific molecular pathways in the brain. For example, a primary objective in the development of neuropharmaceuticals employed in the treatment of neuropsychiatric disorders, such as depression and schizophrenia, as well as neurodegenerative disorders, such as Alzheimer's and Parkinson's, is ensuring brain bioavailability to achieve neurotherapeutic efficacy (Poovaiah et al., 2018). Likewise, the treatment of in-brain cancers is significantly limited by the failure of chemotherapeutics to permeate the blood-brain barrier (BBB) (Park et al., 2012). Understanding how drugs permeate, and conversely, fail to permeate, the BBB is

critical for developing targets and pharmacological manipulations aimed at maintaining therapeutic in-brain concentrations of drugs. Developing methods to accurately and rapidly quantify drug distribution across compartments would significantly advance TDM, improving both pharmacological research and clinical practice.

Because existing methods to quantify drug transport often lack temporal resolution, our understanding of inter-subject pharmacokinetic variability is limited. When generating pharmacokinetic curves using data obtained by blood draw and HPLC, researchers must periodically sample over extended intervals, suggesting the data may not capture critical moments of drug absorption, distribution, metabolism, and elimination. And because drawing enough samples from the same animal to track individual PK repeatedly is often impractical, most of these methods rely on aggregating data across multiple animals to generate a pharmacokinetic profile. While this is valuable for understanding more generalized pharmacokinetic processes, aggregation may obscure important outliers or trends that could inform facets of drug action in specific subpopulations. In contrast, EAB sensors can generate high-density, high-precision data sets for individual animals, enabling the direct evaluation of pharmacokinetic variability that would critically inform therapeutic drug monitoring.

Here, I posit that EAB sensors can significantly advance personalized medicine by enabling real-time therapeutic drug monitoring. To place my work in context, I first begin with an overview of existing techniques utilized to quantify drug concentration across different physiological compartments. I argue that while they have significantly advanced the state of the art of precision monitoring, their limitations, including temporal resolution, reliance on ex vivo quantification, and their inability to generate data in real-time, suggest

they may be ill-equipped to catalyze the advancement of personalized medicine that the field demands. I then introduce the emerging and innovative biosensing platform, EAB sensors. I illustrate how EAB sensors overcome the limitations of prior technology and summarize the work conducted thus far.

1.2 Current methods for quantifying drug concentration

Current methods for quantifying the permeation of drugs into the blood or solid tissues, including the brain, lack the temporal and spatial resolution to analyze the dynamics of drug metabolism, elimination, or transport, particularly with regard to the CNS (M. I. Davies et al., 2000; Sloan et al., 2012). Research suggests that using blood levels as a proxy for CNS concentrations leads to underdosing (Ban et al., 2022; Lonsdale et al., 2013). Modeling drug transport into the CNS is further hampered by incomplete evidence of how therapeutics are distributed into peripheral compartments. Traditional sampling methods to quantify both systemic and peripheral levels of drugs rely on ex vivo analysis and lack the temporal resolution with which we can truly understand and quantify the distribution of these agents into solid tissue.

1.2.1. Quantifying drug levels in blood. Accurately quantifying drug levels in the blood is a fundamental aspect of pharmacokinetic monitoring. Understanding drug levels in the bloodstream is invaluable for minimizing drug-induced toxicity and optimizing therapeutic efficacy.

1.2.1.a. High-Performance Liquid Chromatography (HPLC). HPLC is the most commonly used technique to quantify drug levels in the blood. However, this process requires blood samples obtained through patient blood draws, which greatly restricts the

temporal resolution of the measurements. As a result, clinicians often rely on single time-point measurements, likely due to the invasive nature of the procedure, its cost, and reliance on skilled phlebotomists. Blood samples are drawn from patients and injected into a system where a high-pressure solvent (mobile phase) carries it through a particle column (stationary phase). The drug then separates from other components of the blood based on interactions with the material of the column. The drug level in the sample is quantified using a sensitive detection method, such as UV-VIS or mass spectrometry, which produces a signal proportional to the concentration in the sample (Morikawa et al., 2023; Nikolin et al., 2004). HPLC is significantly limited by numerous factors, including the cost of equipment, the need for specialized personnel, specificity limitations, and the reliance on ex vivo quantification (Ates et al., 2020; Gaspar et al., 2021).

1.2.1.b. Immunoassays. Immunoassays are an analytical method that relies on antibodies as a biorecognition element. Like other techniques, immunoassay is reliant on blood draws, and due to invasiveness, the need for specialized personnel, and cost, these samples are often only single time point measurements. These assays include enzyme-linked immunosorbent assays (ELISAs) and radioimmunoassay. While widely employed in clinical diagnostics because of their commercial utility, immunoassays are significantly limited by their specificity, as experimental antibodies may cross-react to analogs. Antibodies also require in vivo maturation via mammalian expression vectors (Ates et al., 2020; Lippow et al., 2007). Finally, like HPLC, immunoassays require ex vivo quantification of samples, which significantly limits clinical time-to-answer.

1.2.2. Quantifying drug levels in interstitial fluid (ISF). Determining drug levels in ISF is of critical importance for two reasons. First, many drugs exhibit their therapeutic

effects outside of the blood thus necessitating the need to accurately quantify drug levels at their site of action. Second, ISF measurements could potentially circumvent the invasiveness and inconvenience of routine blood draws currently employed for therapeutic drug monitoring.

1.2.2.a. Sampling ISF. Quantifying drug levels in ISF is significantly limited by current extraction methods. Two primary methods to sample ISF include suction blisters and microdialysis. Suction blisters are created by applying negative pressure to the dermis, from which fluid is then collected (Friedel et al., 2023; Vermeer et al., 1979). Microdialysis obtains ISF by the insertion of a semi-permeable membrane into the tissue, through which a perfusion fluid is passed (Davies et al., 2000; Kolluru et al., 2019). These methods are labor-intensive and invasive and require ex vivo benchtop analysis. Collectively, ISF extraction methods are limited to small volumes (~1-15 μL) and likely significantly alter the ISF composition (e.g., by rupturing cells or dilution with dialysate) in the collection process (Friedel et al., 2023; Niedzwiecki et al., 2018; Ribet et al., 2020; Samant & Prausnitz, 2018; Vermeer et al., 1979).

1.2.3. Quantifying drug levels in the brain. Current methods for quantifying the permeation of drugs into the brain lack the temporal and spatial resolution to analyze dynamic changes that occur in the CNS. And many commonly deployed techniques, such as tissue homogenization, provide measurements of only a single time point and often fail to differentiate between tissue levels of target and circulating blood levels in the brain, significantly limiting our understanding of how drugs move across compartments.

1.2.3.a. Homogenization of brain tissue. Drug levels in the brain are often quantified through tissue homogenization. Postmortem tissue is collected and homogenized

through mechanical, chemical, or enzymatic processes (H. Gao et al., 2013). Brain tissue must be extracted and stored carefully to avoid contamination. Finally, the sample analyte is extracted using LC-MS bioanalysis. This method provides information on only a single time point, hampering our ability to capture the seconds-resolved dynamics of drug transport. It is also a terminal procedure and relies on ex vivo quantification. Further, accurate measurements are confounded if there is any residual blood on the brain tissue, which can impact concentration estimates (Timmerman et al., 2014).

1.2.3.b. Cerebrospinal fluid (CSF) extraction. The simplest method to quantify drug distribution in the central nervous system is to measure drug concentrations in CSF. CSF is a clear fluid, formed as an ultra-filtrate of plasma, found in both intracranial and spinal compartments of the central nervous system (de Lange, 2013; Hrishi & Sethuraman, 2019). The most rudimentary method to obtain CSF is via a single lumbar puncture (spinal tap) during a continuous intravenous infusion (de Lange, 2013). This method is significantly limited by its invasiveness and reliance on ex vivo quantification. Additionally, this method does not enable CSF sampling at the site of action, which raises the question of how closely sampled CSF captures CNS target site concentrations (de Lange, 2013; Hrishi & Sethuraman, 2019). There is also evidence to suggest that repeated CSF sampling may influence physiology (Bothwell et al., 2019; Miyakawa et al., 1977).

1.2.3.c. Microdialysis. The current gold standard methodology to quantify drug distribution into the brain is microdialysis. This powerful technique permits the measurement of endogenous and exogenous molecules in the central nervous system and has significantly advanced the field of neuropharmacology and neurochemistry (Anderzhanova & Wotjak, 2013; Deguchi & Morimoto, 2001; Pan et al., 2007). A microdialysis probe with a

semipermeable membrane is inserted into specific brain regions, and buffer solutions are pumped through the probe (Figure 1.1). This permits molecules from the brain's extracellular fluid to diffuse into the solution, after which it is collected and quantified ex vivo. Typically, microdialysis samples are quantified using HPLC or mass spectrometry to determine the concentration of molecules of interest in the brain's extracellular fluid (Anderzhanova & Wotjak, 2013; Shannon et al., 2013). The strengths of this platform lie in its reliance on ex vivo quantification, suggesting it is generalizable across targets of interest. Conversely, because microdialysis is not performed in real-time and requires ex vivo quantification, the temporal resolution is generally limited to the order of tens of minutes (M. I. Davies et al., 2000; Hammarlund-Udenaes, 2017; Yang et al., 2013). Notably, some highly skilled scientists have been able to perform microdialysis with high temporal resolution (sampling every ~10 seconds), but these advancements are more often one-offs rather than the standard for microanalysis (Lada et al., 1997; Schultz & Kennedy, 2008). Dynamic changes in the CNS occur in a matter of seconds, suggesting a platform technology that can provide real-time, highly temporally resolved data would improve our understanding of in-brain physiology and neuropharmaceutical efficacy.

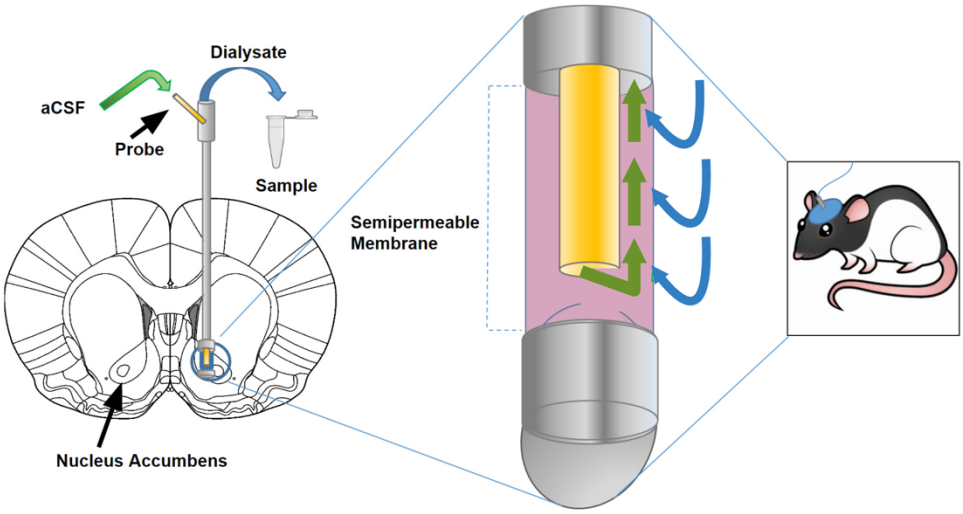

Figure 1.1. Microdialysis Coupled with HPLC-MS. Sombers Lab. 2019. Copyright Leslie Sombers.

1.2.3.d. Cyclic voltammetry. Fast-scan cyclic voltammetry (FSCV) is an electrochemical technique that monitors drug distribution in the brain with high temporal resolution, positioning it as a vast improvement to the abovementioned techniques. In FCSV, a triangular voltage waveform is applied to a working electrode situated in brain tissue at high scan rates (typically 100-400 V/s), thus enabling the detection of electroactive drugs and endogenous metabolites (including neurotransmitters) based on their redox behavior (Castagnola et al., 2020; Hashemi et al., 2009; Heien et al., 2004; Phillips et al., 2003; J. G. Roberts & Sombers, 2017). The current output from these electrode scans can be analyzed based on its magnitude, shape, and position relative to a reference electrode, providing information about the identity of the molecules present. This technique is a powerful advancement from techniques like microdialysis. This electrochemical method is considerably less invasive than other in-brain sensing techniques, with electrode diameters ranging from hundreds of nanometers to tens of micrometers (Burmeister et al., 2008; Ngernsutivorakul et al., 2018; Seymour et al., 2017). Their smaller size minimizes disruption

to local brain tissue, reducing both physical damage and the inflammation typically caused by probe insertion that may cause changes in molecules of interest. FCSV's primary strength lies in its seconds and even sub-seconds temporal resolution, which is a critical strength for capturing rapid neurochemical processes (Marken et al., 2010; Sarter & Kim, 2015).

Electrochemical approaches like FSCV present a powerful research tool enabling the detection of molecules in the brain with high temporal resolution. This technique, however, is significantly limited by the generalizability, or lack thereof, of the platform. FSCV is limited to the detection of species that are redox-active, a constraint that excludes many molecules, including most pharmaceuticals and nearly all drugs of abuse. Due to its reliance on redox as identification, FSCV also suffers from poor selectivity: molecules with similar redox potentials, such as dopamine and serotonin, produce overlapping signals, requiring sophisticated post-hoc data analysis or waveform adjustments to differentiate them (Movassaghi et al., 2024; Rafi & Zestos, 2021).

1.3 Electrochemical aptamer-based (EAB) sensors

1.3.1. Aptamer selection. EAB sensors are a novel biosensing platform that enables real-time monitoring of drugs and metabolites in situ in the living body. EAB sensors utilize aptamers, single-stranded oligonucleotides capable of binding to specific targets with high specificity and selectivity. Aptamer sequences for specific targets are identified in an in vitro process termed the Systematic Evolution of Ligands by Exponential Enrichment (SELEX). SELEX begins with a large, random oligonucleotide library consisting of approximately 10^{15} random sequences. These sequences are then incubated with a target; sequences that fail to

bind target are eluted, while those that bind to the target are amplified through PCR. This iterative process continues for many rounds, decreasing the concentration of target to isolate high-affinity aptamer sequences (Figure 1.2). To ensure aptamer selectivity, SELEX also involves the incubation of sequences with potentially confounding molecules in a process called counter SELEX (Zhuo et al., 2017). Sequences that bind these confounds are eluted, ensuring the final library contains aptamer sequences that have both high affinity and high selectivity for the target of interest (Kohlberger & Gadermaier, 2022; Sampson, 2003). The SELEX process is a significant advantage of EAB platforms, given that aptamers can be synthesized chemically, which allows for rapid, reproducible, and scalable production without the need for cell-based expression systems or animal hosts.

EAB sensors rely on single-stranded DNA as their biorecognition element. We utilize DNA aptamers as opposed to RNA because of its comparative stability. Although both DNA and RNA aptamers can bind targets with high affinity and selectivity, RNA-based aptamer sequences are often more unstable due to the presence of a reactive hydroxyl group which is more susceptible to hydrolysis (D. R. Davies et al., 2012; Ni et al., 2011; Zhu et al., 2015). DNA-based aptamers have higher stability in complex media (fetal bovine serum and human serum (Zhu et al., 2012)) and are resistant to hydrolysis.

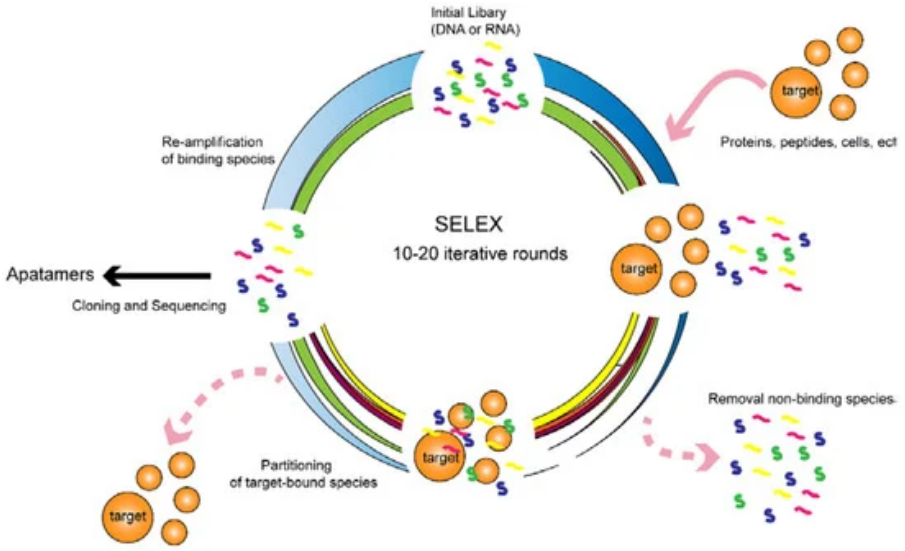

Figure 1.2. Schematic representation of the SELEX (Systematic Evolution of Ligands by Exponential enrichment) process. The cycle begins with a randomized oligonucleotide library incubated with the target molecule. Non-binding sequences are removed through a washing step, while target-bound sequences are eluted. The selected sequences are amplified using PCR (or RT-PCR for RNA aptamers) to generate an enriched pool. This pool undergoes iterative rounds of selection and amplification to refine high-affinity and high-specificity binders. The process concludes with sequencing and characterization of the enriched aptamers for downstream applications. Image from Zhou et al., 2017.

1.3.2. EAB mechanism. To engineer aptamers to function as biorecognition elements, we modify sequences with a covalently attached redox reporter, specifically methylene blue, and attach them to the surface of gold electrodes using thiol surface chemistry. This modification allows us to exploit the structure-switching capabilities of aptamers in the presence of target (Figure 1.3A). When the target is present, the aptamer undergoes a conformational change. This target-induced conformational change causes the methylene blue redox reporter to move closer to the surface of the electrode surface, thus increasing the electron transfer rate (Figure 1.3B). We can quantify this change in electron

transfer rate with an array of electrochemical techniques, including square wave voltammetry (Arroyo-Currás, Somerson, et al., 2017; Dauphin-Ducharme et al., 2019a; Idili et al., 2019), chronoamperometry (Arroyo-Currás, Dauphin-Ducharme, et al., 2018), and cyclic voltammetry (Pellitero et al., 2021). The signal change can then be plotted against increasing target concentration in vitro, allowing for rapid quantification of analyte concentration in vivo.

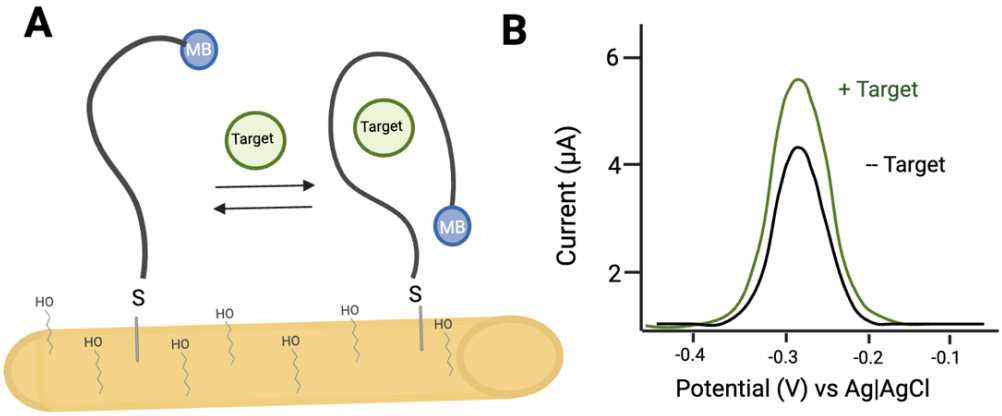

Figure 1.3. (A) Electrochemical aptamer-based (EAB) sensors are composed of a methylene blue (MB)-modified aptamer that is site-specifically attached to the surface of a gold electrode. Target binding produces a conformational change in this aptamer, altering the rate of electron transfer. (B) The binding-induced change in electron transfer results in an easily detectable change in peak current when the sensor is interrogated using square wave voltammetry. Image created in BioRender.

1.3.3. Post-SELEX aptamer modifications. Aptamer sequences can be rationally re-engineered for optimal performance as EAB sensors. Such modifications are often trial-and-error approaches performed to either enhance or decrease the sensitivity and affinity of the aptamer, depending on the application. Such modifications involve iteratively removing or adding base pairs from the terminal end of the aptamer sequence or potentially repositioning

the methylene blue redox reporter (S. Gao et al., 2016; Idili et al., 2021; Mayer & Lai, 2018; Oliveira et al., 2024). Utilization of modeling and structural simulation software, including Mfold, can provide information on secondary structure that can inform modifications that conserve likely target-binding regions (Fallah et al., 2024; S. Gao et al., 2016). This permits the rational reengineering of aptamer sequences in vitro to improve their performance as EAB sensors.

1.4 Advantages of EAB platform

1.4.1. Improved temporal resolution

The temporal resolution provided by EAB sensors is a significant advancement to prior biosensing platforms. EAB sensors can generate data with seconds resolution using interrogation techniques such as square wave voltammetry and sub-seconds resolution with techniques such as chronoamperometry (Arroyo-Currás et al., 2018) and intermittent pulse voltammetry (Santos-Cancel et al., 2018). This improved temporal resolution would significantly expedite clinical time-to-answer, enabling clinicians to adjust drug dosing in real time.

1.4.2. Generalizability

EAB sensors provide significant advantages over existing biosensing techniques, specifically because they are generalizable across targets. Because they rely on aptamers as their biorecognition element, EAB sensors are modular. This implies that the only barrier to target expansion is aptamer generation via SELEX and adaptation into the EAB platform. Aptamer generation and post-SELEX modification is a synthetic process and requires no in

vivo engineering, a primary advantage when considering other biorecognition elements such as antibodies (Rudenko et al., 2021; Sharma et al., 2016). And, unlike other biosensing techniques such as continuous glucose monitoring, EAB sensors do not rely on the chemical reactivity of their target. This renders them generalizable across a wide array of drugs and metabolites, including chemotherapeutics (Arroyo-Currás, Somerson, et al., 2017; Idili et al., 2019; H. Li, Dauphin-Ducharme, Arroyo-Currás, et al., 2017), antibiotics (Arroyo-Currás, Somerson, et al., 2017, 2017; Dauphin-Ducharme et al., 2019a; Vieira et al., 2019; Wu et al., 2022), and endogenous metabolites (Idili et al., 2021; Li et al., 2021).

1.4.3. Supports continuous measurements

The current state of the art for pharmacokinetic monitoring relies on blood draws and subsequent ex vivo quantification, which significantly limits clinical time-to-answer. In comparison, EAB sensors are entirely reagentless, requiring no additional reagents or wash steps, and contain all required incorporated elements to enable autonomous function (Downs et al., 2023; Parolo et al., 2023). Additionally, EAB sensors do not require batch processing, which sets them apart from many traditional analytical methods, such as ELISAs, HPLC, or mass spectrometry. Batch processing typically involves analyzing multiple samples in a time-consuming and multistep protocol, requiring reagents, pre-treatment, and extensive preparation. EAB sensors circumvent this need, given the sensing mechanism is already integrated into the electrode-aptamer system. Aptamers can also reversibly bind targets, capturing both rising and falling concentrations within the body.

1.4.4. Supports real-time measurements

Because aptamers reversibly bind targets, EAB sensors can capture the real-time fluctuations of target concentrations (A. M. Downs et al., 2023). This enables the precise, continuous measurement of drug distribution throughout the body and across distinct physiological compartments. In fact, under typical conditions, the limiting factor in EAB sensor operation is the electrochemical interrogation of the device, rather than the sensor's equilibration rate with the target (A. Downs, 2021). EAB sensors can support the generation of real-time data, enabling high-precision feedback-controlled drug delivery. This would significantly advance both pharmacological research and clinical practice. For example, feedback-controlled drug delivery could eliminate inter-subject pharmacokinetic variability, allowing researchers to study the reproducibility of therapeutic outcomes (Arroyo-Currás, Ortega, et al., 2018). It could further advance TDM by enabling patient-specific, optimized drug dosing in clinical practice, enhancing therapeutic outcomes while minimizing adverse side effects.

1.4.5. Supports in vivo measurements

EAB sensors support measurements in complex biological media. The EAB platform has been demonstrated to enable long-duration measurements in the plasma of live rats for a wide array of clinically relevant targets, including antibiotics (Arroyo-Currás, Somerson, et al., 2017; Arroyo-Currás, Ortega, et al., 2018; Dauphin-Ducharme et al., 2019a; Vieira et al., 2019), chemotherapeutics (Arroyo-Currás, Somerson, et al., 2017; Idili et al., 2021; H. Li, Dauphin-Ducharme, Arroyo-Currás, et al., 2017; S. Lin et al., 2022), anesthetics (Gerson et al., 2023a), and endogenous metabolites (Idili et al., 2021; Li, Dauphin-Ducharme, Ortega, et

al., 2017; Li et al., 2019.). It is important to note that EAB sensors can still be impacted by fouling, specifically when deployed in whole blood (Leung et al., 2021a). To mitigate fouling that results in signal loss in vivo, we utilize a dual frequency drift correction method called Kinetic Differential Measurements (KDM) (Ferguson et al., 2013):

$$\mathrm{KDM} = \frac{(\mathrm{Signal_{on}} - \mathrm{Signal_{off}})}{\frac{1}{2}(\mathrm{Signal_{on}} + \mathrm{Signal_{off}})}$$

We interrogate our sensors with frequencies that both increase and decrease in current in the presence of target, delineated as our "on" and "off" frequencies, respectively, and then subtract the normalized signals. KDM not only corrects for fouling-induced signal loss but also increases the magnitude of the signal gain (Arroyo-Currás, Somerson, et al., 2017; Ferguson et al., 2013; Figure 1.4).

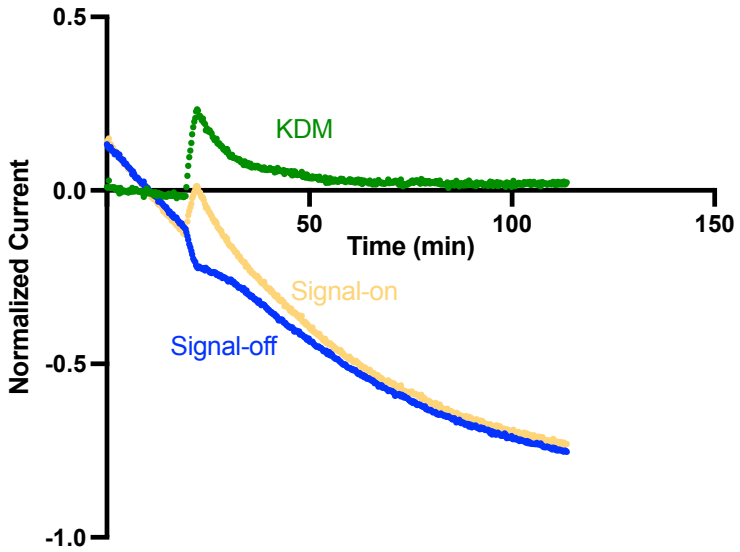

Figure 1.4. KDM, a dual frequency drift correction method, improves signal gain and corrects for signal drift. Two frequency drift correction requires a frequency that increases and decreases in current in the presence and absence of the target, respectively.

1.5. Aims

EAB sensors can be utilized to revolutionize the state of the art of intercompartmental pharmacokinetic modeling. For example, EAB sensors can be utilized to obtain seconds-resolved data that provides unparalleled insight into how drugs distribute from blood to various solid tissues in real-time, information we can utilize to, for example, better infer and predict in-brain drug concentrations from systemic concentrations. Given compartmental pharmacokinetic monitoring is only as strong as the data from which it is derived, vast improvements in temporal resolution would significantly improve our estimations of compartment-specific parameters (Dunvald et al., 2022; Nandi, 2023). For example, determining C_{max} from data obtained by in-brain microdialysis is generally an inference, given the lack of densely sampled data points between baseline and peak CSF concentrations (Pan et al., 2007; Shannon et al., 2013).

The general aim of the work presented by this thesis is to demonstrate how EAB sensors can be utilized to significantly advance the state of the art of personalized medicine, improving our clinical understanding of how drugs are transported into and eliminated from the body. The first three chapters of this work outline methods to improve our understanding of how drugs are distributed into peripheral tissue. The central goal of these projects is to utilize EAB sensors to explore, in real-time with unprecedented, seconds temporal resolution, the pharmacokinetics of chemotherapeutics as they move between major physiological compartments, including the kinetics of drugs crossing (or failure to cross) the blood-brain barrier (Doolittle et al., 2014). The final chapter suggests that EAB sensors can be utilized to discover and analyze individual pharmacokinetic differences. In contrast with existing techniques, such as microdialysis, EAB sensors can provide high-density data sets from individual animals, enabling the precise evaluation of inter-animal differences.

Using doxorubicin as a testbed, I first demonstrate that EAB sensors can capture the seconds-resolved distribution of chemotherapeutics from the bloodstream to the peripheral subcutaneous tissue. I then utilize these measurements to perform high-precision feedback-controlled drug delivery over plasma drug levels. Using the in-brain EAB platform, I further explore how pharmacological manipulations and drug encapsulation methods may improve drug permeation into the brain. Finally, the final chapter of this work demonstrates that individual, subject-specific measurements obtained from EAB sensors can be used to inform inter-patient pharmacokinetic variability. The central aim of this work argues that EAB sensors provide a significant advancement to personalized medicine, enabling high-precision therapeutic drug monitoring.

Chapter 2: Simultaneous, seconds-resolved intravenous and subcutaneous measurements provide a quantitative picture of the relationship between plasma and ISF pharmacokinetics

2.1 Abstract

The kinetics with which chemotherapeutics distribute into solid tissues, including their sites of both action and toxicity, remain poorly characterized. In no small part, this is due to the limited temporal resolution of traditional methods of measuring drug concentrations in the body, all of which employ sample collection (via the withdrawal of biofluids, microdialysis, or ultrafiltration) followed by benchtop analysis. Here, we have used electrochemical aptamer-based (EAB) sensors to perform simultaneous, 12 s resolved measurements of the chemotherapeutic doxorubicin in situ the veins (i.e., plasma) and the subcutaneous space (i.e., interstitial fluid) of live rats. The resulting data sets support the development of unprecedentedly high-temporal-resolution models of the distribution of doxorubicin from the central compartment to a distal physiological compartment and identify and demonstrate predictively strong correlations between plasma and solid-tissue pharmacokinetics in terms of both cumulative (area under the curve) and maximum (Cmax) doxorubicin exposure. In contrast, the correlations between delivered dose and drug exposure in both the plasma and solid tissue are quite poor. The latter observation highlights the need for therapeutic drug monitoring (TDM) and the former the potential value of employing subcutaneous EAB sensors as a convenient, minimally invasive, high-precision means of achieving this end.

2.2 Introduction

Because current methods for monitoring drug levels in the interstitial fluid (ISF), such as microdialysis (Schmidt et al., 2008) and ultrafiltration (Hansen et al., 1999), are

cumbersome and difficult to quantify (due, for example, to dilution effects), almost everything known about pharmacokinetics is based on the measurement of plasma drug concentrations. This is unfortunate for two reasons. First, the sites of action and toxicity of most drugs are the solid tissues and not in the plasma, suggesting that measurements of their pharmacokinetics in the solid tissues could prove of even greater clinical importance than the now standard measurement of their plasma pharmacokinetics. Second, the cumbersome nature of blood draws, microdialysis, ultrafiltration, and the subsequent benchtop analysis of such samples greatly limits the temporal resolution of most pharmacokinetic studies, much less pharmacokinetic measurements performed in the clinic during therapeutic drug monitoring (Reynolds & Aronson, 1993). Against this background, the recent advent of sensors able to measure drug concentrations in situ in the body and in real time provides a means of overcoming these limitations (Arroyo-Currás et al., 2017; Arroyo-Currás, Dauphin-Ducharme, et al., 2018; Wu et al., 2022; Idili et al., 2019; Gerson et al., 2023; Wu et al., 2022). For example, the ability of electrochemical, aptamer-based (EAB) sensors to measure drugs in the brain with seconds resolution has provided quantitative new insights into the kinetics of blood-brain-barrier crossing (Gerson et al., 2024.). By vastly improving the speed, convenience, and precision with which patient-specific pharmacokinetics are determined, such a technology could also revolutionize therapeutic drug monitoring, ultimately leading to, for example, fully autonomous, feedback-controlled drug delivery (Arroyo-Currás, Ortega, et al., 2018; Gerson et al., 2023). The venous sensor placements used in most prior EAB studies, however, are more invasive than is ideal for clinical applications, and thus with widest adaptation of this technology to therapeutic drug monitoring will likely require devices deployed intradermally or in subcutaneous placements. This, in turn, requires that we

improve our understanding of how molecular concentrations in the dermal or subdermal ISF correlate with those in plasma, since, as noted above, the latter forms the basis of all current clinical decision-making. As an added benefit, such studies will also improve our understanding of the transport of drugs from the plasma to the solid tissues that are their sites of action, producing potentially important, if less direct, clinical impact.

A platform technology generalizable to the detection of many molecular analytes, EAB sensors support the seconds or even sub-seconds (Arroyo-Currás, Dauphin-Ducharme, et al., 2018) resolved measurement of specific drugs, metabolites, and biomarkers in situ in the blood (Arroyo-Currás et al., 2017; Arroyo-Currás, Dauphin-Ducharme, et al., 2018; Idili et al., 2019), in cerebrospinal fluid (Gerson et al., 2023), and in the interstitial fluid of solid peripheral tissues (Ferguson et al., 2013; Lin et al., 2022). Comprised of a target-binding aptamer that has been modified with a redox reporter, reengineered to undergo binding-induced folding, and attached to an interrogating electrode, EAB sensors produce an electrochemical signal that is monotonically related to target concentration (Fig. 1A, 1B). The conformation-linked electrochemical signaling mechanism of EAB sensors renders them both reversible, thus supporting the continuous measurement of rising and falling target concentrations, and selective, such that they can be deployed in situ in the body. Building on this, here we have adapted this technology to the problem of simultaneously measuring time-resolved doxorubicin concentrations in the plasma and subcutaneous ISF of live rats, in an effort aimed at defining the relationships between the drug's pharmacokinetics in these physiologically distinct compartments.

2.3 Methods

The appropriately modified aptamer sequences were purchased from Integrated DNA Technologies (Table 4). The other materials employed were obtained and processed as follows. We diluted phosphate-buffered saline (PBS) from a 20x stock obtained from Santa Cruz Biotechnologies. We obtained sodium hydroxide, 6-mercapto-1-hexanol, tris(2-carboxyethyl) phosphine, and sulfuric acid from Sigma Aldrich. We obtained doxorubicin HCl from LC laboratories and dimethyl sulfoxide from Fisher Scientific.

To fabricate intravenous sensors, we first cut and insulated gold (0.2 μm diameter x 10 cm in length; 99.9% purity, A-M systems), platinum (0.125 μm diameter x 10 cm in length; 99.95% purity; A-M Systems), and silver (0.125 μm diameter x 10 cm in length; 99.99% purity, A-M Systems) wires with polytetrafluoroethylene heat-shrink (PTFE, Zeus Inc., HS Sub-Lite-Wall). We bundled the wires with physical gaps separating each wire to prevent shorting. We then trimmed the insulation to produce an exposed length of 3 mm (gold), 5 mm (platinum), and 1 cm (silver). To convert the silver wire to a reference electrode we submerged it in 7.5% sodium hypochlorite (commercial bleach, Clorox) overnight to form a stable silver chloride film. Finally, we rinsed the electrodes in di-ionized water to remove any residual bleach.

To fabricate subcutaneous sensors, we first cut and insulated gold (0.2 μm diameter x 10 cm in length), and silver wire (0.2 μm diameter, 10 cm in length, 99.99% purity, A-M Systems) with polytetrafluoroethylene heat-shrink (PTFE, HS Sub-Lite-Wall). We trimmed the insulation and electrodes to produce an exposed length of 5 mm (gold), and 1 cm (silver). To convert the silver wire to a reference electrode we submerged it in 7.5% sodium hypochlorite (commercial bleach, Clorox) overnight to form a stable silver chloride film,

followed by a di-ionized water wash. We then fabricated a separate counter electrode by heat-shrinking PTFE onto platinum wire (0.25 μm diameter x 10 cm in length). We then fed the counter through a 20-gauge catheter.

Following the above electrode preparations, we then fabricated intravenous and subcutaneous as follows. We reduced the disulfide bond in the methylene-blue modified DNA with 14 mL of 10 mM tris (2-carboxyethyl) phosphine with 2 mL of 100 mM DNA for 1 hour in the dark. After electrode assembly and overnight bleach treatment we rinsed the sensors in water and then cleaned as follows: (a) cycling the potential 1,000 times between -1.0 and -2 V versus Ag|AgCl in a solution of 0.5 M NaOH (1 Vs^{-1}) to remove residual organic or thiol contaminants on the surface; (b) pulsing between 0 and 2 V by applying 32,000 20 ms pulses with a pulse length of 0.02 s in 0.5 M H_2SO_4 to increase the surface area of the electrodes. We then roughened the electrode surface by cycling the potential between 1.5 and -0.35 V at 1 V/s four times in H_2SO_4. We then rinsed the gold electrodes in de-ionized water, fed them through 20 (intravenous) and 22 (subcutaneous)-gauge catheters, and immersed them in 500 nM reduced DNA dissolved in PBS for 1 h. The sensors were then transferred to a 10 mM solution of 6-mercapto-1-hexanol in PBS overnight at room temperature to complete the formation of their self-assembled monolayers. We fed the intravenous and subcutaneous sensors and the external counter of the latter through the lumen of 22 and 20-gauge catheters, respectively (Becton, Dickinson & Company). Before use in vivo, we fill the catheters with 1x PBS.

Sensor interrogation was performed electrochemically using square wave voltammetry on a CH1040C multipotentiostat. To determine relevant calibration curve, we performed a 24-point titration of each aptamer deposited onto the electrodes described above

in 37° bovine blood and determined the "signal-on" (200 Hz) and "signal-off" (40 Hz) frequencies that resulted in the largest relative changes in current. Drift correct was performed with kinetic differential measurements (KDM), obtained by taking the difference in the normalized (to the current seen in the absence of drug prior to the first drug challenge) peak currents seen at these two frequencies ($Signal_{on}$ and $Signal_{off}$):

$$\mathrm{KDM} = \frac{(\mathrm{Signal_{on}} - \mathrm{Signal_{off}})}{\frac{1}{2}(\mathrm{Signal_{on}} + \mathrm{Signal_{off}})} \quad \text{Eq 4.}$$

To fit resulting KDM signals to drug concentrations, we fit in vitro titration data to the equation:

$$[\mathrm{Target}] = \sqrt[\mathrm{n_H}]{\frac{\mathrm{K_{1/2}^{n_H}} * (\mathrm{KDM} - \mathrm{KDM_{min}})}{\mathrm{KDM_{max}} - \mathrm{KDM}}} \quad \text{Eq 5.}$$

where KDM_{max} is the maximum signal gain observed at saturating concentrations, [Target] is the drug concentration, n_H is the Hill Coefficient, and $K_{1/2}$ is the binding half-point of the aptamer (A. M. Downs et al., 2022).

We performed our in vivo experiments using adult male Sprague-Dawley rats (4-5 months old, 300-600 g; Charles River Laboratories, Wilmington, MA, USA). These were pair-housed in a temperature and humidity-controlled vivarium on a 12-h light-dark cycle and provided *ad libitum* access to food and water. All animal procedures were consistent with the guidelines of the NIH *Guide for Care and Use of Laboratory Animals* (8th edition, National Academy Press, 2011) and approved by the Institutional Animal Care and Use Committee (IACUC) of the University of California Santa Barbara.

Rats were induced under 4% isoflurane gas in a Plexiglas anesthesia chamber. Anesthesia was maintained with 2-3% isoflurane gas/oxygen administered via a nose cone

for the experiment's duration. A pulse oximeter (Nonin Medical, Plymouth, MN) was used to measure heart rate and SpO_2 during the experiment. The rat was shaved and the skin above the jugular vein was disinfected with 70% ethanol and betadine. A small incision was made to isolate both veins. A small incision in the jugular vein was made using spring loaded microscissors. A silastic catheter (composed of a bent steel cannula and silastic tubing) was inserted into the left jugular vein for infusions. The EAB sensor was inserted into the right jugular vein for in-vein drug monitoring and stabilized with sterile 6-0 silk sutures (Fine Science Tools, Foster City, CA). Following this insertion, we infused 30 units of heparin through the indwelling infusion line. Insertion of the subcutaneous sensor and external counter electrode was performed using an 18 g catheter inserted just below the surface of the skin on the posterior ventral side of the rat between the two legs after shaving the area.

For drug dosing, a 0.01 M stock of doxorubicin HCl was prepared by diluting a 0.1 M solution dissolved in dimethyl sulfoxide (DMSO, Sigma Alridch) with phosphate buffered saline. A 3 mL syringe containing this stock was connected to the catheter and then inserted into a motorized syringe pump (KDS 200, KD Scientific, Holliston, MA, USA). We performed all measurements using square wave voltammetry on a CH1040C multipotentiostat over a voltage window of approximately -0.1 to -0.45 V (relative to the Ag|AgCl reference). Before infusion of doxorubicin, we waited approximately 20 minutes to establish a stable baseline, ensuring any initial fouling of the electrode was corrected successfully with KDM. Once a stable baseline was determined, doxorubicin was injected over 3 min to better model clinical administration, given most injections of doxorubicin for the treatment of cancer in humans are administered over 10 to 30 minutes (Bronchud et al., 1990; D'Adamo et al., 2005). Target concentration was quantified by fitting KDM values to a

Hill Langmuir equation with parameters for K_D, n_H, KDM_{max} obtained from in vitro calibrations performed in bovine blood at 37°C. All figures were made in BioRender and all graphs were made using Graphpad Prism 9 Software (San Diego, CA).

Pharmacokinetic modeling

For the pharmacokinetic modeling, we only considered data from the peak observed plasma value and forward, effectively removing the pre-infusion and infusion period. That is, for each subject, we removed any plasma data prior to the peak plasma concentration and removed the equivalent ISF data from the respective ISF observations. These data were then considered to start at time 0.

We fitted our data in an iterative process. We first fitted the plasma data using a model based on the single-phase decay equation 12/11/24 8:36:00 AM. That is,

$$C_P(t) = L + (Y - L)e^{-kt}, \qquad \text{Eq 6.}$$

where $C_P(t)$ represents the plasma concentration value (in μM) at time t (in min^{-1}), Y is the value at which the fit crosses the y-axis (in μM), L is the horizontal asymptote of the fit (in μM), and k is the rate constant for the exponential decay (in min^{-1}).

After fitting to the plasma data, we then fitted to the ISF data using four separate multi-compartment models, each of which is represented by a system of first-order, linear ordinary differential equations with initial conditions. In these models, we assumed the contributions from the plasma compartment were fixed and known; specifically, we employed the single-phase decay model fits discussed above as the known plasma values. By setting the plasma compartment as fixed, we effectively reduced these multi-compartmental models to have one less dimension, details of which are subsequently discussed.

The first two of these ISF models we considered are the diffusion and differential transport models (Fig. 6A, B). In these, drugs enter a single compartment (termed "ISF compartment") from a fixed and known plasma compartment. For the diffusion model, the rate constants defining how rapidly the drug enters the ISF compartment, denoted k_D (in min^{-1}), is assumed to be non-negative and equal to the rate constant describing the drug's removal from the compartment. The corresponding ordinary differential equation and initial condition that describes this model can be seen in Equation 1. $C_P(t)$ represents the (fixed and known) drug concentration in the plasma (in μM) at time t (in min) and $C_{ISF}(t)$ represents the concentration in the ISF (in μM) at time t. In contrast, the differential transport model allows the rate constants describing transport into and out of the ISF, k_{IN} and k_{OUT} (both constrained to be non-negative and denoted in min^{-1}), are allowed to differ (seen in Equation 2).

The remaining two models, the distal compartment model and the intermediate compartment model (Fig. 6C, D), extend the two-compartment model systems described above by adding a third compartment. That is, in these models, the drug enters one compartment from the fixed and known plasma compartment, from which it then distributes and redistributes into another compartment that is not in direct communication with the plasma. The underlying ordinary differential system of equations for these models is seen in Equation 3. Here, $C_{ICF}(t)$ represents the concentration (in μM) in the more distal compartment at time t, k_{VI} and k_{IV} are the rate constants describing transport into the intermediate compartment from the plasma and vice versa, and k_{IC} and k_{CI} are the rate constants describing transport into and out of the distal compartment. All rates are non-negative and in min^{-1}, and $C_P(t)$ and $C_{ISF}(t)$ are as defined before. The difference between the distal compartment model and the intermediate compartment model is where we assumed the

ISF concentrations were observed. In the distal compartment model, ISF concentrations were assumed to be observed from the intermediate compartment (presumed to be the ISF); i.e., this is the two-compartment model with the addition of an unobserved distal compartment. In contrast, in the intermediate compartment, we assume there is an unobserved compartment between the plasma and the site of in-tissue measurement concentrations.

We estimated the parameters appropriate for all models using nonlinear regression(Serber & Wild, 2003) in the R software package (RStudio, 2020). In this estimation, we restricted our parameters to be positive, and we assumed the observed values (both for plasma and ISF observations) were the true values ($C_P(t)$ or $C_{ISF}(t)$) plus some additive, normally distributed errors with zero mean and constant variance. To select between the four ISF model fits, we employed the Bayesian Information Criteria (BIC) (Schwarz, 1978) as our model selection method. The model with the lowest BIC value from the set of considered models is deemed the preferred model of the set.

2.4 Results

To perform measurements in the subcutaneous space we employed a previously described, doxorubicin-binding aptamer (Arroyo-Currás, Somerson, et al., 2017; S. Lin et al., 2022) (Figure 2A). We deposited this on a 200 μm diameter, 3 mm long gold working electrode that we bundled together with a chloride-anodized silver wire reference electrode (Leung et al., 2023) (Fig. 1A). To implant this into the subcutaneous space, we first inserted an 18-gauge shielded catheter at a 45° angle below the surface of the skin on the posterior ventral side of the rat, confirming the guide catheter is not embedded in fat or muscle by

touch (the latter offer significant resistance to insertion). We then removed the needle, leaving the catheter in place, and slid the working and reference electrodes through the catheter and into the subcutaneous tissue. To complete our three-electrode setup then we inserted a platinum wire counter electrode into the subcutaneous space approximately 1.5 cm away from the working electrode using the same catheter-based approach (Figure 1C). To ensure that we are sampling ISF and not blood, we confirm the catheter does not backfill with blood during initial insertion and check to ensure a lack of blood on the sensor when it is removed after the experiment; neither of these occurred during any of the collection of any of the data presented in this study.

EAB sensors support the high-precision, high-frequency measurement of doxorubicin in the subcutaneous ISF. Specifically, using dual-frequency, kinetic-differential-measurement-corrected square wave voltammetry (A. M. Downs et al., 2022; Ferguson et al., 2013) to interrogate our sensor, we achieve time resolution of 12 s and a pre-drug-challenge, root-mean-squared (RMS) baseline noise of 0.005 μM (Figure 1D). Upon challenging the animals with intravenous doxorubicin at body-mass adjusted doses of 3 to 10 mg/kg, we observe the ISF concentration of the drug to rise to maximum ISF concentrations, C_{max}(ISF), ranging from approximately 0.3 to 1.4 mM in a dose-dependent manner (Figure 1D). The concentration then falls, returning to near-baseline levels within 1 to 2 h.

The relative ease of employing EAB sensors in the body renders it possible to perform simultaneous, seconds-resolved drug measurements in the plasma and the ISF, providing new insights into the pharmacokinetic relationships between these distinct physiological compartments. An initial difficulty in applying this approach to doxorubicin, however, was that our original doxorubicin-detecting sensor begins to saturate at the few

micromolar peak concentrations seen in plasma, C_{max}(plasma), reducing measurement precision (Figure 2B). To circumvent this, we fabricated a second sensor employing a one-base-pair truncation of the aptamer which, by altering the thermodynamics of the aptamer's conformational switch, pushes the sensor's useful dynamic range to higher concentrations (Shaver et al., 2022). As expected, at 22 ± 2 μM (all reported confidence intervals reflect 95% confidence) the binding midpoint of the resulting sensor is several-fold higher than the 4.5 ± 0.7 μM of the original sensor (Figure 2B). Concomitantly, the sensor's gain (relative change in signal upon addition of high concentrations of target) is also enhanced, presumably because truncation increases the population of the aptamer unfolded in the absence of target (Vallée-Bélisle et al., 2009). Inserting this second sensor into the right jugular vein (approach described previously, (Arroyo-Currás, Somerson, et al., 2017; Arroyo-Currás, Dauphin-Ducharme, et al., 2018; Idili et al., 2019) we achieve the measurement of plasma doxorubicin concentrations with 12 s resolution and 0.06 μM RMS baseline noise (Fig. 3). Of note, the order-of-magnitude higher noise seen in plasma relative to subcutaneous measurements arises due to the proximity of the former sensor to the heart. For example, this noise falls dramatically upon sacrificing the animal (data not shown).

The plasma and ISF pharmacokinetics of doxorubicin vary significantly from animal to animal. For example, the correlations between dose and the doxorubicin exposure (as measured by area under the curve; AUC) seen in the plasma and ISF are, at $R^2 = 0.38$ for both, not statistically significant at $\alpha = 0.05$ (Figure 4A, Table 1). This observation in the rat is consistent with prior literature suggesting high inter- and even intra-patient variability in human doxorubicin pharmacokinetics (Hempel et al., 2002; Hon & Evans, 1998; Jacquet et al., 1990). In contrast, the correlations between dose and C_{max} in both the plasma and the ISF

are, at $R^2 = 0.71$ and $R^2 = 0.98$, respectively, highly significant ($p < 0.01$ and $p < 0.0001$, respectively, Fig. 4B, Table 1). This observation, however, is fairly trivial as, presumably, these correlations simply reflect the strongly proportional relationships between body mass and both blood and ISF volume (Lee & Blaufox, 1985). The fluid volumes the drug is distributed into in both cases are strongly correlated with body mass (Feldschuh & Enson, 1977), and thus body-mass-adjusted dosing leads to significant correlations with the resulting peak drug concentrations.

Despite the significant inter-animal variation in both the plasma and ISF pharmacokinetics of doxorubicin, we nevertheless see strong correlations between the two within individual animals. Specifically, the correlation between $AUC_{(plasma)}$ and $AUC_{(ISF)}$ within individual animals is, at $R^2 = 0.96$ and $p < 0.001$, far more statistically significant than the correlation that either parameter has with dose (Figure 5A, Table 1). These observations are consistent with similar recent studies (S. Lin et al., 2022) finding strong correlations between AUC(plasma) and AUC(ISF) ($R^2 = 0.99$) for the antibiotic vancomycin. Perhaps not surprisingly, C_{max}(plasma) and C_{max}(ISF) are, at $R^2 = 0.86$, $p = 0.005$, likewise strongly correlated within individual animals (Fig. 5B).

Pharmacokinetic modeling

Prompted by the unprecedented time resolution of our EAB-sensor-derived, simultaneous plasma and ISF doxorubicin concentrations we next explored compartmental models of the drug's transport between the two measurement compartments. In the first of these, we assume that the plasma-filled veins and the ISF-filled "solid tissues" are the only significant compartments and that the drug is transported between these via passive diffusion

(Figure 6A). Given that we have knowledge of both the time-resolved plasma, C_P, and ISF, C_{ISF}, drug concentrations, this "diffusion model" is defined by the single parameter k_D, which describes the rate of transport between the two compartments (Eq. 1).

$$\frac{dC_{ISF}(t)}{dt} = k_D(C_P(t) - C_{ISF}(t)) \qquad \text{(Eq. 1)}$$

At the next level of complexity is an "differential transport model." In this case, the rate constant for transport from the vein into the tissues, k_{IN}, and the rate constant describing transport from the tissue to the vein, k_{OUT}, are allowed to differ, thus yielding 2 fitted parameters (Fig. 6B).

$$\frac{dC_{ISF}(t)}{dt} = k_{IN}C_P(t) - k_{OUT}C_{ISF}(t) \qquad \text{(Eq. 2)}$$

In our next two models we added a third, unobserved compartment. In the first of these 3-compartment models, the "distal compartment model," this additional compartment is distal to the ISF compartment in which we are making measurements (Figure 6C). Finally, for completeness, we also investigated an "intermediate compartment model" in which the additional compartment is located between the vein and the ISF site at which we are taking measurements (Figure 6D). Both of these models contain 4 parameters (Equation 3), as we assume asymmetric transport into and between the two tissue compartments present in each.

To apply these models to our results, we first fit our plasma time courses to a one-compartment model (Figure 7, top row). We then used the resulting plasma pharmacokinetic model as input to four models of the resulting ISF drug concentration profiles. To delineate the appropriateness of these models we have employed the Bayesian Information Criterion (BIC), a model selection criterion that weights goodness-of-fit while penalizing model complexity (Schwarz, 1978). The model with the lowest BIC is considered the most

appropriate model with, as a general rule of thumb, models differing in BIC by less than 2 being considered indistinguishably good (or poor) descriptors of the system (Fabozzi et al., 2014). Applying these 4 models to our 7 paired data sets (Figure 7, bottom row) we see that, as judged by BIC (Table 2), the distal compartment model is selected for 5 (with differential transport being ranked second best for all 5) and the differential transport model is ranked most appropriate for the other 2 (with the intermediate model being ranked second best these). That is, the diffusion model is too simple, and the intermediate compartment model provides no significant improvement in fit over the differential transport or distal compartment models for any of our paired data sets. This said, while many of our paired data sets appear to be well-captured (by simple visual inspection) by one or both of the latter models (e.g., F2, M1, M2(1), M2(2), M3), it appears that as yet uncaptured physiology or experimental error (e.g., uncorrected sensor drift, incorrect sensor calibration) remains for some data sets (e.g., F1).

Application of the differential transport model (which, again, is the most appropriate model by BIC for 2 of the 7 data sets, and the second most appropriate for the remainder), estimates rate constants for transport between the plasma and the ISF at the observation site of order 0.06 to 0.16 min^{-1} for all observations. These values are of similar magnitude to the elimination rate constants obtained from our one-compartment modeling of the plasma time courses (Table 3), suggesting that the rate constant for transport of the drug to the site tissue site of measurement is similar to the mean rate constant for the distribution of this drug into the solid tissues. This said, the rate constants for transport to the ISF measurement site are lower than the estimated plasma elimination rate constant for 5 of 7 observations, presumably because the rate constant for elimination from the blood also captures both transport into the

solid tissues and removal of the drug from the body via the kidneys. The observation that the rate constants for transport from (k_{IN}) and to (k_{OUT}) the plasma differ by up to 2-fold could reflect physiological variations between the two compartments, such as a metabolically induced pH gradient that causes the drug to partition unequally between them. Alternatively, this discrepancy could be due to errors in the calibration of either or both sensors (Downs et al., 2022). For 5 of our 7 data sets, BIC ranks the distal compartment model as preferred among our 4 models (Table 2). In this model there is a third, unmeasured compartment that is distal to the measurement site (Fig. 6C). Given that doxorubicin must cross into cells to reach its site of action (the DNA in the cell nucleus), this distal compartment is presumably the intracellular fluid (ICF).

2.5 Discussion

Here we have utilized EAB sensors to simultaneously monitor the concentration of doxorubicin in the blood and ISF of live rats, obtaining densely sampled data sets that capture the distribution of drug between compartments with unprecedentedly high, few-second time resolution. Analyzing these data, we find no significant correlation between body-mass-adjusted dose and the resulting drug exposure (as AUC) in either bodily fluid. Despite the significant animal-to-animal pharmacokinetic variation this poor correlation implies, however, the correlations between the pharmacokinetics observed in the two compartments is exceptionally strong.

The administration of antineoplastic agents, and many other therapeutic drugs, is significantly limited by the relationship between systemic exposure and toxicity. Against this

background, the relatively poor correlations between dose and drug exposure in both the blood and subcutaneous space (Figure 4) highlight the potential clinical importance of performing therapeutic drug monitoring to ensure that dosing is personalized to maximize both safety and efficacy (Paci et al., 2014; Rebollo et al., 2010). Specifically, these observations, which are consistent with prior literature suggesting high inter-patient variability in pharmacokinetics (Hempel et al., 2002; Hon & Evans, 1998; Jacquet et al., 1990), strongly suggest a need for dosing based on individualized pharmacokinetic parameters rather than more generic physical descriptors, such as body mass or sex (Hempel et al., 2002; Jacquet et al., 1990; Redlarski et al., 2016). Fortunately, the predictively strong correlations we observe between drug exposure in the plasma and ISF suggest a convenient, high-precision means to this end. That is, given the strong correlation between AUC(plasma) and AUC(ISF), the ability of EAB sensors to perform real-time, high-frequency measurements of drug concentration in easily accessible subcutaneous space would circumvent the cumbersome blood draws and benchtop analysis traditionally employed in therapeutic drug monitoring (Evans & Relling, 1989; Smita et al., 2022). And it would do so while simultaneously vastly improving the temporal resolution of such measurements, and with that, the accuracy with which patient-specific pharmacokinetics are determined.

Moving beyond the strong correlation we observe between plasma and ISF pharmacokinetics, we suspect that measurements performed in the solid tissues, such as those reported here, may prove of greater clinical value than plasma concentration measurements. Specifically, plasma drug measurements provide only an indirect estimation of drug concentrations in the targeted tissue (Alnaim, 2007; Hon & Evans, 1998). While additional research will be required to confirm this speculation, we hypothesize that subcutaneous ISF

measurements may prove a more accurate estimator than plasma drug concentrations are of drug concentrations in other solid tissues, a question the technology described here is well-placed to investigate. This said, the remarkably strong correlation between the pharmacokinetics of doxorubicin in the plasma and in the subcutaneous ISF (Fig. 5), observations that have also been observed for vancomycin (S. Lin et al., 2022) and tobramycin (Y. Wu et al., 2022) suggest that plasma-based measurements may inform on drug exposure in the solid tissues with more than sufficient accuracy to match clinical needs.

The potential value of EAB-based therapeutic drug monitoring is enhanced by the generalizability of the EAB platform, which can be used in the measurement of a wide variety of drug classes (Arroyo-Currás, Somerson, et al., 2017; Gerson et al., 2023a; Idili et al., 2019). This may prove particularly valuable for the administration of chemotherapeutics, given the narrow therapeutic windows typically associated with these drugs and the high clinical value associated with their therapeutic monitoring (Hon & Evans, 1998; Paci et al., 2014). General dosing of chemotherapeutics is determined using averaged pharmacokinetic data collected from large populations with individualization based on gross and often low-utility metrics such as body surface area (Redlarski et al., 2016). Determining the maximum tolerated dose for these agents is complicated by significant inter-patient pharmacokinetic variability, narrow therapeutic windows, and steep dose-response relationships. To ablate metastasizing cancer cells, chemotherapeutic agents injected intravenously are expected to be distributed to tissue where they must be maintained at relevant therapeutic levels. Providing insight into the pharmacokinetics of drug distribution across compartments can inform clinical interventions tailored to maximize drug levels in tissue while avoiding central toxicity induced by antineoplastic drugs.

2.6 Figures and Tables

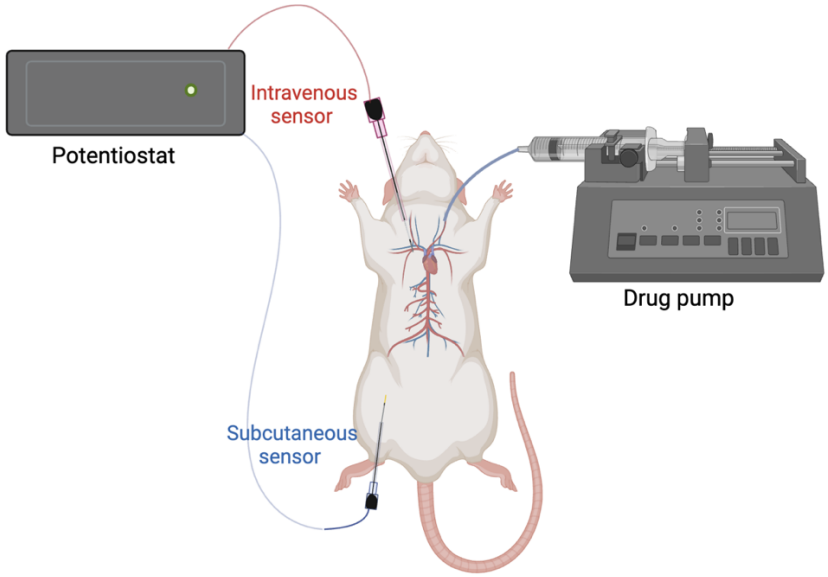

Figure 2.1. (A) Electrochemical aptamer-based (EAB) sensors are composed of a methylene blue (MB)-modified aptamer that is site-specifically attached to the surface of a gold electrode. Target binding produces a conformational change in this aptamer, altering the rate of electron transfer. (B) The binding-induced change in electron transfer results in an easily detectable change in peak current when the sensor is interrogated using square wave voltammetry. (C) To perform simultaneous in-vein and subcutaneous doxorubicin measurements, we insert an EAB sensor into the right jugular vein and a second sensor below the surface of the animal's posterior ventral skin. To administer the drug, we insert a silastic catheter into the left jugular vein. (D) Shown are subcutaneous measurements of doxorubicin assessed after the indicated, sequential intravenous doses, each lasting 4 min.

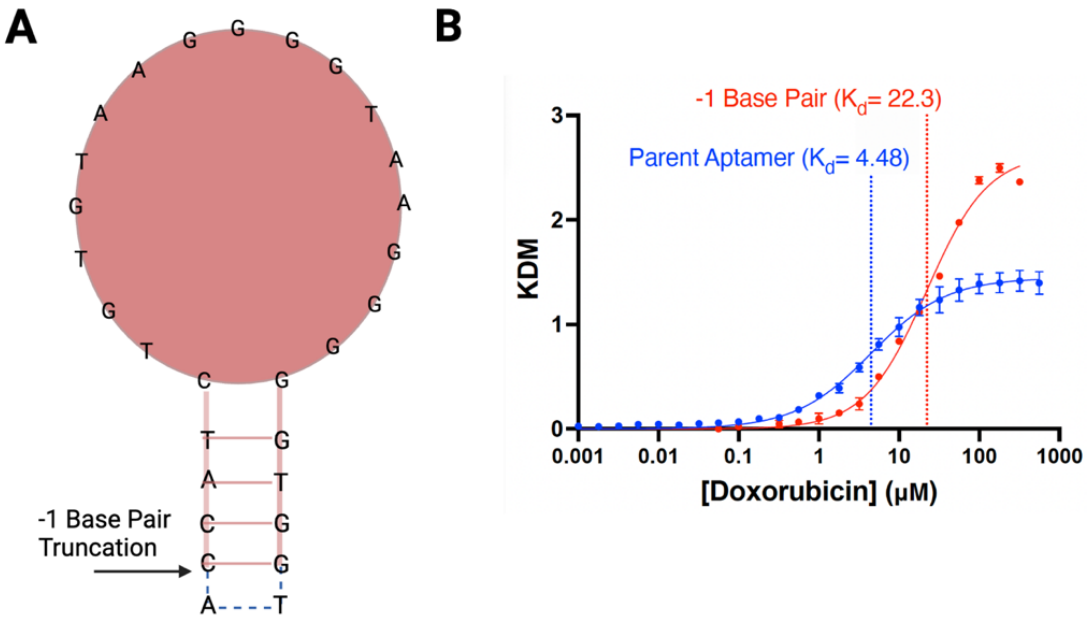

Figure 2.2. To capture the rather wide clinical range of doxorubicin as it distributes from the plasma to the ISF, we have used a pair of EAB sensors differing in their useful dynamic range. (A) These sensors employ either the full-length "parent aptamer" (shown in red and blue) or a 1-base-pair truncation (red), with the latter modification reducing the affinity of the aptamer and pushing the resulting sensor's dynamic range to higher doxorubicin concentrations. (B) Shown are calibration curves for the two sensors, with the sensor employing the parent aptamer ($K_d = 4.5 \pm 0.7$ μM) shown in blue and the -1 base pair aptamer ($K_d = 22 \pm 2$ μM) in red. These data were collected in vitro in whole bovine blood at 37°C, with the error bars shown on this graph reflecting standard deviations across 8 independently fabricated devices to illustrate reproducibility.

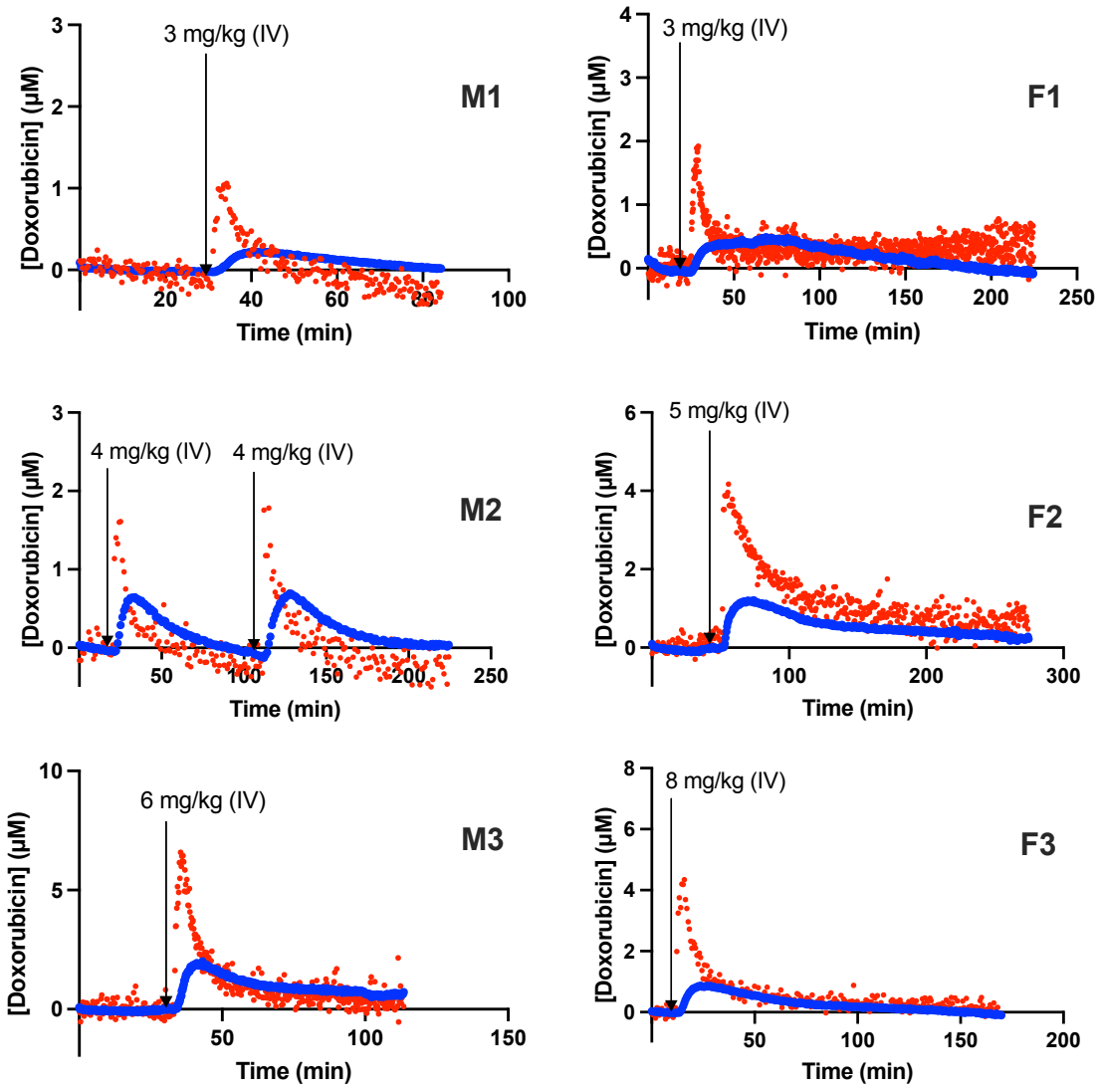

Figure 2.3. Simultaneous jugular and subcutaneous EAB sensor measurements achieve high-temporal-resolution measurement of the distribution of doxorubicin between the plasma and the ISF. Shown are such measurements collected in six individual rats after the indicated body-mass-adjusted doses. The rat ID, shown to the right of each figure (e.g., "F1") refers to animal sex and identification number. All doses were administered intravenously over 3 minutes.

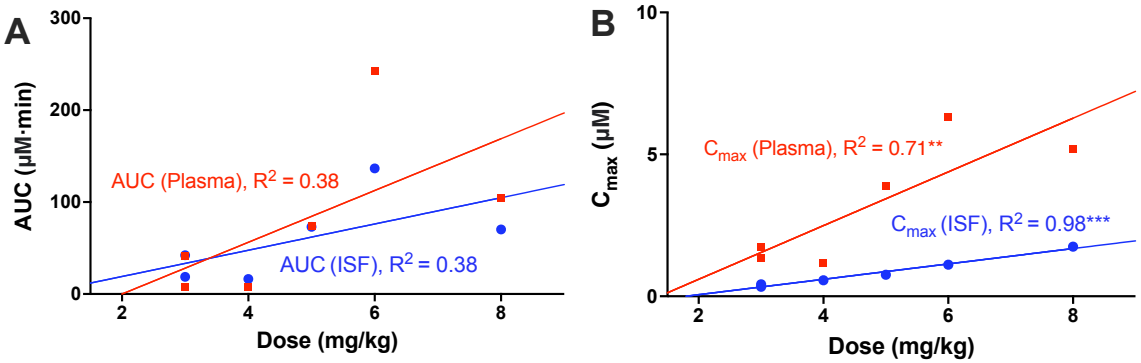

Figure 2.4. (A) Body-mass adjusted dose is poorly correlated with drug exposure (as measured by Area Under the Curve- AUC) in both the plasma and the subcutaneous ISF. Neither of the indicated correlations are significant at the $\alpha = 0.05$ level. (B) In contrast, the correlation between dose and peak observed concentration is significant ($p < 0.01$ and $p < 0.001$) in the plasma and ISF, respectively.

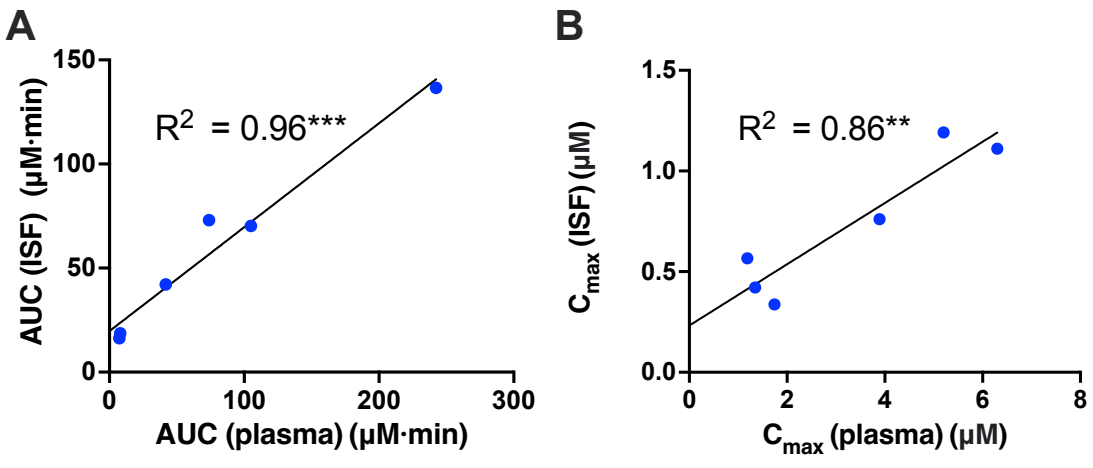

Figure 2.5. The pharmacokinetics of doxorubicin in the subcutaneous ISF are strongly correlated with those seen in the plasma**.** (A) For example, cumulative doxorubicin exposure in the plasma and ISF, calculated as the area under the curve (AUC) obtained from fitting data sets to a single exponential decay model, are strongly correlated ($p < 0.001$) within individual animals. (B) The maximum doxorubicin concentrations, C_{max}, reached in the ISF and plasma are also strongly correlated ($p < 0.01$) within individual animals.

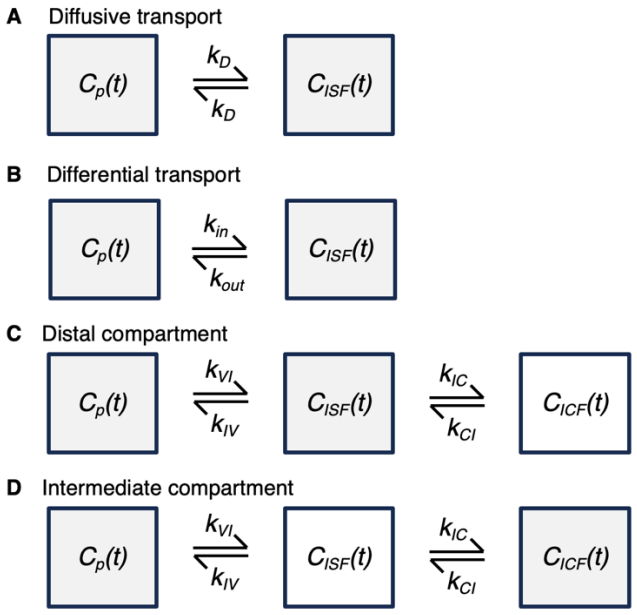

Figure 2.6. Here we have explored 4 compartmental models of drug transport. In each of these, drug enters the ISF compartment by way of the plasma compartment, where the plasma compartment concentration time course, $C_{P(t)}$, is assumed to fixed and known. The two compartments that are being measured are indicated with grey shading. (A) In the diffusive transport model, transport between the plasma and ISF is via passive diffusion, leading to a single fitted rate constant, k_D, that describes transport both to and from the ISF. (B) In the differential transport model, the rate constants for transport into (k_{in}) and out of (k_{out}) of the ISF are asymmetric. (C, D) We also investigated two three-compartment models, which differ regarding which of the three compartments is not under observation. In the distal compartment model, the unobserved compartment is distal to the tissue measurement site; this presumably reflects intracellular fluid. In the intermediate compartment model, the additional, unobserved compartment is between the plasma and the tissue measurement site. This is difficult to rationalize physiologically, but we have included it for completeness.

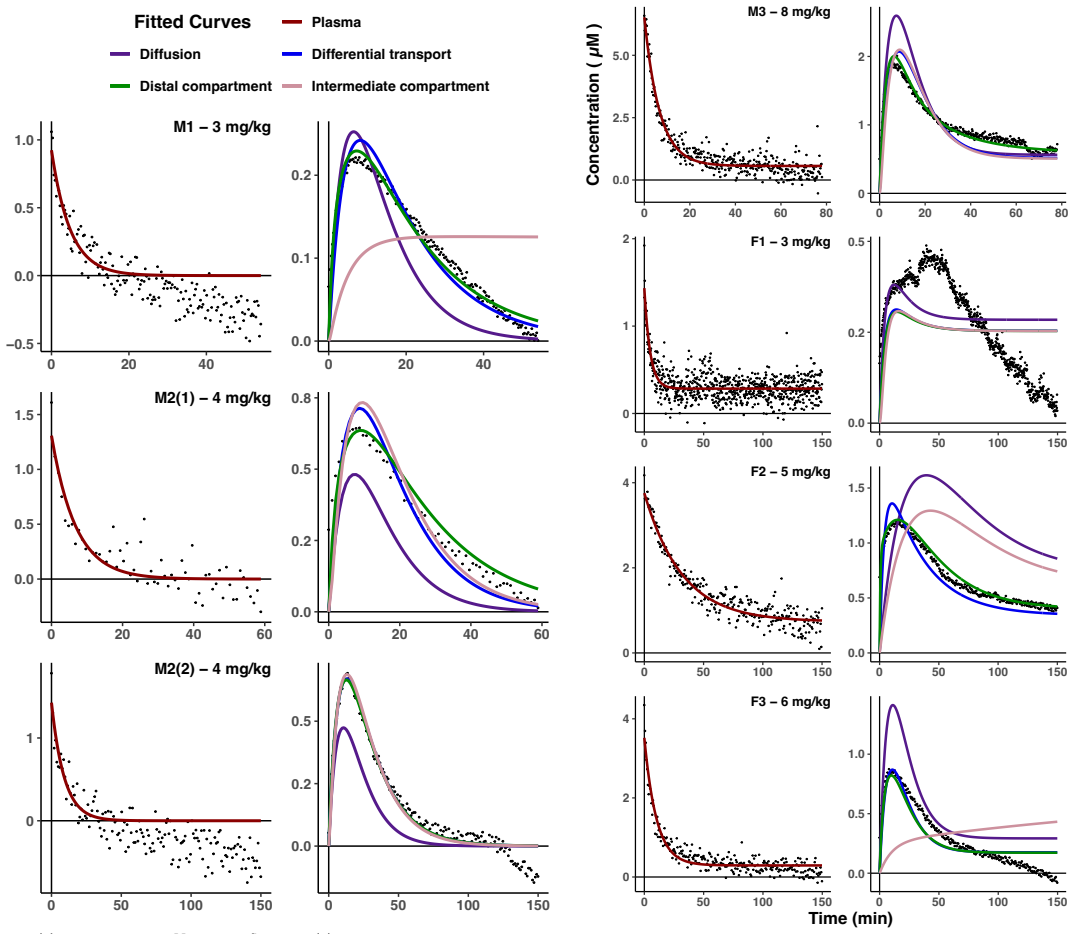

Figure 7. (Left column) To model transport from the plasma into the subcutaneous measurement site we first fit our plasma time courses to a one-compartment model (red). (Right column) While many of our paired data sets appear to be well-captured (by simple visual inspection) 2 or more of our 4 models, it appears that uncaptured physiology (e.g., changing renal function) or experimental error (e.g., uncorrected sensor drift, incorrect sensor calibration) remains for some data sets (e.g., F1).

Table 1: Pharmacokinetic Parameters. Outputted data from single exponential fit for each animal in the current study.

Dose (mg/kg)	**Animal ID**	**AUC (μM·min)**		**C_{max} (μM)**		**Time to C_{max} (min)**		**Half-life (min)**
		Plasma	**ISF**	**Plasma**	**ISF**	**Plasma**	**ISF**	**Plasma**
3	M1	8.0	19	1.35	0.42	2.9	16	2.5
3	F1	42	42	1.74	0.34	3.5	49	1.7
4	M2	7.4	16	1.19	0.57	3.2	11	1.9
5	F2	74	73	3.89	0.76	3.0	16	7.2
6	M3	242	137	6.3	1.11	15	26	3.7
8	F3	105	70	5.20	0.34	2.8	8.5	2.5

Table 1: Pharmacokinetic Parameters**.** Outputted data from a single exponential fit for each animal in the current study.

Table 2: Model Selection*							
Model	**M1**	**M2 (1st)**	**M2 (2nd)**	**M3**	**F1**	**F2**	**F3**
Diffusion	-1554.0	-245.5	-741.3	-245.8	-3397.2	319.2	-440.2
Differential transport	-2017.0	-357.5	-1260.9	-1057.7	-3510.3	-1010.7	-1220.6
Distal compartment	-2153.4	-360.7	-1250.8	-1821.5	-3490.4	-1153.5	-1233.0
Intermediate compartment	-1103.4	-314.0	-1245.3	-729.9	-3459.0	-8.6	-135.5
*Dark grey denotes lowest BIC and thus the preferred model; lighter grey denotes the second lowest BIC.							

Table 2: BIC from each model and selected model.

Table 3: Model Parameters								
	Model	**Plasma ***	**Differential transport**		**Distal compartment**			
Parameter	**/***	k_{elim}	k_{IN}	k_{OUT}	k_{VI}	k_{IV}	K_{CI}	k_{IC}
M1	**Estimate**	0.21	0.089	0.066	0.17	0.12	0.5	0.5
	CI	[0.16, 0.27]	[0.085, 0.095]	[0.064, 0.068]	[0.13, 0.21]	[0.09, 0.15]	[0.1, 2.0]	[0.2, 1.6]
M2 (1st)	**Estimate**	0.15	0.16	0.088	0.23	0.103	0.38	0.35
	CI	[0.11, 0.20]	[0.14, 0.19]	[0.081, 0.097]	[0.14, 0.38]	[0.103, 0.103]	[0.26, 0.54]	[0.09, 1.35]
M2 (2nd)	**Estimate**	0.11	0.096	0.053	0.102	0.056	0.3	0.02
	CI	[0.08, 0.16]	[0.083, 0.111]	[0.050, 0.056]	[0.080, 0.131]	[0.025, 0.126]	[0.0001, 1633]	[0.0003, 1.5]
M3	**Estimate**	0.15	0.103	0.113	0.147	0.141	0.096	0.114
	CI	[0.14, 0.16]	[0.101, 0.105]	[0.113, 0.113]	[0.139, 0.154]	[0.135, 0.146]	[0.069, 0.132]	[0.101, 0.128]
F1	**Estimate**	0.20	0.055	0.061	0.055	0.061	1.1	0.04
	CI	[0.18, 0.23]	[0.043, 0.070]	[0.049, 0.078]	[0.033, 0.092]	[0.036, 0.104]	[0,3.9e7]	[0,3806]
F2	**Estimate**	0.031	0.114	0.246	0.40	0.74	0.14	0.81
	CI	[0.029, 0.034]	[0.106, 0.123]	[0.230, 0.262]	[0.37, 0.44]	[0.74, 0.74]	[0.12, 0.16]	[0.81, 0.81]
F3	**Estimate**	0.098	0.062	0.104	0.077	0.13	0.26	0.09
	CI	[0.090, 0.106]	[0.057, 0.067]	[0.099, 0.109]	[0.071, 0.085]	[0.12, 0.14]	[0.08, 0.90]	[0.05, 0.18]
*Rate constant for one-compartment fit of plasma time course								
**All units are in min^{-1}								
*** Approximate 95% confidence intervals								

Table 3: All model parameters for each experiment.

Table 4: Aptamer sequences	
Name	**Sequence (5' to 3')**
Parent	ACCATCTGTGTAAGGGGTAAGGGGTGGT
-1 Base Pair `	CCATCTGTGTAAGGGGTAAGGGGTGG

Chapter 3: Feedback control over plasma drug concentrations achieves rapid and accurate control over solid-tissue drug concentrations

3.1 Abstract

Electrochemical aptamer-based (EAB) sensors enable the continuous, real-time monitoring of drugs and biomarkers in situ in the blood, brain, and peripheral tissues of live subjects. The real-time concentration information produced by these sensors provides unique opportunities to perform closed-loop, feedback-controlled drug delivery, by which the plasma concentration of a drug can be held constant or made to follow a specific, time-varying profile. Motivated by the observation that the site of action of many drugs, however, is the solid tissues and not the blood, here we experimentally confirm that maintaining constant plasma drug concentrations also produces constant concentrations in the interstitial fluid. Specifically, using an intravenous EAB sensor we performed feedback control over the concentration of doxorubicin, an anthracycline chemotherapeutic, in the plasma of live rats. Using a second sensor placed in the subcutaneous space, we find that drug concentrations in the interstitial fluid of this tissue rapidly (30-60 min) match and then accurately (root mean squared deviation 8% to 21%) remain at the feedback-controlled plasma concentration. This close correspondence validates the use of feedback-controlled plasma drug concentrations as a means of controlling drug concentrations in the solid tissues that are the site of drug action. Following this, we expanded our studies to use pairs of sensors in the subcutaneous space of individual animals undergoing feedback-controlled delivery to the plasma. The output of the two sensors tracks one another with excellent precision (R^2 = 0.95-0.99) and accuracy (mean deviation of 9-13%), confirming that the performance of in vivo EAB sensors matches that in prior, in vitro validation studies. Together, these observations provide further evidence that EAB sensors will prove a powerful new approach to the high-precision personalization of drug dosing.

3.2 Introduction

Electrochemical aptamer-based (EAB) sensors enable real-time, seconds-resolved measurements of the disposition of drugs and biomarkers in the living body (Fig. 1A, 1B). They have been used, for example, to measure an increasing number of drugs and metabolites in situ in the blood (jugular) (Arroyo-Currás, Somerson, et al., 2017; Arroyo-Currás, Dauphin-Ducharme, et al., 2018; Idili et al., 2019, 2021), cerebrospinal fluid (lateral ventricle, hippocampus) (Gerson et al., 2023a), and interstitial fluid (subcutaneous space, muscle, solid tumors) (Ferguson et al., 2013; Y.-L. Lin et al., 2018; Seo et al., 2021). The real-time, in vivo concentration measurements provided by EAB sensors also offer unique opportunities to perform feedback-controlled drug delivery. We have previously demonstrated, for example, feedback control over both plasma (Arroyo-Currás, Ortega, et al., 2018; Dauphin-Ducharme et al., 2019b) and in-brain (Gerson et al., 2023a) drug concentrations, in each case precisely achieving either fixed concentrations or pre-defined, time-varying concentration profiles with the latter, for example, mimicking human pharmacokinetics in a rat. Here we expand on these studies by using feedback control over plasma drug levels to explore two questions regarding the measurement of and control over drug concentrations in the solid peripheral tissues. The first question, which is clinical in focus, is how well and how rapidly control over plasma drug concentrations equates to control over drug concentrations in these tissues? The second question, which is technical in nature, is how accurate is the calibration of subcutaneous EAB sensors?

To motivate the clinical question we address, we note that the argument in favor of performing feedback control over plasma drug concentrations is that, if this is performed for long enough, drug concentrations in the solid tissues will eventually reach and maintain the same level. That is, the assumption that holding plasma drug concentrations constant at their clinically optimal level equates to achieving similarly constant, similarly optimal levels in the solid tissues that are the site of action of most drugs. Such an advance could prove particularly important in the pharmacological treatment of cancer, which generally assumes that achieving adequate plasma drug exposure corresponds to achieving adequate exposure in the solid tissues of a tumor. Here we test this assumption by employing feedback control to maintain a constant drug concentration in the plasma while simultaneously observing the resulting concentration in interstitial fluid (ISF) of the subcutaneous space.

To motivate the technical question we wish to address, we note that the calibration of sensors deployed in ISF has historically proven problematic (Friedel et al., 2023; Rodbard, 2016). As an example, we discuss the situation with EAB sensors. We traditionally calibrate in vivo EAB sensors in vitro in the physiological medium in which they will be deployed. This includes the calibration of intravenous sensors in vitro in undiluted whole blood (Arroyo-Currás, Dauphin-Ducharme, et al., 2018; A. M. Downs et al., 2022; Idili et al., 2019, 2021) and in-brain sensors in vitro in undiluted cerebrospinal fluid (Gerson et al., 2023a), both held at body temperature. For sensors deployed in ISF, however, selecting the appropriate calibration medium is complicated by the difficulty of meaningfully collecting this bodily fluid. That is, ISF extraction methods, including suction blisters, microdialysis, and microneedle extraction, are limited to small volumes (~1-15 μL) and likely significantly alter the ISF composition (e.g., by rupturing cells or dilution with dialysate) in the collection process

(Friedel et al., 2023; Niedzwiecki et al., 2018; Ribet et al., 2020; Samant & Prausnitz, 2018; Vermeer et al., 1979). Given these limitations, some groups have entirely eschewed the calibration of subcutaneous EAB sensors (S. Lin et al., 2022) In contrast, in prior studies we have calibrated subcutaneous EAB sensors using 37˚C whole blood as the calibrant, an approach we justified by observing that, while they are filled with a molecular-weight-limiting "glycocalyx" matrix (Dull & Hahn, 2022; Foote et al., 2022) the junctions between the cells lining the walls of the finest capillaries are "leaky" enough that there is pressure-driven bulk flow between the plasma and ISF (Cserr & Patlak, 1992; Friedel et al., 2023), suggesting that the electrolyte and small-molecule composition of the two should be closely similar. Consistent with this argument, 90% of the metabolites found in the ISF are also found in blood (Friedel et al., 2023; P. R. Miller et al., 2018; Samant et al., 2020; Tran et al., 2018). Here we have coupled feedback control over plasma drug levels with simultaneous measurements performed in the ISF to quantitatively test the accuracy of using blood as a calibrant for the latter. We argue that, if the use of blood as a calibration matrix for sensors deployed in the ISF is accurate, the concentration measured in the ISF should eventually match and remain at the plasma concentration.

3.4 Methods

We diluted phosphate-buffered saline (PBS) from a 20x stock obtained from Santa Cruz Biotechnologies. Sodium hydroxide, 6-mercapto-1-hexanol, tris(2-carboxyethyl) phosphine, and used sulfuric acid (Sigma Aldrich) doxorubicin HCl (LC Laboratories) and dimethyl sulfoxide (Fisher Scientific) as obtained. We purchased methylene blue-and-HO-C 6 S-S-C 6-

modified DNA sequences (Arroyo-Currás, Somerson, et al., 2017; S. Lin et al., 2022) from Integrated DNA Technologies (IDT).

Doxorubicin aptamer sequence

5' – HS- (CH2)6 – ACCATCTGTGTAAGGGGTAAGGGGTGGT – (CH2)7 –NH– Methylene Blue – 3'

Electrode fabrication and functionalization

To fabricate the electrodes of intravenous sensors, we cut and insulated gold (0.2 µm diameter x 10 cm in length; 99.9% purity, A-M systems), platinum (0.125 µm diameter x 10 cm in length; 99.95% purity; A-M Systems), and silver (0.125 µm diameter x 10 cm in length; 99.99% purity, A-M Systems) wires with polytetrafluoroethylene heat-shrink (PTFE, Zeus Inc., HS Sub-Lite-Wall). We bundled the wires with physical gaps separating each wire to prevent shorting. We then trimmed the insulation to produce an exposed length of 3 mm (gold), 5 mm (platinum), and 1 cm (silver). To convert the silver wire to a reference electrode we submerged it in 7.5% sodium hypochlorite (commercial bleach, Clorox) overnight to form a stable silver chloride film. Finally, we rinsed the electrodes in DI water to remove any residual bleach.

To fabricate the electrodes of subcutaneous sensors, we insulated gold (0.2 µm diameter x 10 cm in length), and silver wire (0.2 µm diameter, 10 cm in length, 99.99% purity, A-M Systems) with polytetrafluoroethylene heat-shrink (PTFE, HS Sub-Lite-Wall). We trimmed the insulation and electrodes to produce an exposed length of 5 mm (gold), and 1 cm (silver). To convert the silver wire to a reference electrode we submerged it in 7.5% sodium hypochlorite

(commercial bleach, Clorox) overnight to form a stable silver chloride film, followed by a DI water wash. We then fabricated a separate counter electrode by heat-shrinking PTFE platinum wire (0.25 μm diameter x 10 cm in length). We then fed the counter through a 20-gauge catheter.

We functionalized intravenous and subcutaneous sensors as follows. First, we reduced the disulfide bond in the methylene-blue modified DNA with 14 μL of 10 mM tris (2-carboxyethyl) phosphine with 2 μL of 100 mM DNA for 1 h in the dark. After electrode assembly and overnight bleaching we rinsed the sensors in di-ionized water and cleaned the gold surface via: (a) cycling the potential 1,000 times between -1.0 and -1.6 V versus Ag|AgCl in a solution of 0.5 M NaOH (1 Vs^{-1}) to remove residual organic or thiol contaminants on the surface; (b) pulsing between 0 and 2 V by applying 32,000 pulses with a pulse length of 20 ms in 0.5 M H_2SO_4 to increase the microscopic surface area of the gold (Arroyo-Currás, Scida, et al., 2017). Following this, we rinsed the gold electrodes in de-ionized water, fed them through 20 (intravenous) and 22 (subcutaneous)-gauge catheters, and immersed them in the reduced DNA solution (500 nM in pH = 7.4 PBS) for 1 h. The gold electrodes were then transferred to a 10 mM solution of 6-mercapto-1-hexanol in PBS overnight at room temperature to complete the formation of their self-assembled monolayers. Finally, we fed the intravenous and subcutaneous sensors and the external counter of the latter through the lumen of 22 and 20-gauge catheters, respectively (Becton, Dickinson & Company). Before in vivo insertion, we fill these catheters with 1x PBS.

We performed our in vivo experiments using adult male Sprague-Dawley rats (4-5 months old, 400-650 g; Charles River Laboratories, Wilmington, MA, USA). These were pair-housed in a temperature and humidity-controlled vivarium on a 12-h light-dark cycle and

provided ad libitum access to food and water. All animal procedures were consistent with the guidelines of the NIH Guide for Care and Use of Laboratory Animals (8th edition, National Academy Press, 2011) and approved by the Institutional Animal Care and Use Committee (IACUC) of the University of California Santa Barbara.

We performed sensor placements as follows. Rats were induced under 4% isoflurane gas in a Plexiglas anesthesia chamber. Anesthesia was maintained with 2-3% isoflurane gas/oxygen administered via a nose cone for the experiment's duration. A pulse oximeter (Nonin Medical, Plymouth, MN) was used to measure heart rate and SpO2 during the experiment. The rat was shaved and the skin above the jugular vein was disinfected with 70% ethanol and betadine. A small incision was made to isolate both veins. A small incision in the jugular vein was made using spring-loaded microscissors. A silastic catheter (composed of a bent steel cannula and silastic tubing) was inserted into the left jugular vein for infusions. The EAB sensor was inserted into the right jugular vein for in-vein drug monitoring and stabilized with sterile 6-0 silk sutures (Fine Science Tools, Foster City, CA). Following this insertion, we infused 30 units of heparin through the indwelling infusion line. Insertion of the subcutaneous sensor and external counter electrode was performed using an 18 g catheter inserted just below the surface of the skin on the posterior ventral side of the rat between the two legs after shaving the area. We confirmed the guide catheter is not embedded in fat or muscle by touch (the latter offers significant resistance to insertion). To ensure that we sampled ISF and not blood, we confirmed that the catheter did not backfill with blood during initial insertion and checked to ensure the sensor was free of blood when it was removed after the experiment. Neither of these occurred during the collection of any of the data presented in this study.

Feedback control

To perform feedback control, we employed an adaptive controller we have recently described. After a 20-minute baseline was measured to establish sensor stability, we started the adaptive feedback control algorithm. This algorithm does not use any a priori knowledge of the pharmacokinetics of doxorubicin in the test subject or any other animal. Instead, it uses a simple, pre-defined, time-varying infusion rate until the drug level reaches 65% of the desired set point. Using the injection profile and the resulting plasma concentrations measured up to this point, the control algorithm then fits the individual animal's pharmacokinetics to a two-compartmental pharmacokinetic model. Afterward, the controller continues to update this pharmacokinetic model using the most recent 100 concentration measurements. This allows it to adapt to any changes in the animal's physiology during the experiment. Using this model, the controller then controls the infusion rate to achieve and maintain the set point concentration. The controller also includes a safety feature that halts drug infusion if the drug concentration exceeds 120% of the set point concentration and turns back on it once the concentration falls back below 110% of the set point.

3.4 Results

Given that feedback-controlled drug delivery will presumably be of the greatest value for drugs for which the pharmacokinetic variability between patients is clinically significant (Knezevic & Clarke, 2020; Paci et al., 2014) we have used the chemotherapeutic doxorubicin, a drug whose high inter- and even intra-subject variability is known to impact clinical outcomes significantly (Gil et al., 1983). To measure the plasma doxorubicin concentrations

we placed a 200 μm diameter by 3 mm long EAB sensor into the right external jugular vein (Leung et al., 2023) of anesthetized rats (subject characteristics detailed in Table S1) and a catheter into the left jugular vein for drug delivery. To perform similar measurements in the ISF, we inserted 200 μm diameter by 5 mm long EAB sensors into the subcutaneous space by first inserting 18-gauge shielded catheters below the surface of the skin on the animal's posterior ventral side at a 45° angle. We then removed the needles, leaving the catheters in place to guide the sensors into the subcutaneous tissue (Fig. 2). To interrogate both intravenous and subcutaneous sensors we used square wave voltammetry to perform dual-frequency, kinetic differential measurements (KDM) (A. M. Downs et al., 2022; Ferguson et al., 2013). Using this approach, our sensors achieve a time resolution of 16 s and baseline (pre-drug-challenge), root-mean-squared noise floors of 0.4 μM in the vein, and 0.2 μM in the subcutaneous space. The greater noise in the former compartment arises due to the animal's pulse; this noise falls dramatically upon sacrificing the animal (data not shown). To maintain constant drug concentrations in the plasma we employed an adaptive feedback control algorithm that actively "learns" the pharmacokinetics of each animal. Relative to our earlier, proportional-integral-derivative controllers (Dauphin-Ducharme et al., 2019b; Gerson et al., 2023a) this approach improves the speed with which the set point concentration is reached and the accuracy with which this is maintained.

Feedback control over plasma drug levels leads to rapid equilibration at the same concentration in the interstitial fluid of the subcutaneous space. To see this, in our first experiment we placed an intravenous sensor in the right external jugulars of 3 rats and a second sensor in the subcutaneous space of the right posterior ventral side. After establishing a stable baseline for the plasma sensor (typically after 20 to 30 min, Table 1), we initiated controller-

informed drug infusion (Fig. 3, top row). Under such control, the plasma doxorubicin concentration rose to within 15% of the 2 μM set point in 2 to 11 mins (average of 6.8 min; Table 1), after which the controller maintained the plasma concentration at that set point to an RMS deviation of ±30% (Fig. 4). Of note, the rate of infusion required to maintain the set point concentration, which is evident in infusion rate profiles (Fig. 3, middle row), varied dramatically not only between animals but also within individual animals over time. Specifically, the infusion rate required to maintain plasma drug concentrations at the set point concentration eventually dropped to zero in all 3 animals. This is not due to poor sensor reversibility; the sensor rapidly returns to baseline after being challenged at 3.2 μM in vitro in 37˚C bovine blood for 60 min (Fig. S2). Instead, we believe this is due to doxorubicin-induced kidney failure reducing the elimination rate to zero (Afsar et al., 2020, Burke, 1977) Consistent with this argument, all 3 rats stop urinating during the experiment despite receiving significant intravenous fluid during drug delivery.

Controlling plasma drug concentrations equates to control over drug concentrations in the solid tissue. Specifically, after the ISF has equilibrated with the plasma, (defined here as being when the subcutaneous concentration reaches within 15% of the plasma set point concentration and remains within this window for at least 5 min), the mean measured plasma concentration, and the mean measured ISF concentration differ by between 0.10 and 0.29 μM for our first 3 animals (Fig. 3, bottom row, Table 2). In the face of sensor-to-sensor fabrication variation, which is known to be of similar magnitude for these crudely hand-built devices (A. M. Downs et al., 2022), this rather high degree of correlation validates both the argument that control over plasma drug concentrations leads to rapid and accurate control over drug

concentrations in the solid peripheral tissues and our use of blood as a calibrant for sensors deployed in the ISF.

The reproducibility of subcutaneous EAB sensors is quite good. To see this, we next performed feedback control over plasma levels in 2 rats while performing concentration measurements using a pair of subcutaneous sensors placed ~1 cm apart, roughly 0.5 cm to either side of the animal's midline. Once again, upon initiating feedback control over plasma doxorubicin, the drug's measured concentration at both subcutaneous sites rapidly rises to and maintains the set point concentration (Fig. 4). Despite the possibility of site-specific differences in the rate of transfer from the plasma to the ISF, the concentration measurements produced by the two subcutaneous track one another quite closely. Specifically, measurements following the initiation of feedback control are correlated between the two sensors with R^2 of 0.95 and 0.98 (Fig. 5). That said, the slopes of these correlations differ from the expected value of unity by 9% and 13%. These small, systematic errors presumably arise due to sensor-to-sensor variation in these hand-built devices. For example (and as noted above), we observe similar sensor-to-sensor variation in in vitro experiments (A. M. Downs et al., 2022).

3.5 Discussion

Here we have performed feedback control over plasma drug concentrations in live rats with simultaneous monitoring of the drug in a solid tissue. Doing so we find that, upon holding plasma doxorubicin concentrations steady at a fixed concentration for a few tens of minutes, the measured concentration in the interstitial fluid of the subcutaneous space matches that seen

in plasma to within ~15%, which is well within expected sensor-to-sensor variability. And it achieves this match rapidly relative to the timescale of most drug action.

From the technical perspective, the close correspondence of paired plasma and ISF drug concentration measurements following equilibration of the two compartments strongly supports our prior claim that blood is a suitable proxy for the calibration of sensors placed in the subcutaneous space. Given the difficulty of collecting sufficient volumes of undiluted, unperturbed ISF, this observation should significantly improve the convenience of future efforts to calibrate sensors for such placements. Indeed, given that most solid tissues (the exceptions being the brain and gonads (Goldstein & Betz, 1986; Mruk & Cheng, 2015)) are in direct, fluid communication with the plasma (i.e., are not separated by a transport-limiting membrane, such as the blood-brain-barrier), we believe this approach will work for a wide range of solid-tissue EAB sensor placements.

From the clinical perspective, the relatively rapid rate with which drug concentrations in the subcutaneous ISF equilibrate with constant plasma drug concentrations speaks to the potential therapeutic value of performing feedback control over plasma drug levels. Specifically, our work validates the assumption that holding drug concentrations constant at clinically optimized levels equates to achieving similarly optimal concentrations in the solid tissues that are the site of action of most drugs. This should advance the therapeutic administration of drugs with high interpatient pharmacokinetic variability and narrow therapeutic windows, such as chemotherapeutics.

3.6 Figures and Tables

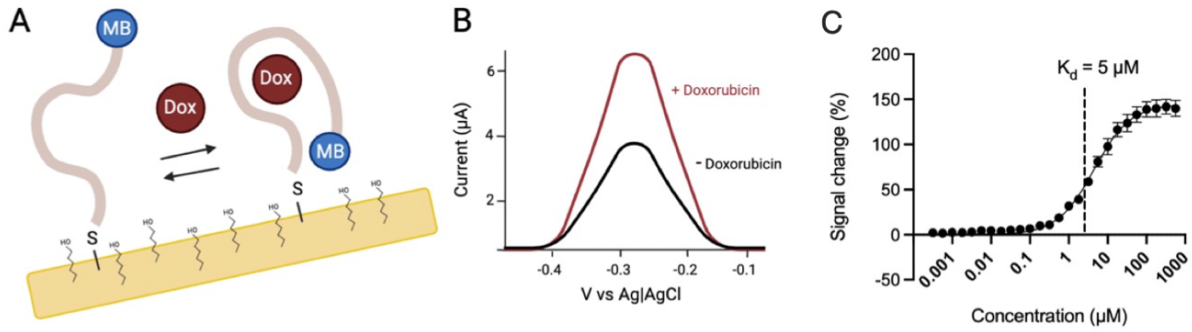

Fig. 3.1. (A) Electrochemical aptamer-based (EAB) sensors are composed of a methylene blue (MB)-modified aptamer that is site-specifically attached to the surface of a gold electrode. Target binding produces a conformational change in this aptamer, altering the rate of electron transfer. **(B)** The binding-induced change in electron transfer results in an easily detectable change in peak current when the sensor is interrogated using square wave voltammetry. **(C)** To perform measurements of doxorubicin in plasma and subcutaneous space, we utilize a doxorubicin aptamer with a K_d of 5 μM. Data was collected in vitro in whole rat blood at 37°C, with the error bars shown on this graph reflecting standard deviations across 8 independently fabricated devices to illustrate reproducibility.

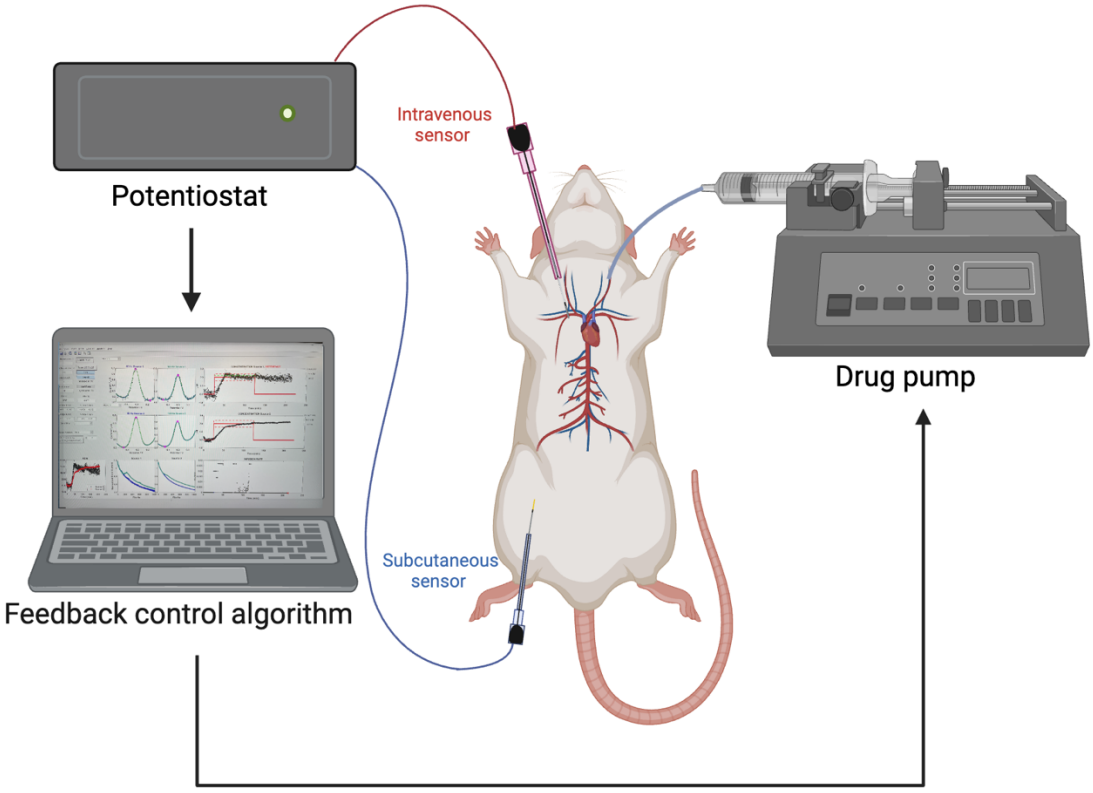

Figure 3.2. To perform feedback control over plasma drug concentrations, we insert an intravenous sensor in the right jugular vein and an indwelling catheter into the left jugular vein and then connect it to a potentiostat for electrochemical interrogation using square wave voltammetry. The real-time data this produces is used to inform an adaptive feedback control algorithm (Gerson et al., 2024) that adjusts the rate with which a drug pump delivers the drug to rapidly reach and accurately maintain the desired set point. Here we also employed 1 or 2 sensors in the ventral subcutaneous space to measure how rapidly these solid tissues equilibrate with the plasma drug concentration.

Table 1. Rise times in plasma and ISF		
Rat	**Rise time in the plasma* (min)**	**Rise time in the ISF** (min)**
Rat 1	6	25
Rat 2	11	29
Rat 3	10	59
Rat 4	5	SubQ1: 59 SubQ1: 37
Rat 5	2	SubQ1: 35 SubQ2: 34
Average	**6.8**	**39.7**

*Rise time (vein) is defined as the time elapsed between the initiation of control and when the plasma concentration reaches 15% of the set point concentration

**Rise time ISF is defined as the time elapsed between the initiation of control and when the subcutaneous concentration reaches 15% of the set point concentration

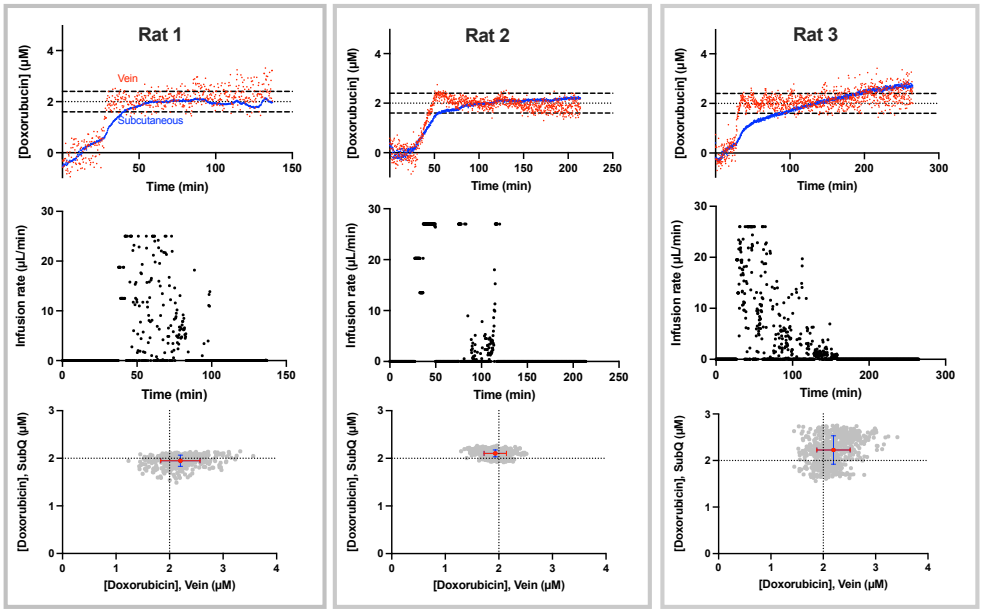

Figure 3.3. After the initiation of feedback control, drug levels in the subcutaneous ISF rapidly equilibrate with those in the plasma. (Top Row) Shown are data sets collected from three different animals (the three columns) illustrating the measured concentration in the plasma (red) and in the ISF (blue). In all three cases the drug concentration in the plasma and ISF rapidly rise to the set point. (Middle Row) Shown are the time-varying infusion rates required to reach and maintain the set-point plasma concentration. Note that the maximum infusion rate differs between rats depending on their body weight. (Bottom Row): After drug concentrations in the plasma and ISF have equilibrated (defined here as subcutaneous concentrations reaching and remaining within 15% of the set point for at least 5 min), the two concentrations remain closely similar. To illustrate this, here we present scatter plots illustrating the correlations between the pairs of measured concentrations after equilibration has been reached. The red points represent the average of vein and subcutaneous measurements obtained over this period, and the error bars reflect the standard deviations of each value. The generally larger standard deviations seen for plasma measurements are due to noise arising from the close placement of these sensors to the animal's heart.

Table 2. The correlation between measured plasma and ISF concentrations		
Rat identifier	**Average and standard deviation of plasma concentration after the 2 µM set point is first reached (µM)**	**Average and standard deviation of subcutaneous concentration after the 2 µM set point is first reached (µM)**
Rat 1	2.2 ± 0.4	2.0 ± 0.1
Rat 2	1.9 ± 0.2	2.10 ± 0.07
Rat 3	2.2 ± 0.3	2.2 ± 0.3
Rat 4	2.0 ± 0.4	SubQ1: 1.8 ± 0.1 SubQ2: 1.9 ± 0.1
Rat 5	2.0 ± 0.2	SubQ1: 1.80 ± 0.09 SubQ2: 1.90 ± 0.14

Average plasma and subcutaneous drug concentrations observed after the set point is reached **(**i.e., after the subcutaneous concentration reaches and remains for 5 min within 15% of the set point).

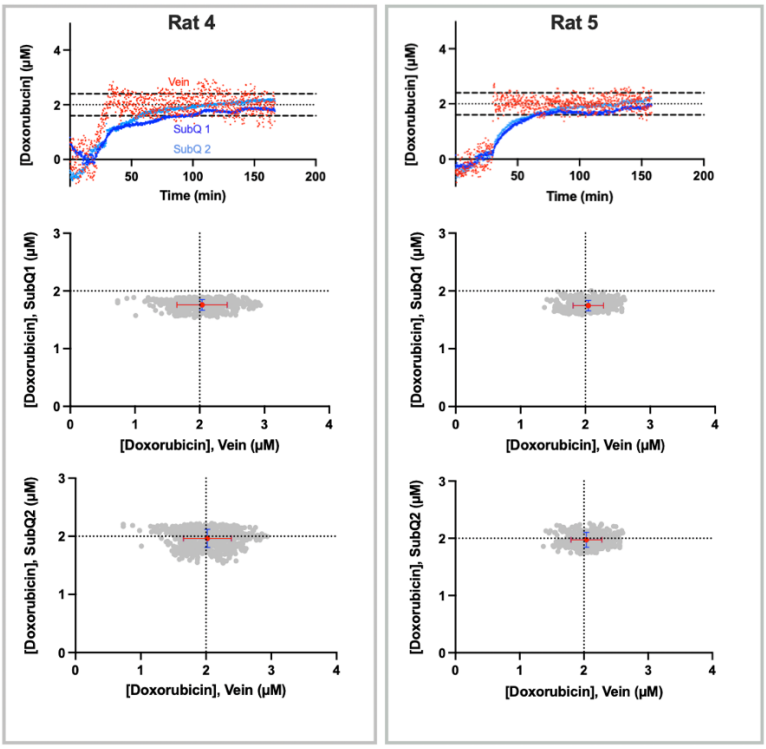

Figure 3.4. The reproducibility of subcutaneous sensors placed within individual animals (light and dark blue) is quite good. (Top row) To see this, here we deployed a pair of sensors in the ventral subcutaneous space located ~1 cm away from one another. (Bottom rows) Once again, after the subcutaneous space has equilibrated with the plasma (determined when the subcutaneous levels reach within 15% of the target concentration and maintain set point concentration for at least 5 min), the correspondence between the measured plasma and ISF drug concentrations is excellent for both sensors in the pair. Red points represent the average vein and subcutaneous concentration across the duration of the experiment following equilibration. Error bars represent the standard deviation of the vein concentrations (red) and subcutaneous concentrations (blue). The corresponding infusion rate data is presented in the SI (Fig. S2).

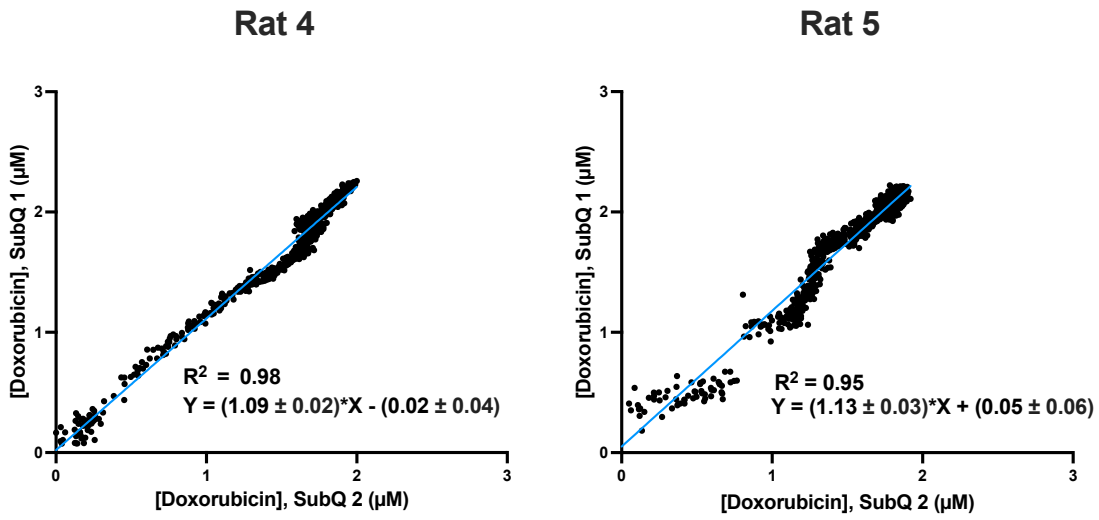

Figure 3.5. Measurements performed simultaneously at two sites in the subcutaneous space track one another with good precision**.** Shown are simple linear regressions of the concentration estimates produced by each of the paired subcutaneous sensors presented in Fig. 4; the correlations between the paired measurements are exceptional: $R^2 = 0.98$, $F(1, 762) = 33167$, $p < 0.0001$ and $R^2 = 0.95$, $F(1, 905) = 16{,}472$, $p < 0.0001$) for rats 4 and 5, respectively. This said, we observe mean, systematic deviations between the two sensors of 9 ± 2% (Rat 4) and 13 ± 3% (Rat 5). This presumably occurs due to sensor to sensor fabrication variation; similar levels of deviation have been reported during in the in vitro characterization of these hand-made devices (A. M. Downs et al., 2022).

3.8 Supplemental Information

Table S1. Rat identification and characteristics.			
Rat Identifier	**Weight (g)**	**Sex**	**Total drug volume administered (µL)**
Rat 1	569	M	461
Rat 2	635	M	756
Rat 3	598	M	688
Rat 4	469	M	1000
Rat 5	483	M	1000

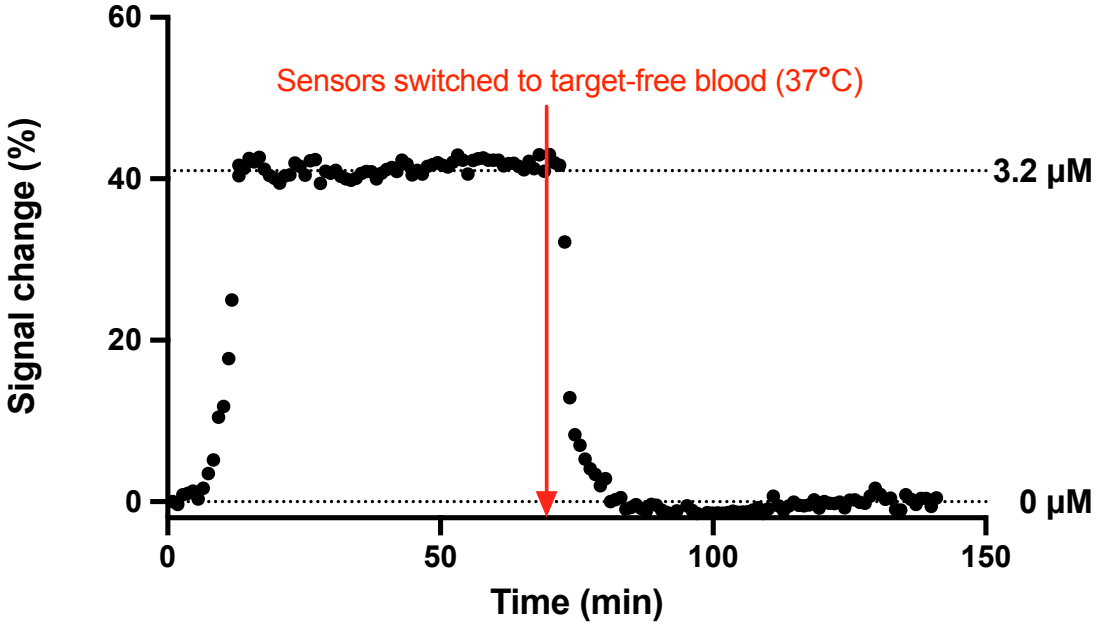

S3.1. The doxorubicin aptamer is rapidly reversible. Here we functionalized gold wire sensors (n=8) with the doxorubicin aptamer in bovine blood at 37°C. The doxorubicin aptamer rapidly responds to the target upon the addition of doxorubicin. We maintained drug levels at 3.2 µM (well above the concentrations used in our in vivo studies) for 60 min before moving the sensors to target-free, 37˚C bovine blood.

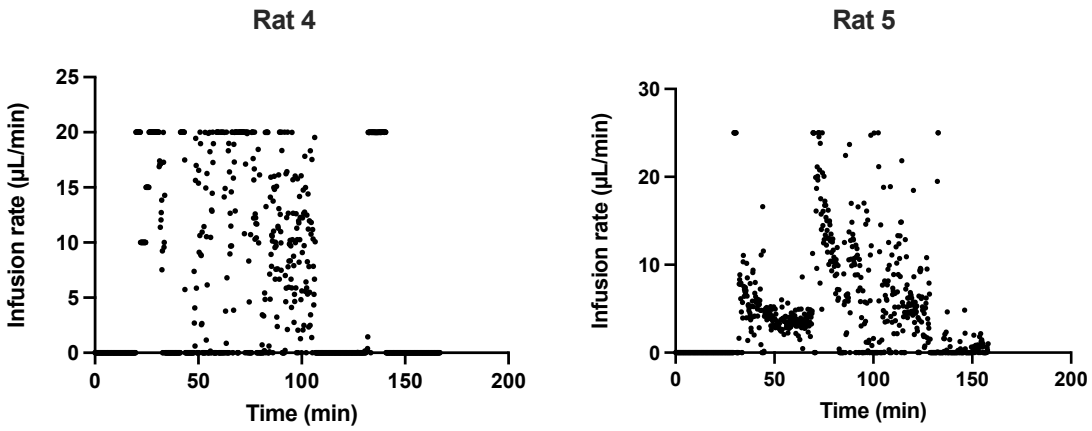

Figure S3.2. Shown are the injection time courses for Rats 4 and 5 (Fig. 4)

Chapter 4: EAB sensors for the seconds-resolved quantification of drug permeation across the blood-brain barrier

4.1 Abstract

A significant barrier to the treatment of in-brain cancers is the generally extremely low (to nil) penetration of chemotherapeutic agents across the blood-brain barrier—a tightly regulated, homeostatic blockade that excludes the passage of most molecules and many neurotherapeutics to the brain. The recent advent of drug formulations and pharmacological interventions aimed at increasing in-brain drug concentrations of therapeutics suggests a means of surmounting this problem. To explore the efficacy of two emerging methods (drug encapsulation and P-glycoprotein inhibition) aimed at enhancing DOX penetration to the brain, we utilize a novel sensing platform, electrochemical aptamer-based (EAB) sensors, to capture the rate of distribution of chemotherapeutic formulations across the blood-brain barrier. In contrast to unmodified doxorubicin, liposomal pegylated doxorubicin (2.5 mg/kg IV) produced detectable changes in doxorubicin concentration in the brain however this occurred inconsistently across subjects (i.e. significant concentration changes in only two of six animals). Ondansetron pretreatment and subsequent administration of doxorubicin produced no significant signal change in the brain. Potential sources of this irreproducibility include storage and transportation of liposomal pegylated doxorubicin, EAB sensor sensitivity, and inter-animal pharmacokinetic variability.

4.2 Introduction

The treatment of in-brain cancers is significantly limited by the failure of chemotherapeutics to permeate the blood-brain barrier (BBB). Doxorubicin, for example, effectively inhibits the proliferation of glioma cells in vitro and is highly toxic to

glioblastoma cell lines in vivo, yet when intravenously administered, its therapeutic efficacy is almost non-existent due to poor permeation across the BBB (Ahmed Juvale et al., 2022). In response, researchers have developed a host of new drug delivery methods aimed at enhancing the permeation of chemotherapeutics (with much of this work focused specifically on doxorubicin), across the BBB, to overcome this obstacle. However, existing methods for detecting in-brain concentrations of drugs lack the temporal resolution to understand how these manipulations dynamically alter the kinetics of drug distribution into the brain.

To improve drug permeation across the blood brain barrier, recent work has focused on have developed methods of increasing the concentration of chemotherapeutics in the brain with pharmacological manipulations, including inhibition of P-gp efflux pumps (Sardi et al., 2013), focused ultrasound (Lin et al., 2018; Park et al., 2012), and encapsulation in a pegylated liposome (Green & Rose, 2006). Here, we evaluate how drug formulation in a pegylated liposomal improves permeation across the BBB. Liposomal doxorubicin formulations have been authorized by the FDA for use in clinical populations specifically for the treatment of ovarian cancer, AIDS-related Kaposi's Sarcoma, and Multiple Myeloma (Barenholz, 2012). Clinical research suggests encapsulating doxorubicin in pegylated liposomes enhances its safety and efficacy, and preclinical research indicates that it may specifically improve the treatment of brain cancers (Birngruber et al., 2014; Gaillard et al., 2014; Ghaferi et al., 2022). This is accomplished by altering the pharmacokinetics of doxorubicin, improving delivery to the tumor while decreasing cardiovascular toxicity. Coating the liposome with polyethylene glycol (PEG), a synthetic hydrophilic polymer, increases circulation time and enhances permeation into the BBB (Birngruber et al., 2014, Xing et al., 2015). In preclinical research conducted by Gaillard et al. (2014), mice

administered [^{14}C]-labeled liposomal pegylated doxorubicin had significantly higher in-brain concentrations of doxorubicin compared to rats administered [^{14}C]-labeled doxorubicin. Researchers quantified brain levels of doxorubicin ex vivo using scintillation. Similarly, compared to free doxorubicin, Birngruber et al. (2014) determined doxorubicin encapsulated in glutathione pegylated liposomes administered intravenously increased in-brain concentrations in a rat brain tumor model. Brain levels of doxorubicin were quantified using cerebral open-flow microperfusion (cOFM). Both tissue homogenization and ex vivo quantification and cOFM are limited by their inability to capture the seconds-resolved temporal dynamics of drug distribution across the blood-brain barrier.

Another strategy employed to maximize brain concentrations of chemotherapeutics is pretreatment with P-glycoprotein (P-gp) inhibitors. Recent evidence suggests the mechanism of BBB-mediated resistance is complicated by the cooperation of P-gp, also aptly named multidrug resistance protein 1 (MDR1) (D. S. Miller et al., 2008). This glycoprotein codes for a plasma membrane protein that functions as a "gatekeeper" efflux pump, which efficiently removes molecules from the CNS, restricting their entry into the brain. Targeting and inhibiting P-gp has received extensive attention in enhancing the efficacy of pharmacotherapies (D. S. Miller et al., 2008). Ondansetron, or Zofran, is a competitive antagonist of the 5-HT_3 receptor and is also a substrate for P-gp (Chong et al., 2019). A study by Sardi et. al illustrated that ondansetron pretreatment led to higher doxorubicin concentrations in all analyzed brain regions following the quantification of brain tissue samples with mass spectrometry (Sardi et al., 2013).

A key challenge in assessing the effectiveness of novel strategies for enhancing drug penetration into the brain is the absence of technology that allows for seconds-resolved

tracking of drug distribution. In this regard, in-brain EAB sensors could serve as a valuable tool for evaluating the impact of various pharmacological interventions. Consisting of a 75 μm, 3-mm long gold wire electrode, EAB sensors can be implanted into the brain following stereotaxic surgery and can be used to analyze in-brain drug concentrations with high temporal resolution, a vast improvement to traditional sampling techniques such as microdialysis (Fig. 1) (Chefer et al., 2009). Utilizing EAB sensors, we have previously demonstrated that doxorubicin does not permeate the BBB in detectable amounts (Fig. 2A). We utilized this finding in prior research as a negative control to confirm that the intracranial surgeries performed for probe insertion do not produce functional changes in BBB integrity (Gerson et al., 2023a), it provides further confirmation that free doxorubicin does not permeate the BBB. Here, in contrast, we utilize EAB sensors to capture, with seconds-resolved resolution, the distribution of liposomal pegylated doxorubicin across the blood-brain barrier. We also evaluate how pretreatment with ondansetron, a P-gp inhibitor, may increase in-brain concentrations of doxorubicin.

4.3 Methods

The materials employed were obtained and processed as follows. We diluted phosphate-buffered saline (PBS) from a 20x stock obtained from Santa Cruz Biotechnologies. We obtained sodium hydroxide, 6-mercapto-1-hexanol, tris(2-carboxyethyl) phosphine, and sulfuric acid from Sigma Aldrich. We obtained doxorubicin HCl from LC laboratories and dimethyl sulfoxide from Fisher Scientific. We obtained liposomal pegylated

doxorubicin from Avanti Polar Lipids. We purchased methylene blue-and-HO-C 6 S-S-C 6-modified DNA sequences from Integrated DNA Technologies.

To functionalize in-brain EAB sensors, we reduced the disulfide bond in the methylene-blue modified DNA with 14 mL of 10 mM tris (2-carboxyethyl) phosphine with 2 mL of 100 mM DNA for 1 hour in the dark. We cleaned the sensors, involving: (a) cycling the potential 1,000 times between -1.0 and -2 V versus Ag|AgCl in a solution of 0.5 M NaOH (1 Vs-1) to remove residual organic or thiol contaminants on the surface; (b) pulsing between 0 and 2 V by applying 32,000 20 ms pulses with a pulse length of 0.02 s in 0.5 M H2SO4 to increase the surface area of the electrodes. We then roughened the electrode surface by cycling the potential between 1.5 and -0.35 V at 1 V/s four times in H2SO4. We then rinsed the gold electrodes in de-ionized water and immersed them in 500 nM reduced DNA dissolved in PBS for 1 h. The sensors were then transferred to a 10 mM solution of 6-mercapto-1-hexanol in PBS overnight at room temperature to complete the formation of their self-assembled monolayers.

Sensor interrogation was performed electrochemically using square wave voltammetry on a CH1040C multipotentiostat. To determine relevant calibration curve, we performed a 24-point titration of each aptamer deposited onto the electrodes described above in 37° bovine cerebrospinal fluid and determined the “signal-on” (200 Hz) and “signal-off” (40 Hz) frequencies that resulted in the largest relative changes in current. Drift correct was performed with kinetic differential measurements (KDM), obtained by taking the difference in normalized peak currents collected at our signal-on and signal-off frequencies:

$$\mathrm{KDM} = \frac{(\mathrm{Signal_{on}} - \mathrm{Signal_{off}})}{\frac{1}{2}(\mathrm{Signal_{on}} + \mathrm{Signal_{off}})} \quad \text{Eq 1.}$$

To fit resulting KDM signals to drug concentrations, we fit in vitro titration data to the equation:

$$\mathrm{KDM} = \mathrm{KDM_{min}} + \frac{(\mathrm{KDM_{max}} - \mathrm{KDM_{min}}) * [\mathrm{Target}]^{\mathrm{n_H}}}{[\mathrm{Target}]^{\mathrm{n_H}} + \mathrm{K_d}^{\mathrm{n_H}}} \quad \text{Eq 2.}$$

where KDM_{max} is the maximum signal gain observed at saturating concentrations, [Target] is the drug concentration, n_H is the Hill Coefficient, and K_D is the binding half-point of the aptamer (A. M. Downs et al., 2022).

We performed our in vivo experiments using adult male Sprague-Dawley rats (4-5 months old, 300-700 g; Charles River Laboratories, Wilmington, MA, USA). These were pair-housed in a temperature and humidity-controlled vivarium on a 12-h light-dark cycle and provided ad libitum access to food and water. All animal procedures were consistent with the guidelines of the NIH Guide for Care and Use of Laboratory Animals (8th edition, National Academy Press, 2011) and approved by the Institutional Animal Care and Use Committee (IACUC) of the University of California Santa Barbara.

Rats were induced under 4% isoflurane gas in a Plexiglas anesthesia chamber. Anesthesia was maintained with 2-3% isoflurane gas/oxygen administered via a nose cone for the experiment's duration. We performed intracranial surgery on rats with a chronic indwelling jugular catheter (Charles River) to surgically implant a permanent 19-gauge stainless steel cannula using stereotaxic coordinates aimed at the lateral ventricle

[anteroposterior (AP) = −0.48, mediolateral (ML) = +1.6, dorsoventral (DV) = −1]. Once the cannula is implanted, we inserted a removable 1.2-cm-long 22-gauge stainless-steel obturator. After the animal had healed for 7 days, we inserted the functionalized EAB sensors into the brain.

For drug dosing, a 0.01 M stock of doxorubicin HCl was prepared by diluting a 0.1 M solution dissolved in dimethyl sulfoxide (DMSO, Sigma Alridch) with phosphate-buffered saline. For injection of liposomal pegylated doxorubicin, concentration was quantified (per batch) with UV-VIS before injection. A 3 mL syringe containing this stock was connected to the catheter and then inserted into a motorized syringe pump (KDS 200, KD Scientific, Holliston, MA, USA). We performed all measurements using square wave voltammetry on a CH1040C multipotentiostat over a voltage window of approximately -0.1 to -0.45 V (relative to the Ag|AgCl reference). Before infusion of doxorubicin, we waited approximately 20 minutes to establish a stable baseline, ensuring any initial fouling of the electrode was corrected successfully with KDM. Once a stable baseline was determined, doxorubicin was injected over 3 min to better model clinical administration, given most injections of doxorubicin for the treatment of cancer in humans are administered over 10 to 30 min. Target concentration was quantified by fitting KDM values to a Hill Langmuir equation with parameters for KD, n_H, KDM_{max} obtained from in vitro calibrations performed in bovine cerebrospinal fluid at 37°C.

For animals in the ondansetron pretreatment group, we pretreated animals following existing protocols (Sardi et al., 2013): 2 mg/kg, intraperitoneally at 10 a.m (Day 0), 2 mg/kg, intraperitoneally at 5 p.m (Day 0), 2 mg/kg intraperitoneally at 10 a.m. (Day 1). Two hours later, we induced rats and administered doxorubicin (8 mg/kg) via an indwelling jugular

catheter. All figures were made in BioRender and all graphs were made using Graphpad Prism 9 Software (San Diego, CA).

4.4 Results

In the brain EAB sensor captures the distribution of liposomal pegylated doxorubicin with a temporal resolution of 20 s and a pre-drug-challenge, root-mean-squared (RMS) baseline noise of 0.005 μM (Fig. 3, top row). This is the first data of its kind to demonstrate, with seconds-resolved resolution, the distribution of this drug formulation across the blood-brain barrier. This, however, was only observed twice, with 4 other replications producing no measurable drug in the brain (Fig. 3, bottom rows). We discuss possible explanations for this lack of replicability below.

Rats pretreated with ondansetron did not show detectable increases in the in-brain level of free doxorubicin (Fig 4A). To verify that this dose is detectable with the aptamer used in the current study, we provide evidence that this same dose measured intravenously produced concentrations of 4.8 μM (Fig 4B).

4.5 Discussion

Here we demonstrated that EAB sensors can capture the distribution of PEG dox across the blood-brain barrier with a few-seconds resolution (Fig. 3, top row). This, however, was not replicable: 4 attempts of the experiment produced no change in signal gain upon the addition of target (Fig. 3, bottom row). Potential sources of this irreproducibility include storage and transportation of liposomal pegylated doxorubicin, EAB sensor sensitivity, and inter-animal pharmacokinetic variability. First, we obtained liposomal pegylated doxorubicin

from a distributor, which required shipping in dry ice. Because maintained temperature is a critical factor in determining liposome stability, minor deviations in temperature could have caused the liposomes to rupture (Pasarin et al., 2023). It is also possible that the aptamer itself was not sensitive enough to detect in-brain concentrations for all animals, as doxorubicin is a drug with incredibly variable inter-patient pharmacokinetics (Bronchud et al., 1990; Jacquet et al., 1990; Park et al., 2012). Thus, our sensor may have only been sensitive enough to detect changes in some animals, but unable to capture the lower in-brain concentrations in others. To improve the sensitivity of our aptamer, we could modify the parent doxorubicin aptamer. We have previously demonstrated our ability to make aptamers more or less sensitive based on modifications (truncations or additions of base pairs) to the termini of the sequence or by modifying the methylene blue reporter location (Idili et al., 2021; Mayer & Lai, 2018). Further work could improve the affinity of the doxorubicin parent aptamer to ensure it could capture lower in-brain concentrations of doxorubicin. Further work could utilize this modified aptamer to explore other methods by which we can increase the blood-brain permeation of chemotherapeutics. Additionally, some work has found an increase in the in-brain concentration of doxorubicin when administering liposomal doxorubicin following focused ultrasound (FUS) mediated blood-brain barrier disruption (Aryal et al., 2015). Future research could evaluate, with high-precision and seconds-resolved temporal resolution, how FUS-mediated BBB disruption improves in-brain drug permeation.

This work also evidenced that pretreatment with ondansetron, a P-gp inhibitor, did not lead to an increase of in-brain concentrations of free doxorubicin. The preliminary work that informed this study was conducted by Sardi et al. (2014), which demonstrated that

ondansetron pretreatment (identical to the pretreatment procedure utilized by this work) led to an accumulation of doxorubicin within the rat brain. To quantify in-brain levels, authors homogenized brain tissue and performed mass spectrometry. A possible explanation for our inability to replicate the study could lie in the limitations of the methods used to quantify brain levels of doxorubicin. Tissue homogenization followed by LC-MS may have led to an overestimation of brain doxorubicin levels if residual blood remained in the brain tissue samples despite perfusion. The presence of doxorubicin in the residual blood could have inadvertently contributed to higher readings, falsely elevating the measured concentrations in the brain tissue.

The successful treatment of in-brain cancers relies on the maintenance of therapeutically efficacious drug concentrations in the brain, which is a particular challenge when chemotherapeutics have a narrow therapeutic window and high inter-patient pharmacokinetic variability (Jacquet et al., 1990; Undevia et al., 2005). The ability to achieve optimal drug levels at the desired site of action for these targets would significantly advance our ability to treat brain cancers, enhancing treatment efficacy while minimizing side effects. And, as brain tumors are notably heterogeneous, advancing personalized precision medicine could ensure individual patients are administered optimal drug dosages based on the unique characteristics of their tumors (Lin et al., 2023).

4.6. Figures and Tables

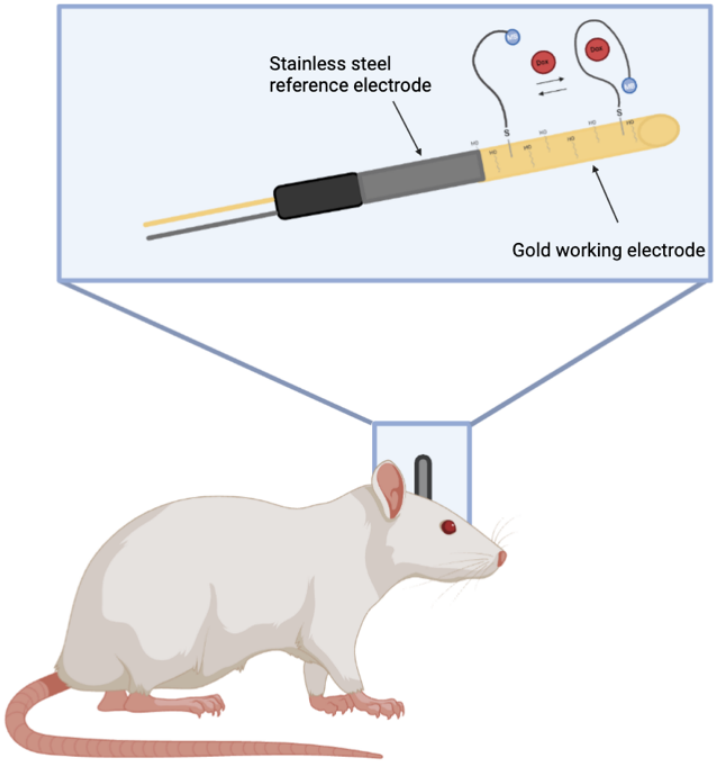

Figure 4.1. The in-brain EAB platform consists of a 75 µm-diameter, 3-mm-long gold electrode that extends from a 22-gauge stainless steel counter/pseudo-reference electrode. These probes are inserted into brain regions of interest following stereotaxic surgery.

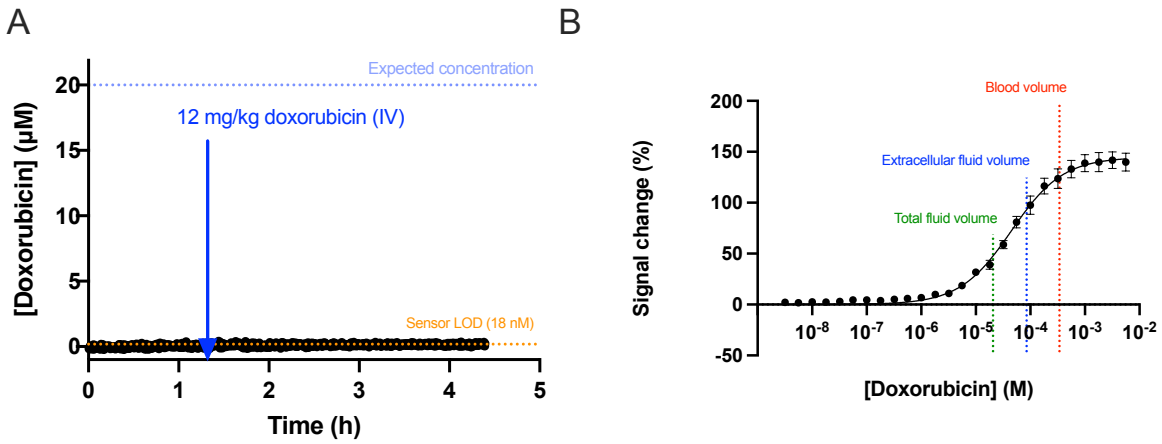

Figure 4.2. Doxorubicin does not permeate the BBB in detectable amounts. (A) Surgical manipulations performed for the placement of EAB sensors do not disrupt the BBB, evidenced by the lack of permeation of doxorubicin into the brain following a large dose of drug. Specifically, some 1.1 hours into this experiment, the drug was dosed intravenously (IV) at 12 mg/kg, a dose that would have saturated the sensor were the drug able to cross into the brain. (B) The doxorubicin aptamer is sensitive to the detection of small amounts of drug, as evidenced by the titration curve in 37°C CSF (K_d = 4.4). If doxorubicin was permeating the BBB, our sensor would be sensitive enough to detect increases in doxorubicin in the brain.

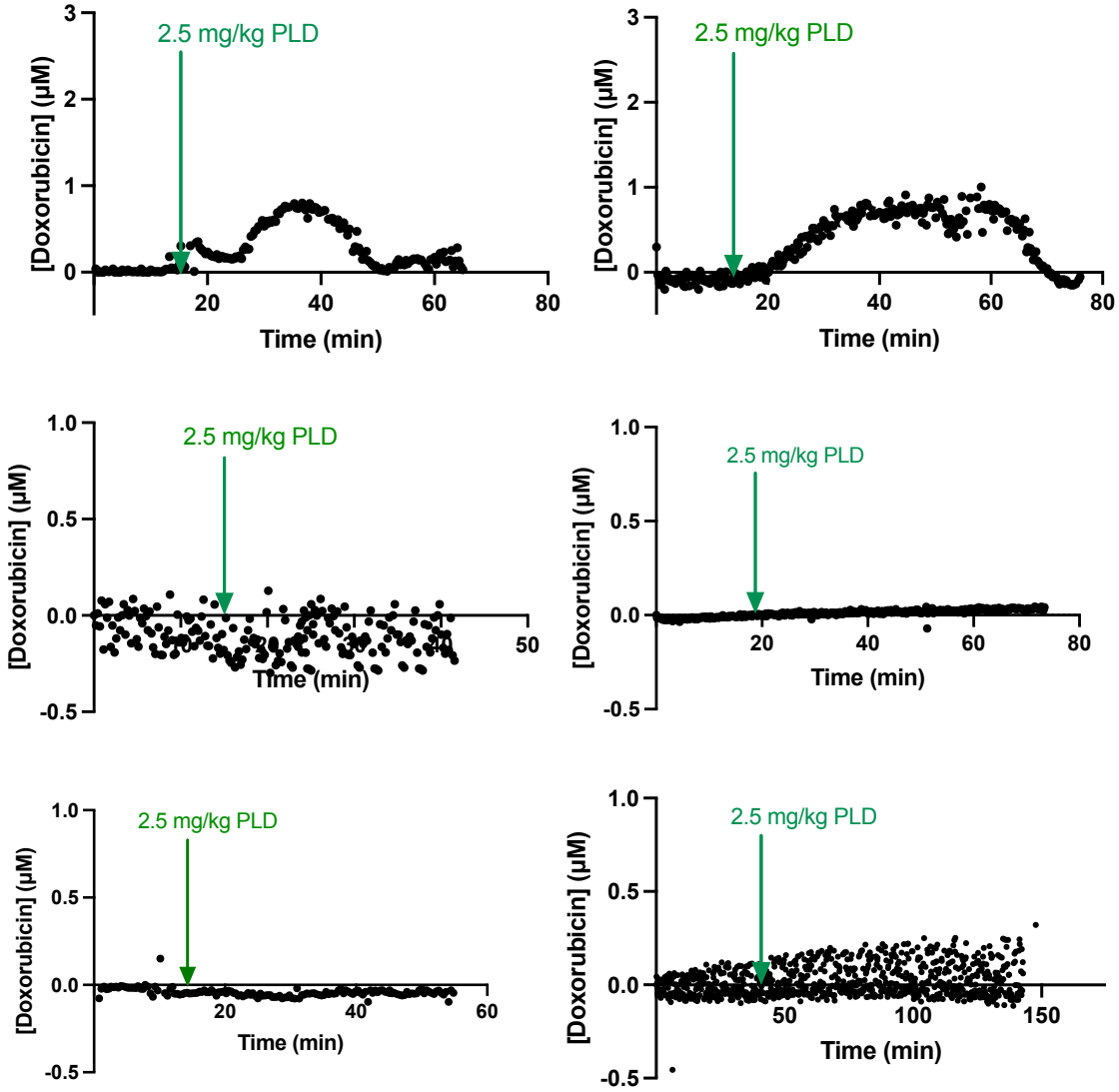

Figure 4.3. (Top row) Successful data sets obtained from the administration of pegylated liposomal doxorubicin. After establishing a baseline, we injected 2.5 mg/kg of pegylated liposomal doxorubicin (Avanti Polar Lipids) into the jugular vein. (Bottom rows) Unsuccessful data collected from the administration of pegylated liposomal doxorubicin. Upon injection of 2.5 mg/kg of commercially available liposomal pegylated doxorubicin, we observed no visible signal change associated with the injection

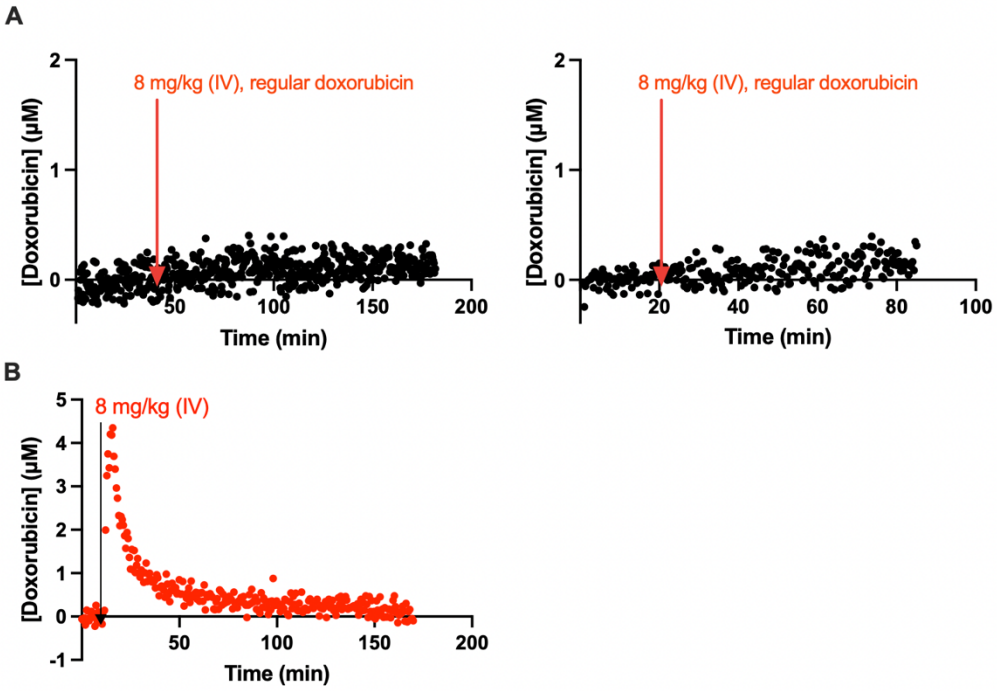

Figure 4.4. (A) Pretreatment with ondansetron does not produce enhanced permeation of doxorubicin across the blood-brain barrier. Shown are experiments in two different animals utilizing the ondansetron pretreatment protocol. (B) This same dose administered intravenously produced high in-vein and subcutaneous concentrations.

Chapter 5: Seconds-resolved, subject-specific plasma pharmacokinetics in male and female rats

5.1 Abstract

Generating real-time, individualized, high-precision pharmacokinetic curves is a critical step in better understanding individuals, including sex-specific, differences in the effects of cocaine that may underlie addiction vulnerability. Thus motivated, here we employ electrochemical aptamer-based (EAB) sensors to generate seconds-resolved measurements of plasma cocaine concentrations to elucidate inter-animal differences (including sex-specific) in cocaine pharmacokinetics. We do not find sex differences in maximum plasma cocaine levels (C_{max}), aligning with previous studies suggesting that sex-specific behavioral disparities in cocaine response may stem from differences in brain transport or pharmacodynamic processes rather than plasma pharmacokinetics alone. Despite the lack of sex differences in cocaine plasma pharmacokinetics, we do observe that females in estrus have significantly higher maximum plasma concentrations (C_{max}) of cocaine compared to females in any other estrus phase. Despite this, we find no significant correlation between estradiol levels, as measured by ELISA, with any pharmacokinetic parameters, including C_{max}, area under the curve (AUC), or half-life. These findings suggest that previously observed heightened behavioral responses to cocaine exhibited by females during estrus may be partially driven by estrus-dependent fluctuations in plasma pharmacokinetics, rather than by the direct effects of estradiol.

5.2 Introduction

Sex is a major predictor of cocaine abuse. For example, although men use and are more likely to become addicted to cocaine than women, women exhibit a faster escalation from initial use to dependence (Brady & Randall, 1999; Lex, 1991; Westermeyer & Boedicker,

2000). Consistent with this, preclinical research has evidenced significant sex differences in the behavioral responses elicited by cocaine in rats, with females acquiring self-administration more rapidly than males (dos Anjos Rosário et al., 2022; Hill & Powell, 1976; Lynch & Carroll, 1999) and exhibiting greater locomotor response to the same body-mass-adjusted dose (Chin et al., 2001; Festa et al., 2004; van Haaren & Meyer, 1991). These sex differences appear to be largely attributable to the effects of gonadal hormones and may be specifically related to their fluctuation across the female reproductive cycle. For example, compared to females in other estrous stages, females in estrus exhibit a larger psychomotor stimulant response to cocaine (Martz et al., 2023; Quiñones-Jenab et al., 1999), will work harder for the delivery of intravenous cocaine (Hecht et al., 1999; Lacy et al., 2016; D. C. Roberts et al., 1989), display a greater preference for larger doses (Lynch et al., 2000), and exhibit fewer hesitations and retreats in obtaining such doses (Kerstetter et al., 2013). Females in estrus likewise exhibit higher relapse-like behavior, as indicated by higher cocaine-seeking behavior under cocaine-primed reinstatement (Feltenstein et al., 2011; Kerstetter et al., 2008; Kippin et al., 2005). Conversely, ovariectomized rats acquire cocaine self-administration more slowly than intact females, a difference that is eliminated upon estradiol administration (Hu et al., 2004; Larson et al., 2005).

A possible mechanism by which these gonadal hormones affect cocaine behavioral responses is via their modulation of cocaine pharmacokinetics, such as the maximum drug concentration, the drug's half-life, or total drug exposure (Festa et al., 2004; Roth et al., 2004). Quantifying differences in these pharmacokinetic parameters, however, has historically proven difficult due to the cumbersome methods required to measure them with precision. That is, prior work quantifying plasma cocaine relied on the drug's ex vivo quantification from blood

draws using LC-MS and HPLC, generating either only single-time-point measurements (i.e., a single concentration measured at a set time after administration) or sparse pharmacokinetic curves obtained from samples drawn every ~10 min (Festa et al., 2004; Niyomchai et al., 2006; Visalli et al., 2005). Such temporal resolution is rather poor relative to the 10-20 min half-life of plasma cocaine (Barbieri et al., 1992; Benuck et al., 1987; Kosten et al., 1997) after behaviorally relevant intravenous dosing, leading to relatively imprecise estimates of the relevant pharmacokinetic parameters. For example, given the lack of densely sampled data points between baseline and peak plasma concentrations, the determination of C_{max} from samples drawn at ~10 min intervals requires inference (Pan et al., 2007; Shannon et al., 2013). Adding to this ambiguity, existing research often combines pharmacokinetic data from multiple subjects to achieve statistically significant results and to better understand generalized pharmacokinetic processes at the expense of understanding individual differences. Against this background, here we report seconds-resolved cocaine concentration measurements collected in situ in the jugular veins of live rats (Arroyo-Currás, Dauphin-Ducharme, et al., 2018; Arroyo-Currás, Somerson, et al., 2017; Arroyo-Currás Netzahualcóyotl et al., 2017; Dauphin-Ducharme et al., 2019a; Gerson et al., 2024; Idili et al., 2019), which we use to characterize individualized and sex-based cocaine pharmacokinetic differences with unprecedented precision.

To resolve cocaine's plasma pharmacokinetics on the seconds timescale here we have used EAB sensors, a molecular monitoring technology supporting the seconds or even sub-second-resolved (Arroyo-Currás, Dauphin-Ducharme, et al., 2018) measurement of specific drugs, metabolites, and biomarkers in situ in the blood (Arroyo-Currás, Somerson, et al., 2017; Gerson et al., 2023b, 2024; Idili et al., 2019; S. Lin et al., 2022), cerebrospinal fluid (Gerson

et al., 2023b, 2024), or interstitial fluid (Ferguson et al., 2013; S. Lin et al., 2022) of live subjects. Composed of a target-recognizing aptamer modified with a redox reporter and attached to an interrogating electrode, EAB sensors generate an electrochemical signal monotonically related to target concentration (Fig. 1A, 1B). Here, we use a cocaine-detecting, intravenous EAB sensor to obtain high-temporal-resolution plasma cocaine measurements and use these to explore relationships between the drug's plasma pharmacokinetics and range of potential pharmacokinetic effectors.

5.3 Methods

The appropriately modified aptamer sequences were purchased from Integrated DNA Technologies. The other materials employed were obtained and processed as follows. We diluted phosphate-buffered saline (PBS) from a 20x stock obtained from Santa Cruz Biotechnologies. We obtained sodium hydroxide, 6-mercapto-1-hexanol, tris(2-carboxyethyl) phosphine, and sulfuric acid from Sigma Aldrich, and cocaine HCl from NIDA.

To fabricate intravenous sensors, we first cut and insulated gold (0.2 μm diameter x 10 cm in length; 99.9% purity, A-M systems), platinum (0.125 μm diameter x 10 cm in length; 99.95% purity; A-M Systems), and silver (0.125 μm diameter x 10 cm in length; 99.99% purity, A-M Systems) wires with polytetrafluoroethylene heat-shrink (PTFE, Zeus Inc., HS Sub-Lite-Wall). We bundled the wires with physical gaps separating each wire to prevent shorting. We then trimmed the insulation to produce an exposed length of 3 mm (gold), 5 mm (platinum), and 1 cm (silver). To convert the silver wire to a reference electrode we submerged it in 7.5% sodium hypochlorite (commercial bleach, Clorox) overnight to form a stable silver

chloride film. Finally, we rinsed the electrodes in di-ionized water to remove any residual bleach.

Following the above electrode preparations, we then fabricated intravenous and subcutaneous as follows. We reduced the disulfide bond in the methylene-blue modified DNA with 14 mL of 10 mM tris (2-carboxyethyl) phosphine with 2 mL of 100 mM DNA for 1 hour in the dark. After electrode assembly and overnight bleach treatment we rinsed the sensors in water and then cleaned the as follows: (a) cycling the potential 1,000 times between -1.0 and -2 V versus Ag|AgCl in a solution of 0.5 M NaOH (1 Vs^{-1}) to remove residual organic or thiol contaminants on the surface; (b) pulsing between 0 and 2 V by applying 32,000 20 ms pulses with a pulse length of 0.02 s in 0.5 M H_2SO_4 to increase the surface area of the electrodes. We then roughened the electrode surface by cycling the potential between 1.5 and -0.35 V at 1 V/s four times in H_2SO_4. We then rinsed the gold electrodes in de-ionized water, fed them through 20--gauge catheters, and immersed them in 500 nM reduced DNA dissolved in PBS for 1 h. The sensors were then transferred to a 10 mM solution of 6-mercapto-1-hexanol in PBS overnight at room temperature to complete the formation of their self-assembled monolayers. We fed the intravenous sensors through the lumen of a 20-gauge catheter (Becton, Dickinson & Company). Before use in vivo, we fill the catheters with 1x PBS.

Sensor interrogation was performed electrochemically using square wave voltammetry on a CH1040C multipotentiostat. To determine the relevant calibration curve, we performed a 24-point titration of the aptamer deposited onto the electrodes described above in 37° bovine blood and determined the “signal-on” (150 Hz) and “signal-off” (20 Hz) frequencies that resulted in the largest relative changes in current. Drift correct was performed with kinetic differential measurements (KDM), obtained by taking the difference in the normalized (to the

current seen in the absence of drug prior to the first drug challenge) peak currents seen at these two frequencies ($Signal_{on}$ and $Signal_{off}$):

$$\mathrm{KDM} = \frac{(\mathrm{Signal_{on}} - \mathrm{Signal_{off}})}{\frac{1}{2}(\mathrm{Signal_{on}} + \mathrm{Signal_{off}})} \quad \text{Eq 4.}$$

To fit resulting KDM signals to drug concentrations, we fit in vitro titration data to the equation:

$$[\mathrm{Target}] = \sqrt[n_H]{\frac{K_{1/2}^{n_H} * (\mathrm{KDM} - \mathrm{KDM_{min}})}{\mathrm{KDM_{max}} - \mathrm{KDM}}} \quad \text{Eq 5.}$$

where KDM_{max} is the maximum signal gain observed at saturating concentrations, [Target] is the drug concentration, n_H is the Hill Coefficient, and K_D is the binding half-point of the aptamer (A. M. Downs et al., 2022).

We performed our in vivo experiments using adult female (n = 8) and male (n = 5) Sprague-Dawley rats (2-5 months old, 300-550 g; Charles River Laboratories, Wilmington, MA, USA). These were pair-housed in a temperature and humidity-controlled vivarium on a 12-h light-dark cycle and provided *ad libitum* access to food and water. All animal procedures were consistent with the guidelines of the NIH *Guide for Care and Use of Laboratory Animals* (8th edition, National Academy Press, 2011) and approved by the Institutional Animal Care and Use Committee (IACUC) of the University of California Santa Barbara.

Prior to induction, we took vaginal swabs of female rats using a lightly saline-dampened cotton swab. Cells were transferred onto microscope slides. Rats were induced under 4% isoflurane gas in a Plexiglas anesthesia chamber. Anesthesia was maintained with 2-3% isoflurane gas/oxygen administered via a nose cone for the experiment's duration. A pulse oximeter (Nonin Medical, Plymouth, MN) was used to measure heart rate and SpO_2 during the

experiment. The rat was shaved and the skin above the jugular vein was disinfected with 70% ethanol and betadine. A small incision was made to isolate both veins. A small incision in the jugular vein was made using spring loaded microscissors. A silastic catheter (composed of a bent steel cannula and silastic tubing) was inserted into the left jugular vein for infusions. The EAB sensor was inserted into the right jugular vein for in-vein drug monitoring and stabilized with sterile 6-0 silk sutures (Fine Science Tools, Foster City, CA). Following this insertion, we infused 30 units of heparin through the indwelling infusion line. Prior to insertion of the EAB sensor, blood was drawn from the inserted catheter and let to sit at room temp for 15 mins before refrigeration. Samples were then centrifuged for 15 min at 1000xg. We collected the supernatant and froze samples for later processing using a rat estradiol ELISA (Novus Biologicals, Centennial, CO).

For drug dosing, a 0.003 M stock of cocaine HCl was prepared. A 3 mL syringe containing this stock was connected to the catheter and then inserted into a motorized syringe pump (KDS 200, KD Scientific, Holliston, MA, USA). We performed all measurements using square wave voltammetry on a CH1040C multipotentiostat over a voltage window of approximately -0.1 to -0.45 V (relative to the Ag|AgCl reference). Before infusing cocaine, we waited approximately 20 minutes to establish a stable baseline, ensuring any initial fouling of the electrode was corrected successfully with KDM. Once a stable baseline was determined (evaluated as within 5% of baseline noise), we injected 1 mg/kg cocaine HCl was injected over 3 min. Target concentration was quantified by fitting KDM values to a Hill Langmuir equation with parameters for K_D, n_H, KDM_{max} obtained from in vitro calibrations performed in bovine blood at 37°C. Pharmacokinetic curves were fit to each data set using Graphpad Prism 9 Software (San Diego, CA).

We stained vaginal cytology slides by first fixing slides in methanol for 1 min and then allowing to try. We stained slides with Giesma stain (Hi Media Laboratories, India), diluted 1 part to 19 parts 1/15 M PBS, pH 7.2 for 10 min (Khatoon et al., 2014) Two blind independent reviewers evaluated the slides and categorized them into estrus groups.

5.4 Results

For this work, we utilized a previously published cocaine-detecting EAB sensor (Fig. 1C) supporting measurements of plasma cocaine with excellent limits of detection and temporal resolution (Alkhamis et al., 2024). The sensor is comprised of a cocaine-binding aptamer deposited on a 200 μm diameter, 3 mm long gold working electrode bundled together with a 1 cm chloride-anodized silver wire reference electrode and a 0.5 cm platinum counter (Fig. 1D) (Leung et al., 2023). This is placed into the jugular vein and a catheter placed into the other jugular vein is used for the intravenous dosing of cocaine; here we employed 1 mg/kg over 3 min for all animals. Using dual-frequency, kinetic-differential-measurement-corrected square wave voltammetry (A. M. Downs et al., 2022; Ferguson et al., 2013) to interrogate this sensor, we achieve a time resolution of 15 s and a pre-drug-challenge, root-mean-squared (RMS) baseline noise of 80 nM in the rat jugular (Fig. 1E).

EAB sensors easily capture the rapid increase in plasma cocaine seen upon intravenous infusion of the drug followed by its subsequent elimination (Fig. 2). Across the 13 animals we investigated (5 males and 8 females), we observed peak cocaine concentrations, C_{max}, of 0.6 to 2.7 μM (mean ± standard deviation = 1.7 ± 0.6 μM), which are reached between 3.0 and 6.7 min after the end of infusion (mean ± standard deviation = 4.2 ± 1.0 min). The subsequent

elimination of the drug is well-described by a simple, one-compartment model (Fig. 2B). In contrast, the parameter estimates are unstable for two animals (Female 7 and Female 8) when we fit these data with a two-compartment model. Based on the single-compartmental model, the drug's plasma half-life ranges from 5.0 to 26.5 min (mean ± standard deviation = 12 ± 6 min). Finally, total drug exposure, defined as the area under the curve (AUC), varied from 19 to 107 μM·min (mean ± standard deviation = 57 ± 27 μM·min).

Despite employing the same body-mass-adjusted dose for all animals, the pharmacokinetics we observe vary rather widely, suggesting that subject-specific factors significantly influence cocaine's disposition in the body. To explore this, we next evaluated the relationships between the various pharmacokinetic parameters and the animal's weight (Fig. 3, top row) and age (Fig. 3, bottom row). Doing so we found a modest, yet statistically significant correlation between weight and AUC ($R^2 = 0.35$, $p = 0.03$; Table 1). In contrast, we find no significant correlation between weight and C_{max} ($R^2 = 0.07$, $p = 0.4$), half-life ($R^2 = 0.0007$, $p = 0.93$), or t_{cmax} ($R^2 = 0.02$, $p = 0.65$). We also identified a modest, yet statistically significant, correlation between age and half-life ($R^2 = 0.42$, $p = 0.01$), but no significant relationship between age and between age and t_{cmax} ($R^2 = -0.19$, $p = 0.13$), C_{max} ($R^2 = 0.26$, $p = 0.07$), or AUC ($R^2 = 0.01$, $p = 0.72$) (Figure 3, bottom row; Table 1).

The positive, statistically significant correlation between body weight and AUC suggests that heavier animals experienced higher cumulative drug exposure than lighter animals when given the same body-mass-adjusted dose. It also suggests that, for non-body-mass-adjusted doses, drug exposure is not inversely proportional to body mass, but instead falls off less rapidly, but because we only employed body-mass-adjusted dosing in this work we are unable to identify the correct functional relationship between the two. Finally, this

observation suggests that simple body-mass-adjusted dosing might not be sufficient to achieve consistent exposure across animals of different weights.

Despite the well-established sex-linked differences in cocaine-induced behaviors, we see no statistically significant differences in plasma cocaine pharmacokinetics between male and female rats (Fig. 2). Specifically, an unpaired t-test found no significant difference C_{max} ($t(11) = 1.58$, $p = 0.14$), AUC ($t(11) = 1.57$, $p = 0.4$), t_{cmax} ($t(11) = 1.94$, $p = 0.32$), or half-life ($t(11) = 0.36$, $p = 0.73$) between the sexes (Table 1). Because an F-test for equality of two variances revealed significant differences in variances for half-life (males: $M = 11.1$, $\sigma^2 = 0.8$; females: $M = 12.4$; $\sigma^2 = 60.8$) and t_{cmax} (males: $M = 3.8$, $\sigma^2 = 0.10$; females: $M = 4.45$, $\sigma^2 = 1.22$), we ran a secondary unpaired t-test with Welch's correction and found no significant differences between groups ($t(7.3) = 0.46$, $p = 0.67$; $t(8.8) = 1.28$, $p = 0.23$). Thus, it appears unlikely that behavioral sex differences in cocaine responses are not attributable to sex differences in cocaine pharmacokinetics. The difference in variances in both time to C_{max} and half-life suggests that these pharmacokinetic parameters may prove more variable to fluctuating hormone levels.

To consider the impact of estrous cycle on resulting pharmacokinetic parameters, we determined the estrus stage of the female animals using vaginal cytology. Since metestrus only persists for 5 to 6 h, animals deemed in either diestrus or metestrus were combined into the diestrus group (Ajayi & Akhigbe, 2020; Ji et al., 2008; Long, 1922). And given we were only able to obtain a single animal in the proestrus phase (likely due to the short, ~14 h duration of the phase (Ajayi & Akhigbe, 2020; Grasso et al., 1998; Long, 1922)) and we found no statistically significant differences in any pharmacokinetic parameters in diestrus or proestrus, we combined the proestrus animal into the diestrus group. Estradiol concentrations were higher

for females in estrus (mean ± standard deviation = 25 ± 3 pg/mL) and lower for females in all other phases (mean ± standard deviation = 17 ± 6 pg/mL), though this difference was not statistically significant ($t(6) = 2.56$, $p = 0.06$). Animals in estrus achieved significantly higher maximum plasma concentrations of cocaine ($M = 2.2$ μM) compared to animals in all other phases ($M = 1.14$ μM), ($t(6) = 3.76$, $p = 0.009$; Fig. 3A). In contrast, we found no statistically significant differences between any other pharmacokinetic parameters across the estrus phases, including half-life ($t(6) = 1.15$, $p = 0.30$; Fig. 5B), AUC ($t(6) = 1.38$, $p = 0.21$; Fig. 5C), or t_{cmax} ($t(6) = 0.39$, $p = 0.71$; Fig. 5D).

We next evaluated the influence of circulating estradiol concentrations on cocaine's plasma pharmacokinetics. To determine the former, we drew a single blood sample from the intravenous catheter before drug injection and measured it using a competitive ELISA for rat estradiol. We found the average estradiol concentration in females was 19.6 pg/mL, with a coefficient of variation (CV) for all samples being below 11%. This concentration is within the ranges suggested by prior literature, suggesting estradiol concentrations in female rats range from 5-140 pg/mL.(Isaksson et al., 2011; Ström et al., 2012) Estradiol concentrations were highest for females in estrus (mean/SD = 25 ± 3 pg/mL) and lowest for females in all other phases (mean/SD = 17 ± 6 pg/mL), however, this difference was not statistically significant ($t(6) = 2.56$, p = 0.06). We found no significant correlations between any pharmacokinetic parameters and estradiol concentration for females (Table 3, Figure 5E-H).

5.5 Discussion

Here, using datasets with an order of magnitude improved temporal resolution over prior studies, we find no sex differences in cocaine pharmacokinetics. This is a vast improvement to prior research, which has only been able to generate pharmacokinetic "curves" from aggregated data across multiple subjects with single time point blood draws (Festa et al., 2004) or blood samples drawn every ~10 min (Visalli et al., 2005). We demonstrate that EAB sensors can enable the generation of individualized, high-precision data sets with individualized pharmacokinetic curves with concentration measurements performed every 8 seconds.

The findings from this study reveal that interindividual variability in pharmacokinetic parameters was evident although all rats received the same body-mass-adjusted dose of cocaine. Specifically, our analysis showed that weight was not correlated with maximum concentration (C_{max}), half-life, or time to maximum concentration (t_{cmax}). However, a significant correlation was found between weight and the area under the curve (AUC), suggesting that while weight does not affect the peak levels or timing of cocaine in plasma, it does influence overall drug exposure. This indicates that AUC, a measure of total drug exposure over time, may be more sensitive to variations in body weight than other pharmacokinetic parameters, potentially due to differences in drug absorption, distribution, or clearance influenced by body size. The finding of a significant correlation between age and half-life suggests that age influences how long cocaine remains in the system, with older subjects likely experiencing a prolonged duration of drug presence. However, age does not appear to significantly affect other pharmacokinetic parameters, such as time to reach maximum concentration (t_{cmax}), maximum concentration (C_{max}), or total drug exposure

(AUC). This indicates that while age may impact the rate at which the drug is cleared, it does not substantially affect the peak levels or the overall exposure to the drug. These results highlight the importance of considering age-related factors when assessing drug clearance rates, as age may play a role in determining the duration of drug effects without altering peak exposure levels. Moreover, this indicates that the ubiquitously employed strategy of body mass-adjusted dosing fails to equate drug exposure even in a relatively homogenous set of rats (i.e., all young adults).

We find no overall sex differences in any measures of cocaine pharmacokinetics (including plasma cocaine levels (C_{max}), AUC, t_{cmax}, and half-life), which is generally consistent with prior studies based on blood sampling and ex vivo measurement (Festa et al., 2004; Niyomchai et al., 2006; Visalli et al., 2005). Collectively, this work suggests sex differences in the behavioral response to cocaine administration are not attributable to substantial differences in plasma cocaine pharmacokinetics and are more likely attributable to in-brain pharmacokinetic or other pharmacodynamic processes. However, we did observe that females in estrus had significantly higher maximum plasma concentrations than females in other stages. This is consistent with prior literature, which suggests females in estrus demonstrate increased behavioral responses to cocaine (Kerstetter et al., 2013; Kerstetter & Kippin, 2011; Quiñones-Jenab et al., 1999). The exact cause of increased plasma concentration during estrus is unclear. Altered cocaine metabolism is unlikely to explain the higher C_{max}, as we observed no estrous cycle impact on half-life. Conversely, the administration of at least one reproductive hormone (LH) has been shown to regulate the protein binding of cocaine in plasma, but it is unclear if a similar effect is observed during the estrous cycle (Mendelson et al., 1999). Another possible explanation for higher maximum

plasma concentrations observed in females in estrus following IV administration is that changes in body composition, for instance, reduced body fat during estrus, could alter cocaine distribution (Dakic et al., 2024; Wade & Gray, 1979), resulting in higher plasma concentrations of cocaine in estrus females.

In contrast to the estrus effect, we found no relationship between estradiol levels and any resulting pharmacokinetic parameters levels, including C_{max}, AUC, t_{cmax}, and half-life. Our finding that C_{max} is higher during estrus, but does not correlate with estradiol concentration, indicates that the effects of the estrus cycle on pharmacokinetics are not a simple reflection of circulating estradiol levels at any given moment. Estradiol, a potent steroid hormone, exerts its physiological effects through both rapid, non-genomic mechanisms and slower, genomic actions (Mendelsohn, 2002; Vasudevan & Pfaff, 2008) with the latter involving gene expression and protein synthesis (Bossé et al., 1997; Iqbal et al., 2020; Kovács et al., 2020) which have a delayed impact on physiological responses; for example, the ability of estradiol to promote reproductive behavior occurs over days in both rats and humans (Blaustein, 2008; Powers, 1970; Roney & Simmons, 2013; Whalen, 1974). Such delayed genomic changes could impact pharmacokinetic processes and explain why estrus status, but not estradiol concentration, at a single time point is more strongly associated with the observed pharmacokinetic outcome. Further, estrus is not only characterized by changes in estradiol concentrations but is also associated with fluctuations in other hormones, including progesterone and luteinizing hormone (Ajayi & Akhigbe, 2020; Brown-Grant et al., 1970). The demonstrated relationship between estrus stage and C_{max} could reflect cumulative, non-linear effects of hormonal fluctuations over time. To better

understand this relationship, it would be valuable to consider continuous or multiple measurements of estradiol and other hormones across the estrous cycle.

Future work should likely evaluate potential sex differences in brain cocaine pharmacokinetics, given that the brain is the primary site of action. Fortunately, EAB sensors remain well-positioned to answer that question, given they have been demonstrated to obtain real-time measurements of drugs in both brain tissue and ventricular spaces (Gerson et al., 2023b, 2024; Shaver et al., 2022). The individual variability observed within each sex further strengthens the argument for personalized pharmacokinetic approaches. For example, females in the current study achieved maximum plasma concentrations to the same dose of cocaine ranging from 0.63 μM to 2.46 μM. Reliance on methods that require data aggregation across multiple subjects risks obscuring critical individual differences that may underlie important behavioral phenomena. EAB sensors present a powerful tool to overcome the limitations of existing methods, obtaining high-density, patient-specific measurements that could be used to transform our understanding of variability in pharmacokinetics.

5.6 Figures and Tables

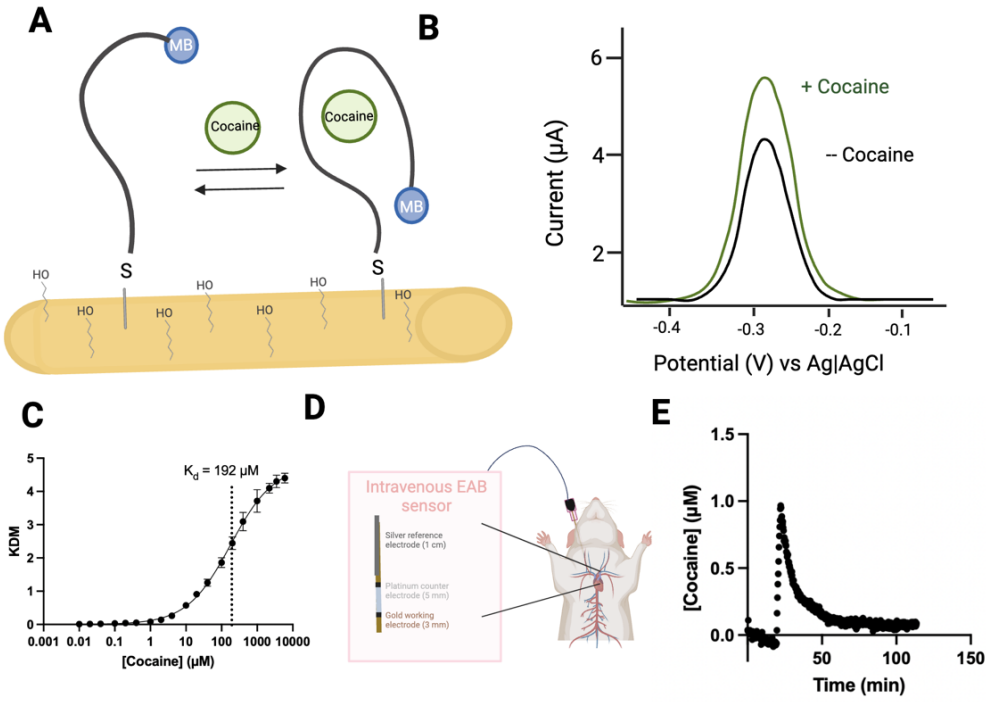

Figure 5.1. Electrochemical aptamer-based (EAB) sensors are composed of a methylene blue (MB)-modified aptamer that is site-specifically attached to the surface of a gold electrode. **(A)** Target binding produces a conformational change in this aptamer, altering the rate of electron transfer. (**B**) The binding-induced change in electron transfer results in an easily detectable change in peak current when the sensor is interrogated using square wave voltammetry**. (C)** To perform in-vein measurements of cocaine measurements, we utilize a previously published aptamer with a K_d of 192 μM. **(D)** We then insert an EAB sensor into the right jugular. To intravenously administer cocaine, we insert a silastic catheter into the left jugular vein. **(E)** EAB sensors enable the real-time, high-precision monitoring of cocaine pharmacokinetics in the blood

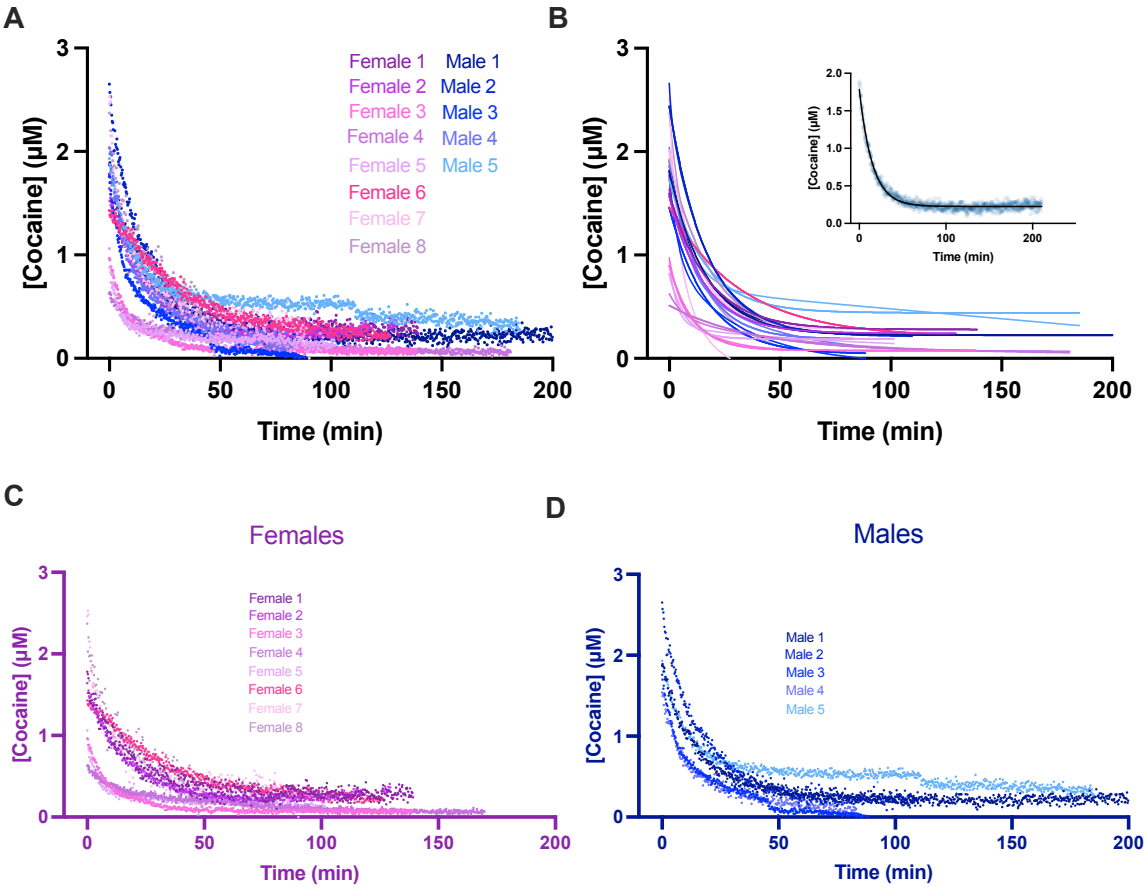

Figure 5.2. EAB sensors enable seconds resolved pharmacokinetics of cocaine in live rats. (A) Shown here is all data (n = 13) overlayed. (B) We fit data to single exponential models to extract pharmacokinetic parameters. Shown are the resulting curve fits including (inset) an example of the single exponential model fit overlayed on data obtained from Male 1. (C) Plasma pharmacokinetic curves of cocaine for (C) females and (D) males.

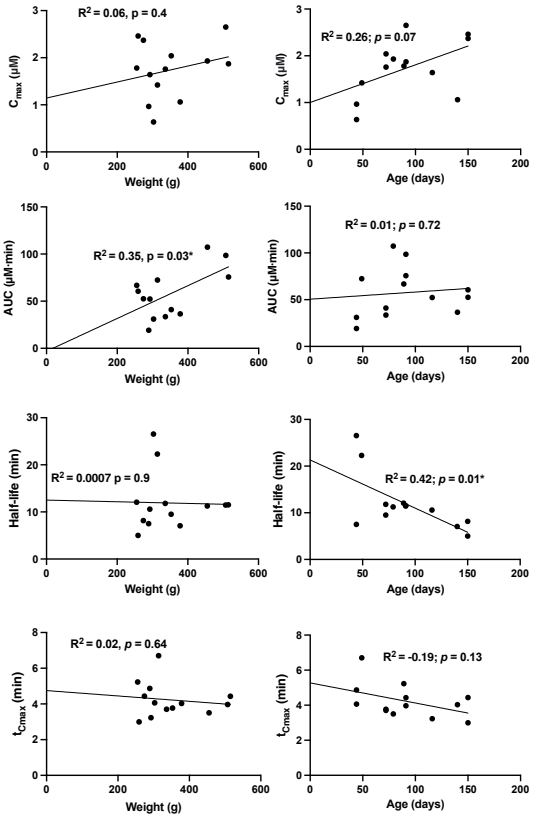

Figure 5.3. Despite uniformly dosing animals with body-mass-adjusted 1 mg/kg cocaine, we observed substantial interindividual variability in the resulting pharmacokinetic parameters, suggesting that subject-specific factors significantly influenced drug disposition. Here, we evaluate the correlation between pharmacokinetic parameters and (left row) weight and (right row) age. (Left) We found no correlation between weight and C_{max} ($R^2 = 0.07$, $p = 0.4$), half-life ($R^2 = 0.0007$, $p = 0.93$), or t_{cmax} ($R^2 = 0.02$, $p = 0.65$), but found a significant correlation between weight and area under the curve (AUC) ($R^2 = 0.35$, $p = 0.03$). (Right) We found a significant correlation between age and half-life ($R^2 = 0.42$, $p = 0.01$), but no significant relationship between age and t_{cmax} ($R^2 = -0.19$, $p = 0.13$), C_{max} ($R^2 = 0.26$, $p = 0.07$), or AUC ($R^2 = 0.01$, $p = 0.72$).

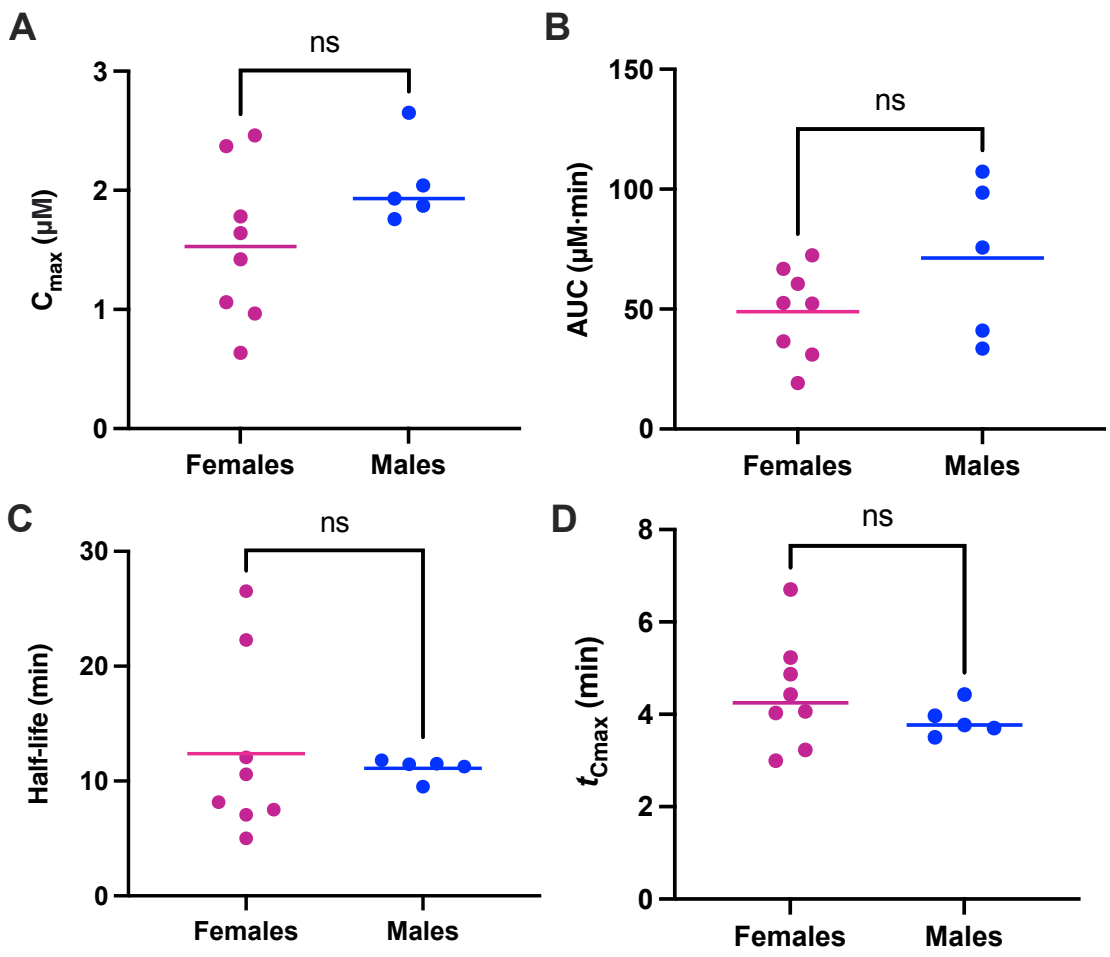

Figure 5.4. We find no sex-specific differences in plasma cocaine pharmacokinetics between males and females. After fitting data to single exponential models, an unpaired t-test found no significant difference between males in females in (A) maximum plasma concentration (Cmax), $t(11) = 1.58$, $p = 0.14$ (B) total cumulative exposure (AUC), $t(11) = 1.57$, $p = 0.14$; (C) half-life, $t(11) = 0.36$, $p = 0.73$, or (D) tc_{max}, $t(11) = 1.04$, $p = 0.32$.

Animal ID	Female 1	Female 2	Female 3	Female 4	Female 5	Female 6	Female 7	Female 8	Male 1	Male 2	Male 3	Male 4	Male 5
tcmax (min) (Average by sex)	4.44375								3.876				
tcmax (min)	5.23	3.23	4.87	4.06	4.03	6.7	3	4.43	4.43	3.97	3.7	3.78	3.5
Half-life (Average by sex) (min)	6.58								11.11				
Half-life (95% CI) (min)	12	10.6	7.5	26.5	4.8	22.3	5	8.17	11.5	11.5	11.8	9.5	11.3
AUC (Average by sex)(μM · min)	48.9								71.25				
AUC (μM · min)	66.86	52.28	19.15	31.03	36.59	72.48	60.62	52.56	75.71	98.61	33.6	31.02	107.3
C_{max} (Average by sex) (μM)	1.54								2.05				
C_{max} (μM)	1.78	1.64	0.966	0.635	1.06	1.42	2.46	2.37	1.89	2.65	1.75	1.54	1.93
[Estradiol] (pg/mL)	21.95	9.62	11.76	23.43	19.4	18.23	24.18	27.8	19	25.5	14.45	22.55	21.35

Table 1. Compiled pharmacokinetic parameters across all animals.

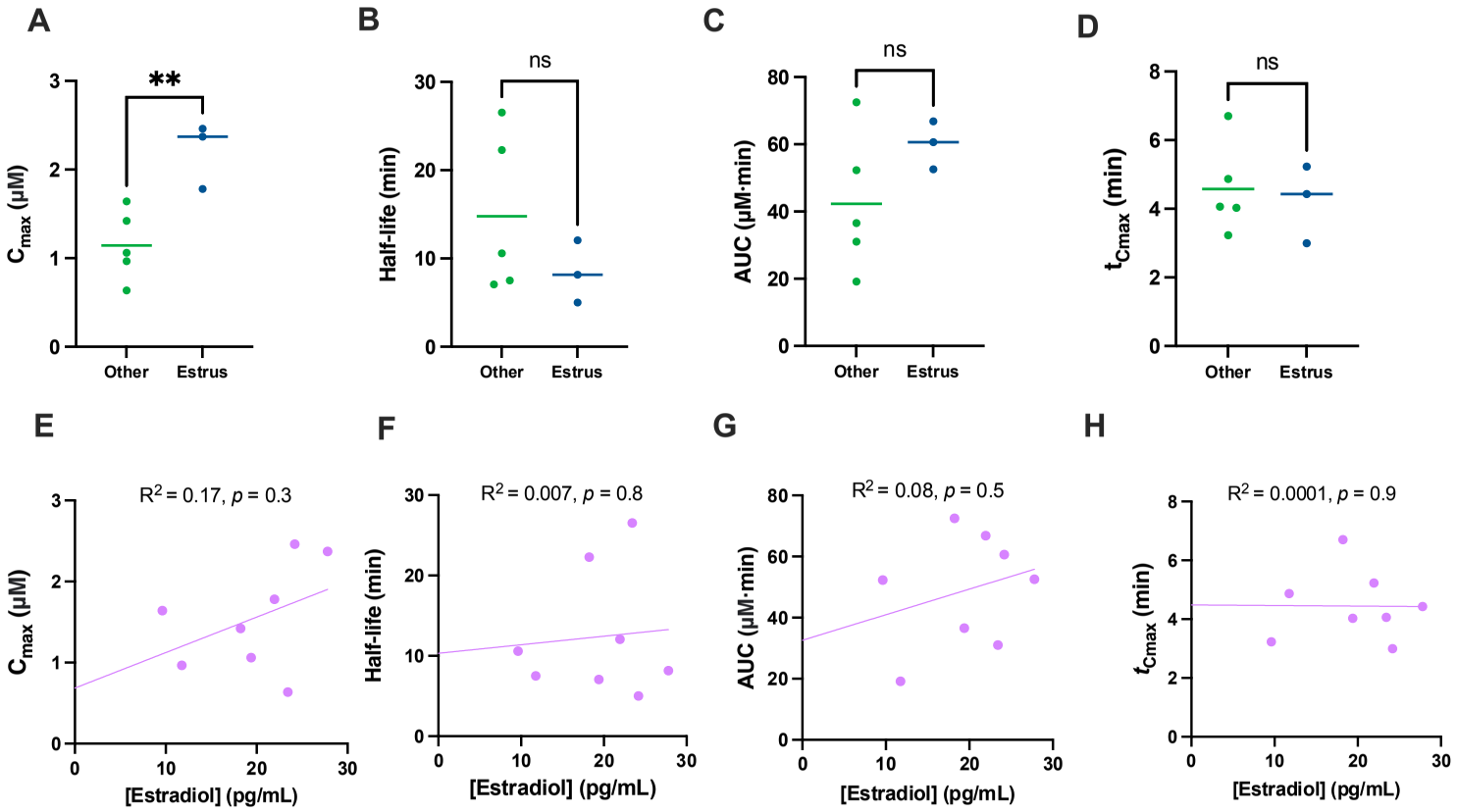
A
B
C
D
**
ns
ns
ns
C_{max} (μM)
Half-life (min)
AUC (μM·min)
t_{Cmax} (min)
Other
Estrus
E
F
G
H
R^2 = 0.17, p = 0.3
R^2 = 0.007, p = 0.8
R^2 = 0.08, p = 0.5
R^2 = 0.0001, p = 0.9
[Estradiol] (pg/mL)

Figure 5.5. (A) Animals in estrus achieved significantly higher maximum plasma cocaine concentrations than females in other estrus phases, $t(6) = 3.76$, $p = 0.009$. We found no significant differences between AUC, half-life, and t_{cmax} for females in estrus vs. non-estrus. (E-F) Estradiol concentration is not correlated with any pharmacokinetic parameters. The average estradiol concentration in females was 19.5 pg/mL. We found no correlation between estradiol concentration and AUC, $R^2 = 0.08$, $p = 0.49$. We found no correlation between estradiol concentration and C_{max}, $R^2 = 0.17$, $p = 0.30$. We found no correlation between estradiol concentration and half-life, $R^2 = 0.007$, $p = 0.84$.

		Weight (g)	Age (months)
AUC (µM · min)	Pearson correlation	0.59	0.23
	Sig. (2-tailed)	0.03*	0.44
	N	13	13
Cmax (µM)	Pearson correlation	0.25	0.36
	Sig. (2-tailed)	0.4	0.23
	N	13	13
Half-life (min)	Pearson correlation	-0.03	-0.56
	Sig. (2-tailed)	0.93	0.04*
	N	13	13
tcmax (min)	Pearson correlation	-0.14	-0.39
	Sig. (2-tailed)	0.65	0.18
	N	13	13

Table 2. Pearson correlation of pharmacokinetic parameters by weight and age.

		Estradiol level (pg/mL)
AUC (µM · min)	Pearson correlation	0.28
	Sig. (2-tailed)	0.5
	N	8
Cmax (µM)	Pearson correlation	0.09
	Sig. (2-tailed)	0.84
	N	8
Half-life (min)	Pearson correlation	0.08
	Sig. (2-tailed)	0.84
	N	8
tcmax (min)	Pearson correlation	-0.01
	Sig. (2-tailed)	0.98
	N	8

Table 3. Pearson correlation of pharmacokinetic parameters by estradiol levels.

Animal ID	Weight (g)	Average Weight (g) ± σ	Age (days)
Female 1	255.3	305 ± 41	89
Female 2	292.6		116
Female 3	289.1		44
Female 4	302.8		44
Female 5	378		140
Female 6	313.7		49
Male 1	514.7	433 ± 84	150
Male 2	507		150
Male 3	336.3		91
Male 4	352.8		91
Male 5	455.0		72

Table 4. Descriptive sample characteristics of all animals in the study.

5.7 Supplemental Information

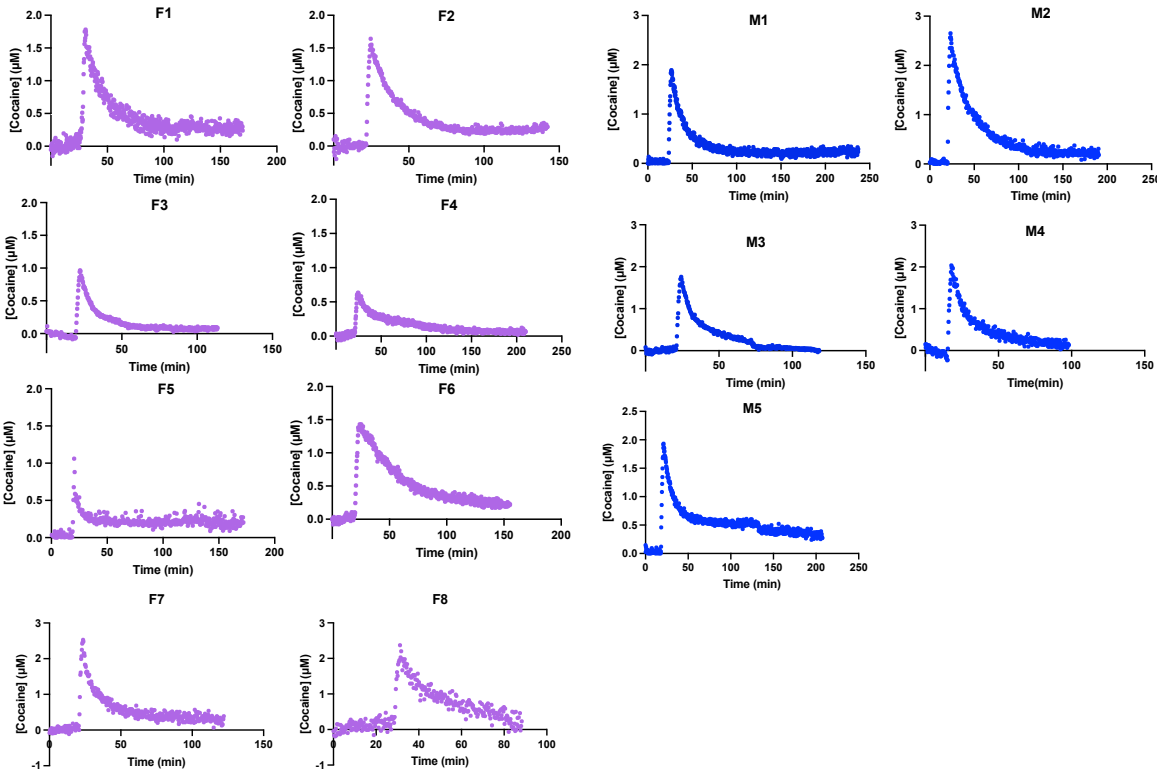

Figure S5.1. Individual data sets from each subject in the current study, with males (blue) and females (purple). Cocaine HCl was administered intravenously (1 mg/kg over 3 mins) for all animals in the current study.

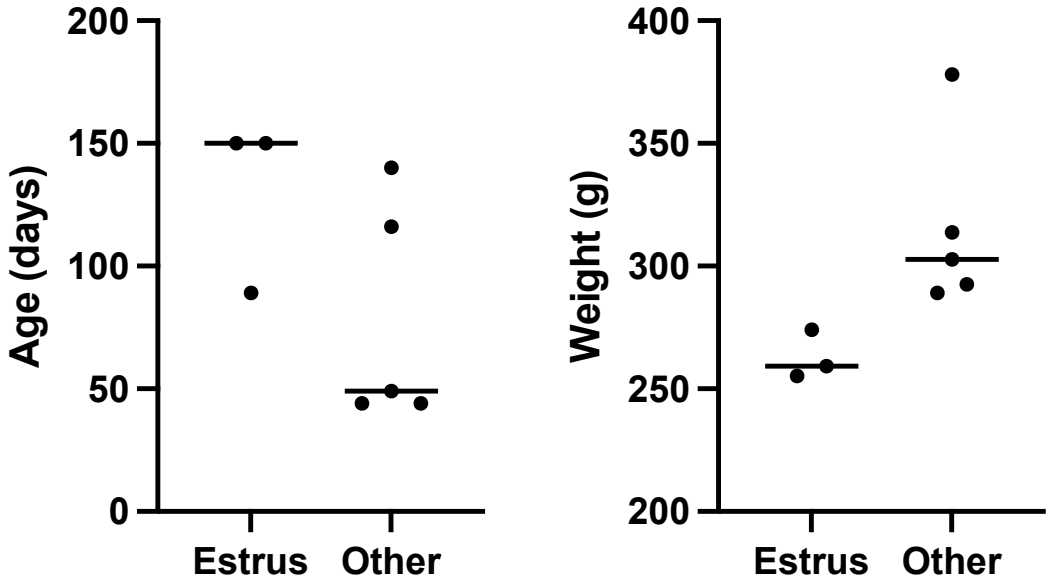

Figure S2.2. We found no significant difference in age or weight between estrus and non-estrus females used in the current study, $t(6) = 1.6$; $p = 0.15$; $t(6) = 2.4$; $p = 0.06$, respectively.

Chapter 6: Discussion

6.1 Summary

Comprehensively, the findings presented here suggest that EAB sensors are well-positioned to significantly advance the state of the art of personalized medicine, improving our ability to perform minimally invasive drug monitoring and enabling the individualization of patient pharmacokinetics, and thus patient care. In the first data chapter of my research (Chapter 2), I demonstrated that EAB sensors could perform real-time monitoring of drug distribution across physiological compartments. This is of value for understanding the pharmacokinetics of drug distribution for drugs whose site of action is not the blood. Additionally, we found strong correlations between pharmacokinetic parameters in the plasma and ISF, suggesting concentration data obtained from minimally invasive subcutaneous sensors could reliably inform plasma concentrations—the latter of which forms the gold standard sample source for therapeutic drug monitoring. In the second portion of the research (Chapter 3), I utilized a novel adaptive feedback control platform to demonstrate how maintaining plasma levels of drugs equates to achieving similarly maintained drug levels in tissue. This close correspondence validates the use of feedback-controlled plasma drug concentrations to control drug concentrations in the solid tissues that are often the site of drug action. We further demonstrated that two sensors side-by-side in the ISF track each other with high precision and accuracy, validating the reproducibility of these hand fabricated sensors. In Chapter 4, I utilized the in-brain EAB platform to evaluate the success of putative pharmacological and encapsulation techniques to enhance blood-brain-barrier crossing, which are in high demand for treating central nervous system conditions. Future work with the EAB platform should evaluate drug transport across physiological barriers in relevant disease states in which the BBB is compromised, such as tumor models (Arvanitis et al.,

2020; Aryal et al., 2015; Mitusova et al., 2022), to better inform how this platform could inform neuropharmaceutical efficacy. Finally, Chapter 5 evaluates how EAB sensors can be used to examine inter-animal pharmacokinetic differences, utilizing cocaine as a testbed. We found high correlations between body weight-adjusted dose and cumulative drug exposure, suggesting that body-weight-adjusted doing may not be sufficient to achieve consistent drug exposure across subjects of different weights. We also found a significant correlation between half-life and age, highlighting the importance of considering age-related factors when evaluating drug clearance. Finally, we found statistically higher maximum plasma cocaine concentrations in females in estrus compared to males and females in any other stage. This work suggests that behavioral differences evidenced in estrus females may be, in part, due to pharmacokinetic differences in plasma cocaine levels.

Collectively, the work presented in this thesis demonstrates the varied applications of EAB sensors with use across different physiological compartments. I have demonstrated the ability to monitor drug concentrations in the bloodstream, interstitial fluid, and the brains of live rats with seconds-resolved resolution. This work demonstrates how EAB sensors could significantly advance the state of the art of personalized medicine, by enabling the seconds resolved, subject-specific measurements of drugs in the body.

6.2 Limitations

6.2.1. Generation of new aptamer sequences

Although the work presented here showcases the strengths of EAB sensing platforms, a major notable limitation of this technology remains, at present, its current limited

adaptability to a broader range of targets. Although, in the last decade, our group has been able to develop EAB sensors against well over a dozen targets (outpacing the few optical sensors developed across various labs in the same period), those targets are generally small molecules whose physiological and/or clinical ranges are micromolar to high nanomolar. The central limitation to the generation of new EAB sensors is the isolation of sufficiently sensitive and selective aptamer sequences, which is currently universally achieved by variants of the SELEX process. While this is also a significant advantage for the platform, as it does not require in vivo engineering (antibodies, for example, require animal hosts or cell-based expression systems (Sharma et al., 2016)), the SELEX process itself has some critical limitations. First, the SELEX process requires iterative rounds to isolate high-affinity aptamer sequences, which can take months to complete (Bowser, 2005; Liu & Yu, 2018). The time-consuming nature of the SELEX process impedes the rapid development of novel EAB sensors (Liu & Yu, 2018). SELEX also requires the generation of massive oligonucleotide libraries, which require extensive reagent consumption and costly laboratory equipment. In addition to these practical limitations, SELEX is also often performed in controlled environments at room temperature, suggesting isolated aptamers may not perform well in complex media or at physiologically relevant temperatures for in vivo applications. Additionally, SELEX is performed in the solution phase, whereas EAB sensors utilize surface-bound aptamers. To combat these limitations, several modifications to the SELEX process, including automation, the integration of bioinformatics tools, and the introduction of capillary electrophoresis SELEX (CE-SELEX) have been developed to expedite the process (Liu & Yu, 2018). Modifying and adapting the SELEX protocol with both surface adherence

and condition optimization may generate aptamers that have higher target affinity when adapted to the EAB platform.

A notable limitation of the SELEX process is that not all target molecules are viable candidates for aptamer generation. Target molecules that reliably produce successful aptamer sequences are often positively charged and contain hydrogen-bond donors and acceptors (Wilson & Szostak, 1999). However, generating aptamer sequences for targets that are hydrophobic and negatively charged, however, remains challenging due to the necessary intermolecular interactions between the aptamer and the target (Liu & Yu, 2018). Further, the success of SELEX is also dependent on the size of the target molecule, which is difficult to ensure with very small or very large targets. Ensuring specificity remains a critical hurdle for small molecule targets, as aptamer sequences must be able to distinguish small structural features. Conversely, large targets may contain a variety of biomolecular structures, thus increasing the likelihood of non-specific binding. Because of their size, aptamers generated for large molecules often offer slow dissociation (Kohlberger & Gadermaier, 2022; Liu & Yu, 2018). The expansion of targets may be better facilitated by exploring modified or unnatural nucleobases, expanding beyond the possible 4^n (where n is the number of nucleotide bases) oligonucleotides possible for synthesis (D. R. Davies et al., 2012; Y. X. Wu & Kwon, 2016). Not only would these non-natural nucleobases expand our potential library for aptamer sequences, but research suggests unnatural nucleotide aptamers show an improved affinity for their targets (Kimoto et al., 2013).

6.2.2. Successful adaptation of aptamer sequences into EAB platform

Successfully adapting aptamer sequences to the EAB platform presents a significant challenge, as not all aptamers that demonstrate high affinity in solution are inherently suitable for electrochemical signaling. While aptamers may exhibit strong target binding in traditional assays, their integration into the EAB platform requires them to undergo binding-induced conformational changes that produce a measurable electrochemical signal by altering the position of the redox reporter relative to the sensor surface. Unfortunately, many high-affinity aptamers fail to achieve this due to their structural rigidity or lack of appropriate folding dynamics. Integrating these aptamers into the platform "as-selected," their signal gain is often minimal (Downs & Plaxco, 2022). Fortunately, we have been able to remedy this via the introduction of post-SELEX modifications that improve the performance of aptamers in the EAB platform. Modifications such as truncation, or the removal of base pairs, destabilize the folded state of the aptamer sequence so it equilibrates between the bound and unbound state (Dauphin-Ducharme et al., 2019a; A. M. Downs & Plaxco, 2022; White et al., 2010). The integration of spectroscopic methods employed to explore the necessary binding-induced conformational changes has better informed the transition of a generated sequence into the EAB platform (Y. Wu et al., 2023).

6.2.3. EAB sensor performance

6.2.3.a. Calibration. Engineering accurate and effective novel biosensing methods depend critically on the ability to generate reliable calibration methods. To improve calibration methods, our lab has generally calibrated sensors in the medium and conditions in which they are to be deployed (A. M. Downs & Plaxco, 2022). For example, calibrating an in

vivo sensor for use in a rat jugular vein is calibrated in 37°C bovine blood. These are necessary approximations given that “titrating” in an animal would require continuous blood draws and secondary ex-vivo analysis. Although we have performed secondary validation for some in vivo targets, quantifying blood draws with traditional “gold standard” methods, I believe future work should continue to verify concentrations to ensure the accuracy and validity of EAB sensors.

Because the relationship between the target molecule concentration and EAB sensor signal is not linear, the calibration of EAB sensors is complicated. Measurement precision is thus limited in parts of the curve that are particularly high or low, where sensor response may plateau or change less predictably. In addition, some aptamers exhibit nonlinear responses at higher target concentrations, which often deviate from the behavior predicted by the Langmuir absorption model. Further, the Langmuir model assumes a homogenous binding surface, in which each binding site offers the same affinity and where binding is a single-step process with no interactions between bound and unbound molecules (Johnson & Arnold, 1995; Swenson & Stadie, 2019; Umpleby et al., 2004). Practically, however, the homogeneity of the binding sites on EAB sensors is unknown and aptamers may undergo multiple conformational changes upon target binding. These deviations from the assumptions proposed by the Langmuir model may complicate the accuracy of EAB calibration. Future work should evaluate more flexible and realistic modeling approaches and data analysis techniques to better capture the complexity of binding interactions in dynamic biological environments.

Aptamers are highly sensitive to changes in pH, ionic strength, and temperature. To perform in vivo, EAB sensors must remain stable in complex biological media in the face of

potentially rapidly fluctuating conditions. This presents a challenge, for example, if EAB sensors cannot demonstrate stability in mediums like sweat, where pH is often an index of hydration state and can vary from 5.0 to 7.5 (Koh et al., 2016; S. Li et al., 2022). Further, in some disease states such as acidosis, the pH of blood can vary significantly (Misbin, 1977). Aptamer calibration can vary with deviations in temperature, ionic strength, and pH (Hianik et al., 2007). Some work has evaluated the performance of pH-independent redox reporters, specifically π-extended tetrathiafulvalene (exTTF) to enable continuous monitoring in pH-variable media (S. Li et al., 2022).

Recent work from the Plaxco lab (Fetter et al., 2024) carefully examined the extent to which physiological fluctuations impact the accuracy of EAB sensors and explored methods to mitigate these effects. Using three distinct EAB sensors for vancomycin, phenylalanine, and tryptophan, the authors found that fluctuations in ionic strength, cation composition, and pH within normal physiological limits minimally impacted the accuracy of EAB sensors. Deviations in temperature produced more significant errors, but these effects can be effectively corrected when the temperature is known, effectively restoring measurement accuracy. Therefore, physiologically induced environmental fluctuations do not appear to pose a significant barrier to the clinical adoption of this in vivo molecular monitoring technology (Fetter et al., 2024).

6.2.3.b. Cross-reactivity. The generation of new aptamer sequences via SELEX prioritizes the generation of aptamers with high affinity for their target, often compromising selectivity. The advent of techniques such as counter-SELEX, which integrates rounds of SELEX screening in the presence of similar target molecules, presents an opportunity to generate aptamers with both high affinity and selectivity (Zhuo et al.,

2017). Regardless of whether counter-SELEX was performed, it is imperative to perform cross-reactivity studies after adaptation as an EAB sensor. Ideally, potential confounds produce no signal response on the target aptamer, or if they do induce signal change, they are at concentrations far beyond physiological relevance. Minimizing non-specific adsorption is a critical and promising strategy to address cross-reactivity in EA B sensors, particularly when operating in complex biological matrices. Surface modifications of the electrode, such as coating with antifouling materials like polyethylene glycol (PEG) and zwitterionic polymers can effectively reduce the nonspecific binding of proteins and other biomolecules (Jiang et al., 2020; Saxena et al., 2024; Zhou et al., 2022). These approaches enhance the specificity of the aptamer-target interaction, ensuring that the signal generated by the EAB sensor accurately reflects the presence of the intended analyte, even in the presence of potential interferents in complex media. This remains a laborious effort that must be determined empirically at some stage of development of an EAB sensor.

6.2.3.c. Longevity and stability. A critical hurdle in advancing the applications of EAB sensors is overcoming signal drift, whereby sensor signal decreases over time. To correct for signal drift, we employ Kinetic Differential Measurements (KDM; described in prior chapters), but the cumulative loss in total signal gain over time still leads to a reduction in the overall signal-to-noise ratio of the biosensor resulting in an inability to overcome noise with signal change. Our lab has demonstrated that signal drift can be split into two phases: an initial exponential signal decrease followed by a secondary linear decrease, attributable to fouling and monolayer loss, respectively (Leung et al., 2021b). Electrode fouling occurs when the electrode surface absorbs proteins or molecules found in complex biological media, decreasing sensor longevity by decreasing the electron transfer rate from the redox reporter

to the gold working electrode (A. M. Downs & Plaxco, 2022; Leung et al., 2021b). Leung et al. (2021) determined this initial exponential signal loss was due to electrode fouling, given the same sensor degradation did not occur in a simple buffer solution. The authors concluded the secondary linear drift phase was attributable to redox-driven monolayer loss and was evident in both simple and complex media. Authors suggest this secondary phase is caused by the desorption of the monolayer, demonstrated by the dependence of the rate of linear drift on the width of the potential window. Narrowing the potential window used to interrogate the EAB sensor markedly decreases the linear drift phase (Leung et al., 2021b).

Overcoming signal loss is a critical hurdle in ensuring EAB sensor longevity. The initial exponential drift observed in a complex biological media could be minimized by introducing novel monolayers that reduce electrode fouling, such as hydrogels (Leung et al., 2021b; S. Li et al., 2023). Additionally, implementing different monolayer chemistry could reduce signal drift. Implementing longer-chain monolayers would improve the stability of the monolayer, but conversely may slow electron transfer (Lai et al., 2006; H. Li, Dauphin-Ducharme, Arroyo-Currás, et al., 2017). Future work should evaluate how potential modifications in monolayer chemistry may improve the longevity of aptamer-based biosensors. To mitigate the loss of the monolayer that gives rise to the linear drift phase, electrochemical methods that rely on scanning relatively narrow potential windows, such as FT-EIS, should be further evaluated. Further, modifying the composition of the surface-assembled monolayer (SAM) could help reduce the impact of fouling and voltammetric scanning on signal loss, thereby enhancing the long-term stability of the sensor. For example, utilization of a 1-hexanethiol monolayer exhibits greater resistance to desorption and capacitance-related faradaic signal loss, even when challenged in undiluted blood for 60

hours (Shaver et al., 2020). Although the 1-hexanethiol monolayer can influence an aptamer's target response, combining mercaptohexanol and 1-hexanethiol monolayers enhances sensor stability without compromising the aptamer's target response. Finally, recent work suggests the integration of synthetic, non-natural "xenonucleic acid" backbones may improve the performance of in vivo EAB sensors. Non-natural "xeno" nucleic acids (XNAs) impart significant resistance to enzymatic degradation (Leung et al., 2024), improving the longevity of EAB sensors.

Another alternative to minimizing the impact of signal degradation is to increase signal gain. A promising method for improving the performance of EAB sensors by improving signal gain is via codeposition, in which the thiol-modified aptamer and the mercaptohexanol dilutant are simultaneously deposited on the electrode surface. Recent work has suggested that codeposition generates higher signal gain than sequential deposition methods (Y. Wu et al., 2024). Codeposition also substantially cuts down on the functionalization time of EAB sensors (requiring only an hour, versus overnight incubation for sequential deposition), which would significantly advance the scalability of EAB sensors for clinical applications.

The ability to obtain long-duration measurements, over days or even weeks, would drastically expand the potential applications of EAB sensors. Enabling long-term continuous monitoring could posit EAB sensors as a technology rivaling the ubiquity of the continuous glucose monitor, collecting seconds-resolved personalized data as a wearable, portable device. EAB sensors could provide continuous insights into conditions requiring long-term management, such as diabetes, cardiovascular disease, or chronic infections. And, given that certain physiological or pathological processes require extended observation periods,

including fibrosis development, slow disease progression, or long-term metabolic changes, prolonging sensor longevity could expand the application of the platform to both inform how these changes occur and inform clinical intervention. Future work must carefully evaluate methods to improve the longevity and stability of EAB sensors, further strengthening the technology's position a revolutionary healthcare device.

6.3 Applications and future directions

6.3.1. Clinical advancements

EAB sensors could revolutionize clinical care, improving how we detect and treat disease. We foresee this advancement in the integration of EAB technology into a platform analogous to a continuous glucose monitor, enabling the real-time measurement of drugs and biomarkers. Because EAB sensors are generalizable, the sheer number of clinical conditions and disease states that EAB sensors could both inform and diagnose is presumably endless. EAB sensors could drastically improve our ability to both diagnose and treat disease. For example, EAB sensors could be particularly useful in diagnosing sepsis: high levels of procalcitonin (PCT) in the blood can be utilized to determine a patient's risk of progression to severe sepsis (Vijayan et al., 2017). Not only could EAB sensors enable the detection of sepsis but could also be used to improve clinical treatment outcomes: EAB sensors for vancomycin, for example, could monitor drug levels within individual patients, maintaining efficacious concentrations.

Real monitoring of endogenous metabolite levels could revolutionize the diagnosis and treatment of disease. For example, renal malfunction, acute kidney injury, and chronic

kidney disease are clinically diagnosed by measuring creatinine concentration in serum (Gonzalez-Gallardo et al., 2022; Saddique et al., 2023). Likewise, urea is a marker of uremic retention in chronic kidney disease (Vanholder et al., 2018). Developing and optimizing EAB sensors for creatinine and urea would not only expedite and improve our diagnosis of kidney-related disease but could also be used to evaluate treatment efficacy and develop novel therapeutics to improve or regulate kidney function. Monitoring levels of c-reactive protein (CRP) levels, a critical serum biomarker of acute inflammatory response, could quickly and accurately inform vulnerability to cardiovascular disease (Luan & Yao, 2018; Noh et al., 2021).

Another foreseeable clinical advantage of EAB sensors would be monitoring drug levels for compliance in addiction medicine. EAB sensors could present as a powerful tool to empower individuals suffering from addiction. For example, EAB sensors could be applied to support drug-free compliance monitoring for individuals convicted of drug-related offenses, providing an alternative to incarceration by enabling continuous, non-invasive tracking of sobriety. This could help keep individuals out of prison while they rebuild their lives in their communities. EAB sensors could further assist individuals undergoing medication-assisted therapy (MAT), enabling continuous monitoring of therapeutic drug levels to ensure patients are safely weaned off drugs of abuse. This would potentially better enable “rehabilitation-at-home” contexts, in which individuals are empowered to safely detox from substances of abuse without the financial burden of detoxification in hospitals or costly rehabilitation centers. EAB sensors could be likewise used to better evaluate biomarkers that precipitate relapse, such as cortisol levels (Lovallo, 2006), to inform the necessity of behavioral intervention. It is in this author’s opinion that the deployment of EAB sensors

should remain focused on empowering individuals, rather than enabling law enforcement or regulatory bodies to monitor or penalize drug use, as this could undermine trust and discourage individuals from utilizing such technologies in their recovery journey.

EAB sensors represent a powerful tool that would drastically improve the state of the art of personalized pharmacokinetics, enabling a future where individuals are dosed based on their distinct metabolic processes in contrast to the current reliance on archaic metrics like body surface area, sex, or weight. Given that most pharmaceutical dosing is based on overgeneralized assumptions about how the average individual metabolizes and processes drugs, EAB sensors could revolutionize therapeutic outcomes, personalizing drug dosing to maximize therapeutic outcomes and minimize toxicity-related side effects.

Finally, EAB sensors offer transformative potential for clinical drug development. Taking a drug from its initial conception to market is an expensive and time-consuming product, costing an average of 515 million dollars (Sertkaya et al., 2024) and taking an average of 12 to 15 years (Brown et al., 2022). EAB sensors can significantly streamline this process by providing real-time, high-resolution data on drug behavior in vivo, reducing the reliance on labor-intensive and costly traditional sampling methods. EAB enables the generation of both individualized and generalized pharmacokinetics with exceptional accuracy, which can help optimize dosing regimens, predict therapeutic windows, and identify potential safety concerns early in development. By accelerating the iteration and refinement of drug candidates, EAB sensors have the potential to shorten timelines, reduce development costs, and increase the likelihood of successful market approval.

6.3.1.a. Barriers to clinical deployment

Developing EAB sensors as a practical clinical tool to monitor both endogenous and exogenous drugs and metabolites would drastically revolutionize healthcare, but there remain critical barriers to overcome to ensure successful adaptation.

6.3.1.a.a. Miniaturization

A primary hurdle for transitioning this preclinical research tool to a mainstay in clinical practice is miniaturization: developing small and thus minimally invasive prototypes that retain high signal gain. Many efforts have been made to evaluate methods to maximize signal gain while minimizing both the length and width of working electrodes, from the utilization of nanoporous gold to the integration of organic electrochemical transistors (Bidinger et al., 2022; A. M. Downs et al., 2021).

6.3.1.a.b. Sterilization

A significant advantage of EAB sensors for clinical deployment is that aptamers are generally considered non-immunogenic, eliciting little to no immune response (Y.-P. Wang et al., 2024). Regardless, rigorous preclinical evaluation, including tests for cytokine release and antibody production, is essential to confirm the biocompatibility of EAB sensors. Addressing immunogenicity concerns is crucial for the safe and effective use of EAB sensors in personalized medicine, particularly for applications requiring repeated or prolonged use in patients. To be clinically approved as an implantable device, EAB sensors must be able to be fully sterilized to ensure safety. Recent work has carefully evaluated different sterilization methods and determined treatment with CIDEX OPA (0.55% *ortho*-phthalaldehyde) successfully decreased pathogen load while not significantly altering sensor performance

(Chung et al., 2022). Further addressing these considerations and the myriad other factors that will ensure FDA compliance will be essential for translating EAB sensors from research to practical, clinically viable devices.

6.3.2. Scientific advancements

In addition to advancing clinical care, EAB sensors present a powerful research tool that could significantly advance biomedical research. This tool could advance many areas of research, including pharmacology (drug metabolism and pharmacokinetics), neuropharmacology and neurochemistry, and endocrinology.

EAB sensors could rapidly advance the field of neuropharmacology, enabling the seconds-resolved quantification of the distribution of psychoactive drugs and the concurrent monitoring of associated hormones and neurotransmitters that fluctuate in response to their administration. The EAB platform has been demonstrated to work in awake, ambulatory animals, enabling concurrent in-brain concentrations of various drugs and metabolites and behavioral assays. This could be utilized to, for example, better elucidate the relationship between circulating hormone levels, such as estradiol, and cognitive performance. The attributes of EAB sensors suggest they could provide the opportunity to perform closed-loop feedback-controlled optogenetics. Closed-loop optogenetics could enable the precise, dynamic modulation of biological activity based on real-time neurochemical signals, drastically improving our understanding of neurobiology (Potter et al., 2014). EAB sensors could be utilized to link quantitative events (ex., the concentration of a drug in a specific brain region) to an immediate modulation of neuronal response. These systems could be used

to dynamically alter optogenetic stimulation to maintain or modulate biological processes, including gene expression, metabolic activity, or neurotransmitter release. EAB sensors could revolutionize optogenetics, enabling closed-loop systems that provide real-time feedback based solely on biochemical cues.

EAB sensors could also be used for the real-time monitoring of cell cultures. To date, they have been utilized to monitor ATP release in astrocytes and detect serotonin with glass nanopipettes (Nakatsuka et al., 2021; Santos-Cancel et al., 2019). There are numerous foreseeable applications of EAB sensors in cell culture applications. EAB sensors could be utilized to measure growth factors necessary for cell proliferation and differentiation in tissue or stem cell engineering or used to monitor critical metabolites or environmental markers to improve cell proliferation. EAB sensors would reduce the reliance on static endpoint assays, better informing the dynamics of cellular processes.

EAB sensors would be a powerful tool in the field of pharmacology, specifically because of the ability to perform feedback-controlled drug delivery. Feedback-controlled drug delivery using EAB sensors would not only advance clinical research but also advance pharmacological research. The high precision control of drug concentrations would permit researchers to treat inter-animal differences in pharmacokinetic response as an experimentally controllable variable. This, in turn, would enable further exploration of the reproducibility of therapeutic outcomes when this variability is eliminated.

6.3.2.a. Barriers to widespread adaptation as a research tool

EAB sensors present a powerful research tool that would vastly advance numerous fields, including pharmacology, neuroscience, and endocrinology. Aside from the general

limitations outlined in this section, there are specific hurdles for the adaptation of this platform as a widespread research tool.

6.3.2.a.a. Miniaturization

The EAB sensor platform is a significant advancement over previous methods for quantifying drug concentrations in the brain, such as microdialysis and cyclic voltammetry. The in-brain EAB platform is currently composed of a 76 μm diameter, 3 mm long working electrode. While the current dimensions provide the spatial resolution to distinguish larger brain regions, such as the lateral ventricle and hippocampus, it is not well suited to target functionally distinct brain subregions with high precision (Beauchamp et al., 2022; Herculano-Houzel et al., 2006). Miniaturizing the platform could provide higher spatial resolution, enabling detailed functional studies of these and other neural subregions. Miniaturization of the in-brain EAB architecture would enable measurements in smaller animal models, such as mice, which offer specific advantages over rats for specific research areas.

6.3.2.a.b. Continued adaptation into behavioral paradigms

To fully realize their potential as a transformative tool in neuroscience, EAB sensors must be adapted to a wide array of behavioral paradigms. We have been able to adapt our platform to perform concurrent in-brain monitoring of drugs with behavioral locomotive output, which is a critical hurdle in evaluating how drugs elicit behavioral responses (Gerson et al., 2023b). Future work should examine how to best implement this research tool in tandem with other behavioral paradigms, including cognitive assays, spatial navigation tasks, and operant behavior paradigms.

A critical hurdle in adapting this technique to behavioral studies is the reality that these tasks often require subjects to be active, whether exploring environments, engaging in tasks, or responding to stimuli. This movement introduces mechanical and electrical noise that can significantly impact the stability and accuracy of EAB sensor readings. These artifacts are especially problematic in dynamic behavioral paradigms, including locomotor activity tests, self-administration studies, or cognitive tasks requiring free movement, where stable, high-resolution molecular data are required for correlating physiological changes with behavior. Potential routes forward include introducing novel signal processing techniques that distinguish genuine molecular signals from movement-induced artifacts or optimizing and refining EAB sensor platform design with more flexible materials that reduce sensitivity to mechanical stress while ensuring stable placements in vivo.

6.3.2.a.c. Standardization

Another critical challenge for the widespread adoption of EAB sensors in research is standardization. The lack of universally accepted protocols for using and interpreting EAB sensor data can lead to inconsistencies across different laboratories and research settings. Variations in sensor calibration, experimental conditions, and data analysis methods can affect the reproducibility and reliability of results. To overcome this barrier, establishing standardized operating procedures, validation protocols, and data interpretation frameworks is essential to ensure consistency across studies, build confidence in the technology, and accelerate its integration into diverse research applications.

6.3.2.a.d. Secondary validation

Finally, one of the primary barriers to the widespread adoption of EAB sensors as a revolutionary research tool is convincing fellow scientists of their reliability and accuracy in comparison to “gold standard” methods. EAB sensor research must continue to integrate secondary ex-vivo analysis using widely accepted techniques to confirm the sensor's accuracy, providing researchers with a benchmark for comparison to build confidence in the precision of the platform. By demonstrating that EAB sensors produce comparable or superior results to well-established methods, the scientific community is more likely to adopt them as a reliable tool for real-time, high-precision pharmacokinetics studies, ultimately advancing personalized medicine.

References

Afsar, T., Razak, S., Almajwal, A., & Al-Disi, D. (2020). Doxorubicin-induced alterations in kidney functioning, oxidative stress, DNA damage, and renal tissue morphology; Improvement by Acacia hydaspica tannin-rich ethyl acetate fraction. *Saudi Journal of Biological Sciences*, *27*(9), 2251–2260. https://doi.org/10.1016/j.sjbs.2020.07.011

Ahmed Juvale, I. I., Abdul Hamid, A. A., Abd Halim, K. B., & Che Has, A. T. (2022). P-glycoprotein: New insights into structure, physiological function, regulation and alterations in disease. *Heliyon*, *8*(6), e09777. https://doi.org/10.1016/j.heliyon.2022.e09777

Ajayi, A. F., & Akhigbe, R. E. (2020). Staging of the estrous cycle and induction of estrus in experimental rodents: An update. *Fertility Research and Practice*, *6*(1), 5. https://doi.org/10.1186/s40738-020-00074-3

Alkhamis, O., Canoura, J., Wu, Y., Emmons, N. A., Wang, Y., Honeywell, K. M., Plaxco, K. W., Kippin, T. E., & Xiao, Y. (2024). High-Affinity Aptamers for In Vitro and In Vivo Cocaine Sensing. *Journal of the American Chemical Society*. https://doi.org/10.1021/jacs.3c11350

Alnaim, L. (2007). Therapeutic drug monitoring of cancer chemotherapy. *Journal of Oncology Pharmacy Practice: Official Publication of the International Society of Oncology Pharmacy Practitioners*, *13*(4), 207–221. https://doi.org/10.1177/1078155207081133

Anderzhanova, E., & Wotjak, C. T. (2013). Brain microdialysis and its applications in experimental neurochemistry. *Cell and Tissue Research*, *354*(1), 27–39. https://doi.org/10.1007/s00441-013-1709-4

Arroyo-Currás, N., Dauphin-Ducharme, P., Ortega, G., Ploense, K. L., Kippin, T. E., & Plaxco, K. W. (2018). Subsecond-Resolved Molecular Measurements in the Living Body Using Chronoamperometrically Interrogated Aptamer-Based Sensors. *ACS Sensors*, *3*(2), 360–366. https://doi.org/10.1021/acssensors.7b00787

Arroyo-Currás, N., Ortega, G., Copp, D. A., Ploense, K. L., Plaxco, Z. A., Kippin, T. E., Hespanha, J. P., & Plaxco, K. W. (2018). High-Precision Control of Plasma Drug Levels Using Feedback-Controlled Dosing. *ACS Pharmacology & Translational Science*, *1*(2), 110–118. https://doi.org/10.1021/acsptsci.8b00033

Arroyo-Currás, N., Scida, K., Ploense, K. L., Kippin, T. E., & Plaxco, K. W. (2017). High Surface Area Electrodes Generated via Electrochemical Roughening Improve the Signaling of Electrochemical Aptamer-Based Biosensors. *Analytical Chemistry*, *89*(22), 12185–12191. https://doi.org/10.1021/acs.analchem.7b02830

Arroyo-Currás, N., Somerson, J., Vieira, P. A., Ploense, K. L., Kippin, T. E., & Plaxco, K. W. (2017). Real-time measurement of small molecules directly in awake, ambulatory animals. *Proceedings of the National Academy of Sciences of the United States of America*, *114*(4), 645–650. https://doi.org/10.1073/pnas.1613458114

Arroyo-Currás Netzahualcóyotl, Somerson Jacob, Vieira Philip A., Ploense Kyle L., Kippin Tod E., & Plaxco Kevin W. (2017). Real-time measurement of small molecules directly in awake, ambulatory animals. *Proceedings of the National Academy of Sciences*, *114*(4), 645–650. https://doi.org/10.1073/pnas.1613458114

Arvanitis, C. D., Ferraro, G. B., & Jain, R. K. (2020). The blood–brain barrier and blood–tumour barrier in brain tumours and metastases. *Nature Reviews. Cancer*, *20*(1), 26–41. https://doi.org/10.1038/s41568-019-0205-x

Aryal, M., Vykhodtseva, N., Zhang, Y.-Z., & McDannold, N. (2015). Multiple sessions of liposomal doxorubicin delivery via focused ultrasound mediated blood-brain barrier disruption: A safety study. *Journal of Controlled Release : Official Journal of the Controlled Release Society*, *204*, 60–69. https://doi.org/10.1016/j.jconrel.2015.02.033

Ates, H. C., Roberts, J. A., Lipman, J., Cass, A. E. G., Urban, G. A., & Dincer, C. (2020). On-Site Therapeutic Drug Monitoring. *Trends in Biotechnology*, *38*(11), 1262–1277. https://doi.org/10.1016/j.tibtech.2020.03.001

Ban, W., You, Y., & Yang, Z. (2022). Imaging Technologies for Cerebral Pharmacokinetic Studies: Progress and Perspectives. *Biomedicines*, *10*(10), 2447. https://doi.org/10.3390/biomedicines10102447

Barbieri, E. J., Ferko, A. P., DiGregorio, G. J., & Ruch, E. K. (1992). The presence of cocaine and benzoylecgonine in rat cerebrospinal fluid after the intravenous administration of cocaine. *Life Sciences*, *51*(22), 1739–1746. https://doi.org/10.1016/0024-3205(92)90303-7

Barenholz, Y. (Chezy). (2012). Doxil® — The first FDA-approved nano-drug: Lessons learned. *Journal of Controlled Release*, *160*(2), 117–134. https://doi.org/10.1016/j.jconrel.2012.03.020

Beauchamp, A., Yee, Y., Darwin, B. C., Raznahan, A., Mars, R. B., & Lerch, J. P. (2022). Whole-brain comparison of rodent and human brains using spatial transcriptomics. *eLife*, *11*, e79418. https://doi.org/10.7554/eLife.79418

Benuck, M., Lajtha, A., & Reith, M. E. (1987). Pharmacokinetics of systemically administered cocaine and locomotor stimulation in mice. *Journal of Pharmacology and Experimental Therapeutics*, *243*(1), 144–149.

Bidinger, S. L., Keene, S. T., Han, S., Plaxco, K. W., Malliaras, G. G., & Hasan, T. (2022). Pulsed transistor operation enables miniaturization of electrochemical aptamer-based sensors. *Science Advances*, *8*(46), eadd4111. https://doi.org/10.1126/sciadv.add4111

Birngruber, T., Raml, R., Gladdines, W., Gatschelhofer, C., Gander, E., Ghosh, A., Kroath, T., Gaillard, P. J., Pieber, T. R., & Sinner, F. (2014). Enhanced Doxorubicin Delivery to the Brain Administered Through Glutathione PEGylated Liposomal Doxorubicin (2B3-101) as Compared with Generic Caelyx,®/Doxil®—A Cerebral Open Flow Microperfusion Pilot Study. *Journal of Pharmaceutical Sciences*, *103*(7), 1945–1948. https://doi.org/10.1002/jps.23994

Blaustein, J. D. (2008). Neuroendocrine regulation of feminine sexual behavior: Lessons from rodent models and thoughts about humans. *Annual Review of Psychology*, *59*, 93–118. https://doi.org/10.1146/annurev.psych.59.103006.093556

Bossé, R., Rivest, R., & Di Paolo, T. (1997). Ovariectomy and estradiol treatment affect the dopamine transporter and its gene expression in the rat brain. *Molecular Brain Research*, *46*(1), 343–346. https://doi.org/10.1016/S0169-328X(97)00082-X

Bothwell, S. W., Janigro, D., & Patabendige, A. (2019). Cerebrospinal fluid dynamics and intracranial pressure elevation in neurological diseases. *Fluids and Barriers of the CNS*, *16*(1), 9. https://doi.org/10.1186/s12987-019-0129-6

Bowser, M. T. (2005). SELEX: Just another separation? *The Analyst*, *130*(2), 128–130. https://doi.org/10.1039/b412492h

Brady, K. T., & Randall, C. L. (1999). GENDER DIFFERENCES IN SUBSTANCE USE DISORDERS. *Psychiatric Clinics of North America*, *22*(2), 241–252. https://doi.org/10.1016/S0193-953X(05)70074-5

Bronchud, M. H., Margison, J. M., Howell, A., Lind, M., Lucas, S. B., & Wilkinson, P. M. (1990). Comparative pharmacokinetics of escalating doses of doxorubicin in patients with metastatic breast cancer. *Cancer Chemotherapy and Pharmacology*, *25*(6), 435–439. https://doi.org/10.1007/BF00686055

Brown, D. G., Wobst, H. J., Kapoor, A., Kenna, L. A., & Southall, N. T. (2022). Clinical development times for innovative drugs. *Nature Reviews. Drug Discovery*, *21*(11), 793. https://doi.org/10.1038/d41573-021-00190-9

Brown-Grant, K., Exley, D., & Naftolin, F. (1970). *PERIPHERAL PLASMA OESTRADIOL AND LUTEINIZING HORMONE CONCENTRATIONS DURING THE OESTROUS CYCLE OF THE RAT*. https://doi.org/10.1677/joe.0.0480295

Burke, J. F. (1977). Doxorubicin Hydrochloride-Associated Renal Failure. *Archives of Internal Medicine*, *137*(3), 385. https://doi.org/10.1001/archinte.1977.03630150079022

Burmeister, J. J., Pomerleau, F., Huettl, P., Gash, C. R., Werner, C. E., Bruno, J. P., & Gerhardt, G. A. (2008). Ceramic-based multisite microelectrode arrays for simultaneous measures of choline and acetylcholine in CNS. *Biosensors and Bioelectronics*, *23*(9), 1382–1389. https://doi.org/10.1016/j.bios.2007.12.013

Castagnola, E., Robbins, E. M., Woeppel, K. M., McGuier, M., Golabchi, A., Taylor, I. M., Michael, A. C., & Cui, X. T. (2020). Real-Time Fast Scan Cyclic Voltammetry Detection and Quantification of Exogenously Administered Melatonin in Mice Brain. *Frontiers in Bioengineering and Biotechnology*, *8*. https://doi.org/10.3389/fbioe.2020.602216

Chan, I. S., & Ginsburg, G. S. (2011). Personalized Medicine: Progress and Promise. *Annual Review of Genomics and Human Genetics*, *12*(Volume 12, 2011), 217–244. https://doi.org/10.1146/annurev-genom-082410-101446

Chefer, V. I., Thompson, A. C., Zapata, A., & Shippenberg, T. S. (2009). Overview of Brain Microdialysis. *Current Protocols in Neuroscience / Editorial Board, Jacqueline N. Crawley ... [et Al.]*, *CHAPTER*, Unit7.1. https://doi.org/10.1002/0471142301.ns0701s47

Chin, J., Sternin, O., Wu, H. B., Fletcher, H., Perrotti, L. I., Jenab, S., & Quiñones-Jenab, V. (2001). Sex differences in cocaine-induced behavioral sensitization. *Cellular and Molecular Biology (Noisy-Le-Grand, France)*, *47*(6), 1089–1095.

Chong, Y. E., Chiang, M., Deshpande, K., Haroutounian, S., Kagan, L., & Lee, J. B. (2019). Simultaneous quantification of ondansetron and tariquidar in rat and human plasma using HPLC-UV. *Biomedical Chromatography : BMC*, *33*(11), e4653. https://doi.org/10.1002/bmc.4653

Chung, J., Sepunaru, L., & Plaxco, K. W. (2022). On the Disinfection of Electrochemical Aptamer-Based Sensors. *ECS Sensors Plus*, *1*(1), 011604. https://doi.org/10.1149/2754-2726/ac60b2

Cserr, H. F., & Patlak, C. S. (1992). Secretion and Bulk Flow of Interstitial Fluid. In M. W. B. Bradbury (Ed.), *Physiology and Pharmacology of the Blood-Brain Barrier* (pp. 245–261). Springer. https://doi.org/10.1007/978-3-642-76894-1_9

D'Adamo, D. R., Anderson, S. E., Albritton, K., Yamada, J., Riedel, E., Scheu, K., Schwartz, G. K., Chen, H., & Maki, R. G. (2005). Phase II Study of Doxorubicin and

Bevacizumab for Patients With Metastatic Soft-Tissue Sarcomas. *Journal of Clinical Oncology*, *23*(28), 7135–7142. https://doi.org/10.1200/JCO.2005.16.139

Dakic, T., Velickovic, K., Lakic, I., Ruzicic, A., Milicevic, A., Plackic, N., Vujovic, P., & Jevdjovic, T. (2024). Rat brown adipose tissue thermogenic markers are modulated by estrous cycle phases and short-term fasting. *BioFactors (Oxford, England)*, *50*(1), 101–113. https://doi.org/10.1002/biof.1993

Dauphin-Ducharme, P., Yang, K., Arroyo-Currás, N., Ploense, K. L., Zhang, Y., Gerson, J., Kurnik, M., Kippin, T. E., Stojanovic, M. N., & Plaxco, K. W. (2019a). Electrochemical Aptamer-Based Sensors for Improved Therapeutic Drug Monitoring and High-Precision, Feedback-Controlled Drug Delivery. *ACS Sensors*, *4*(10), 2832–2837. https://doi.org/10.1021/acssensors.9b01616

Dauphin-Ducharme, P., Yang, K., Arroyo-Currás, N., Ploense, K. L., Zhang, Y., Gerson, J., Kurnik, M., Kippin, T. E., Stojanovic, M. N., & Plaxco, K. W. (2019b). Electrochemical Aptamer-Based Sensors for Improved Therapeutic Drug Monitoring and High-Precision, Feedback-Controlled Drug Delivery. *ACS Sensors*, *4*(10), 2832–2837. https://doi.org/10.1021/acssensors.9b01616

Davies, D. R., Gelinas, A. D., Zhang, C., Rohloff, J. C., Carter, J. D., O'Connell, D., Waugh, S. M., Wolk, S. K., Mayfield, W. S., Burgin, A. B., Edwards, T. E., Stewart, L. J., Gold, L., Janjic, N., & Jarvis, T. C. (2012). Unique motifs and hydrophobic interactions shape the binding of modified DNA ligands to protein targets. *Proceedings of the National Academy of Sciences*, *109*(49), 19971–19976. https://doi.org/10.1073/pnas.1213933109

Davies, M. I., Cooper, J. D., Desmond, S. S., Lunte, C. E., & Lunte, S. M. (2000). Analytical considerations for microdialysis sampling. *Advanced Drug Delivery Reviews*, *45*(2), 169–188. https://doi.org/10.1016/S0169-409X(00)00114-9

de Lange, E. C. M. (2013). Utility of CSF in translational neuroscience. *Journal of Pharmacokinetics and Pharmacodynamics*, *40*(3), 315–326. https://doi.org/10.1007/s10928-013-9301-9

Deguchi, Y., & Morimoto, K. (2001). Application of an in vivo brain microdialysis technique to studies of drug transport across the blood-brain barrier. *Current Drug Metabolism*, *2*(4), 411–423. https://doi.org/10.2174/1389200013338216

dos Anjos Rosário, B., de Fátima SantanaNazaré, M., de Souza, D. V., Le Sueur-Maluf, L., Estadella, D., Ribeiro, D. A., & de Barros Viana, M. (2022). The influence of sex and reproductive cycle on cocaine-induced behavioral and neurobiological alterations: A review. *Experimental Brain Research*, *240*(12), 3107–3140. https://doi.org/10.1007/s00221-022-06479-4

Downs, A. (2021). *Improving the accuracy and resolution of electrochemical aptamer-based sensors* [UC Santa Barbara]. https://escholarship.org/uc/item/6405f6sk

Downs, A. M., Bolotsky, A., Weaver, B. M., Bennett, H., Wolff, N., Polsky, R., & Miller, P. R. (2023). Microneedle electrochemical aptamer-based sensing: Real-time small molecule measurements using sensor-embedded, commercially-available stainless steel microneedles. *Biosensors and Bioelectronics*, *236*, 115408. https://doi.org/10.1016/j.bios.2023.115408

Downs, A. M., Gerson, J., Hossain, M. N., Ploense, K., Pham, M., Kraatz, H.-B., Kippin, T., & Plaxco, K. W. (2021). Nanoporous Gold for the Miniaturization of In Vivo

Electrochemical Aptamer-Based Sensors. *ACS Sensors*, *6*(6), 2299–2306. https://doi.org/10.1021/acssensors.1c00354

Downs, A. M., Gerson, J., Leung, K. K., Honeywell, K. M., Kippin, T., & Plaxco, K. W. (2022). Improved calibration of electrochemical aptamer-based sensors. *Scientific Reports*, *12*(1), Article 1. https://doi.org/10.1038/s41598-022-09070-7

Downs, A. M., & Plaxco, K. W. (2022). Real-Time, In Vivo Molecular Monitoring Using Electrochemical Aptamer Based Sensors: Opportunities and Challenges. *ACS Sensors*, *7*(10), 2823–2832. https://doi.org/10.1021/acssensors.2c01428

Dull, R. O., & Hahn, R. G. (2022). The glycocalyx as a permeability barrier: Basic science and clinical evidence. *Critical Care*, *26*(1), 273. https://doi.org/10.1186/s13054-022-04154-2

Dunvald, A. D., Iversen, D. B., Svendsen, A. L. O., Agergaard, K., Kuhlmann, I. B., Mortensen, C., Andersen, N. E., Järvinen, E., & Stage, T. B. (2022). Tutorial: Statistical analysis and reporting of clinical pharmacokinetic studies. *Clinical and Translational Science*, *15*(8), 1856–1866. https://doi.org/10.1111/cts.13305

Evans, W. E., & Relling, M. V. (1989). Clinical Pharmacokinetics-Pharmacodynamics of Anticancer Drugs. *Clinical Pharmacokinetics*, *16*(6), 327–336. https://doi.org/10.2165/00003088-198916060-00001

Fallah, A., Imani Fooladi, A. A., Havaei, S. A., Mahboobi, M., & Sedighian, H. (2024). Recent advances in aptamer discovery, modification and improving performance. *Biochemistry and Biophysics Reports*, *40*, 101852. https://doi.org/10.1016/j.bbrep.2024.101852

Feltenstein, M. W., Henderson, A. R., & See, R. E. (2011). Enhancement of cue-induced reinstatement of cocaine-seeking in rats by yohimbine: Sex differences and the role of the estrous cycle. *Psychopharmacology*, *216*(1), 53–62. https://doi.org/10.1007/s00213-011-2187-6

Ferguson, B. S., Hoggarth, D. A., Maliniak, D., Ploense, K., White, R. J., Woodward, N., Hsieh, K., Bonham, A. J., Eisenstein, M., Kippin, T. E., Plaxco, K. W., & Soh, H. T. (2013). Real-time, aptamer-based tracking of circulating therapeutic agents in living animals. *Science Translational Medicine*, *5*(213), 213ra165. https://doi.org/10.1126/scitranslmed.3007095

Festa, E. D., Russo, S. J., Gazi, F. M., Niyomchai, T., Kemen, L. M., Lin, S.-N., Foltz, R., Jenab, S., & Quinones-Jenab, V. (2004). Sex differences in cocaine-induced behavioral responses, pharmacokinetics, and monoamine levels. *Neuropharmacology*, *46*(5), 672–687. https://doi.org/10.1016/j.neuropharm.2003.11.017

Fetter, L. C., McDonough, M. H., Kippin, T. E., & Plaxco, K. W. (2024). Effects of Physiological-Scale Variation in Cations, pH, and Temperature on the Calibration of Electrochemical Aptamer-Based Sensors. *ACS Sensors*. https://doi.org/10.1021/acssensors.4c02274

Foote, C. A., Soares, R. N., Ramirez-Perez, F. I., Ghiarone, T., Aroor, A., Manrique-Acevedo, C., Padilla, J., & Martinez-Lemus, L. A. (2022). Endothelial Glycocalyx. *Comprehensive Physiology*, *12*(4), 3781–3811. https://doi.org/10.1002/cphy.c210029

Friedel, M., Thompson, I. A. P., Kasting, G., Polsky, R., Cunningham, D., Soh, H. T., & Heikenfeld, J. (2023). Opportunities and challenges in the diagnostic utility of dermal

interstitial fluid. *Nature Biomedical Engineering*. https://doi.org/10.1038/s41551-022-00998-9

Gaillard, P. J., Appeldoorn, C. C. M., Dorland, R., Kregten, J. van, Manca, F., Vugts, D. J., Windhorst, B., Dongen, G. A. M. S. van, Vries, H. E. de, Maussang, D., & Tellingen, O. van. (2014). Pharmacokinetics, Brain Delivery, and Efficacy in Brain Tumor-Bearing Mice of Glutathione Pegylated Liposomal Doxorubicin (2B3-101). *PLOS ONE*, *9*(1), e82331. https://doi.org/10.1371/journal.pone.0082331

Gao, H., Ho, S., & Williams, J. (2013). LC-MS Bioanalysis of Drugs in Tissue Samples. In *Handbook of LC-MS Bioanalysis* (pp. 297–306). John Wiley & Sons, Ltd. https://doi.org/10.1002/9781118671276.ch23

Gao, S., Zheng, X., Jiao, B., & Wang, L. (2016). Post-SELEX optimization of aptamers. *Analytical and Bioanalytical Chemistry*, *408*(17), 4567–4573. https://doi.org/10.1007/s00216-016-9556-2

Gaspar, V. P., Ibrahim, S., Zahedi, R. P., & Borchers, C. H. (2021). Utility, promise, and limitations of liquid chromatography-mass spectrometry-based therapeutic drug monitoring in precision medicine. *Journal of Mass Spectrometry*, *56*(11), e4788. https://doi.org/10.1002/jms.4788

Gerson, J., Erdal, M. K., Dauphin-Ducharme, P., Idili, A., Hespanha, J. P., Plaxco, K. W., & Kippin, T. E. (2024). A high-precision view of intercompartmental drug transport via simultaneous, seconds-resolved, in situ measurements in the vein and brain. *British Journal of Pharmacology*, *181*(20), 3869–3885. https://doi.org/10.1111/bph.16471

Gerson, J., Erdal, M. K., McDonough, M. H., Ploense, K. L., Dauphin-Ducharme, P., Honeywell, K. M., Leung, K. K., Arroyo-Curras, N., Gibson, J. M., Emmons, N. A.,

Meiring, W., Hespanha, J. P., Plaxco, K. W., & Kippin, T. E. (2023a). High-precision monitoring of and feedback control over drug concentrations in the brains of freely moving rats. *Science Advances*, *9*(20), eadg3254. https://doi.org/10.1126/sciadv.adg3254

Gerson, J., Erdal, M. K., McDonough, M. H., Ploense, K. L., Dauphin-Ducharme, P., Honeywell, K. M., Leung, K. K., Arroyo-Curras, N., Gibson, J. M., Emmons, N. A., Meiring, W., Hespanha, J. P., Plaxco, K. W., & Kippin, T. E. (2023b). High-precision monitoring of and feedback control over drug concentrations in the brains of freely moving rats. *Science Advances*, *9*(20), eadg3254. https://doi.org/10.1126/sciadv.adg3254

Ghaferi, M., Raza, A., Koohi, M., Zahra, W., Akbarzadeh, A., Ebrahimi Shahmabadi, H., & Alavi, S. E. (2022). Impact of PEGylated Liposomal Doxorubicin and Carboplatin Combination on Glioblastoma. *Pharmaceutics*, *14*(10), Article 10. https://doi.org/10.3390/pharmaceutics14102183

Gil, P., Favre, R., Durand, A., Iliadis, A., Cano, J. P., & Carcassonne, Y. (1983). Time dependency of adriamycin and adriamycinol kinetics. *Cancer Chemotherapy and Pharmacology*, *10*(2), 120–124. https://doi.org/10.1007/BF00446223

Goetz, L. H., & Schork, N. J. (2018). Personalized medicine: Motivation, challenges, and progress. *Fertility and Sterility*, *109*(6), 952–963. https://doi.org/10.1016/j.fertnstert.2018.05.006

Goldstein, G. W., & Betz, A. L. (1986). The blood-brain barrier. *Scientific American*, *255*(3), 74–83. https://doi.org/10.1038/scientificamerican0986-74

Gonzalez-Gallardo, C. L., Arjona, N., Álvarez-Contreras, L., & Guerra-Balcázar, M. (2022). Electrochemical creatinine detection for advanced point-of-care sensing devices: A review. *RSC Advances*, *12*(47), 30785–30802. https://doi.org/10.1039/D2RA04479J

Grasso, P., Rozhavskaya, M., & Reichert, L. E. (1998). In vivo effects of human follicle-stimulating hormone-related synthetic peptide hFSH-beta-(81-95) and its subdomain hFSH-beta-(90-95) on the mouse estrous cycle. *Biology of Reproduction*, *58*(3), 821–825. https://doi.org/10.1095/biolreprod58.3.821

Green, A. E., & Rose, P. G. (2006). Pegylated liposomal doxorubicin in ovarian cancer. *International Journal of Nanomedicine*, *1*(3), 229–239.

Hammarlund-Udenaes, M. (2017). Microdialysis as an Important Technique in Systems Pharmacology—A Historical and Methodological Review. *The AAPS Journal*, *19*(5), 1294–1303. https://doi.org/10.1208/s12248-017-0108-2

Hashemi, P., Dankoski, E. C., Petrovic, J., Keithley, R. B., & Wightman, R. M. (2009). Voltammetric Detection of 5-Hydroxytryptamine Release in the Rat Brain. *Analytical Chemistry*, *81*(22), 9462–9471. https://doi.org/10.1021/ac9018846

Hecht, G. S., Spear, N. E., & Spear, L. P. (1999). Changes in progressive ratio responding for intravenous cocaine throughout the reproductive process in female rats. *Developmental Psychobiology*, *35*(2), 136–145.

Heien, M. L. A. V., Johnson, M. A., & Wightman, R. M. (2004). Resolving Neurotransmitters Detected by Fast-Scan Cyclic Voltammetry. *Analytical Chemistry*, *76*(19), 5697–5704. https://doi.org/10.1021/ac0491509

Hempel, G., Flege, S., Würthwein, G., & Boos, J. (2002). Peak plasma concentrations of doxorubicin in children with acute lymphoblastic leukemia or non-Hodgkin

lymphoma. *Cancer Chemotherapy and Pharmacology*, *49*(2), 133–141. https://doi.org/10.1007/s00280-001-0392-4

Herculano-Houzel, S., Mota, B., & Lent, R. (2006). Cellular scaling rules for rodent brains. *Proceedings of the National Academy of Sciences*, *103*(32), 12138–12143. https://doi.org/10.1073/pnas.0604911103

Hianik, T., Ostatná, V., Sonlajtnerova, M., & Grman, I. (2007). Influence of ionic strength, pH and aptamer configuration for binding affinity to thrombin. *Bioelectrochemistry*, *70*(1), 127–133. https://doi.org/10.1016/j.bioelechem.2006.03.012

Hill, S. Y., & Powell, B. J. (1976). Cocaine and morphine self-administration: Effects of differential rearing. *Pharmacology, Biochemistry, and Behavior*, *5*(6), 701–704. https://doi.org/10.1016/0091-3057(76)90315-4

Hon, Y. Y., & Evans, W. E. (1998). Making TDM work to optimize cancer chemotherapy: A multidisciplinary team approach. *Clinical Chemistry*, *44*(2), 388–400.

Hrishi, A. P., & Sethuraman, M. (2019). Cerebrospinal Fluid (CSF) Analysis and Interpretation in Neurocritical Care for Acute Neurological Conditions. *Indian Journal of Critical Care Medicine : Peer-Reviewed, Official Publication of Indian Society of Critical Care Medicine*, *23*(Suppl 2), S115–S119. https://doi.org/10.5005/jp-journals-10071-23187

Hu, M., Crombag, H. S., Robinson, T. E., & Becker, J. B. (2004). Biological Basis of Sex Differences in the Propensity to Self-administer Cocaine. *Neuropsychopharmacology*, *29*(1), 81–85. https://doi.org/10.1038/sj.npp.1300301

Idili, A., Arroyo-Currás, N., Ploense, K. L., Csordas, A. T., Kuwahara, M., Kippin, T. E., & Plaxco, K. W. (2019). Seconds-resolved pharmacokinetic measurements of the

chemotherapeutic irinotecan in situ in the living body. *Chemical Science*, *10*(35), 8164–8170. https://doi.org/10.1039/C9SC01495K

Idili, A., Gerson, J., Kippin, T., & Plaxco, K. W. (2021). Seconds-Resolved, In Situ Measurements of Plasma Phenylalanine Disposition Kinetics in Living Rats. *Analytical Chemistry*, *93*(8), 4023–4032. https://doi.org/10.1021/acs.analchem.0c05024

Iqbal, J., Tan, Z.-N., Li, M.-X., Chen, H.-B., Ma, B., Zhou, X., & Ma, X.-M. (2020). Estradiol Alters Hippocampal Gene Expression during the Estrous Cycle. *Endocrine Research*, *45*(2), 84–101. https://doi.org/10.1080/07435800.2019.1674868

Isaksson, I.-M., Theodorsson, A., Theodorsson, E., & Strom, J. O. (2011). Methods for 17β-oestradiol administration to rats. *Scandinavian Journal of Clinical and Laboratory Investigation*, *71*(7), 583–592. https://doi.org/10.3109/00365513.2011.596944

Jacquet, J. M., Bressolle, F., Galtier, M., Bourrier, M., Donadio, D., Jourdan, J., & Rossi, J. F. (1990). Doxorubicin and doxorubicinol: Intra- and inter-individual variations of pharmacokinetic parameters. *Cancer Chemotherapy and Pharmacology*, *27*(3), 219–225. https://doi.org/10.1007/BF00685716

Ji, Y., Tang, B., & Traub, R. J. (2008). The visceromotor response to colorectal distention fluctuates with the estrous cycle in rats. *Neuroscience*, *154*(4), 1562–1567. https://doi.org/10.1016/j.neuroscience.2008.04.070

Jiang, C., Wang, G., Hein, R., Liu, N., Luo, X., & Davis, J. J. (2020). Antifouling Strategies for Selective In Vitro and In Vivo Sensing. *Chemical Reviews*, *120*(8), 3852–3889. https://doi.org/10.1021/acs.chemrev.9b00739

Johnson, R. D., & Arnold, F. H. (1995). The temkin isotherm describes heterogeneous protein adsorption. *Biochimica et Biophysica Acta (BBA) - Protein Structure and Molecular Enzymology*, *1247*(2), 293–297. https://doi.org/10.1016/0167-4838(95)00006-G

Kang, J.-S., & Lee, M.-H. (2009). Overview of Therapeutic Drug Monitoring. *The Korean Journal of Internal Medicine*, *24*(1), 1–10. https://doi.org/10.3904/kjim.2009.24.1.1

Kerstetter, K. A., Aguilar, V. R., Parrish, A. B., & Kippin, T. E. (2008). Protracted time-dependent increases in cocaine-seeking behavior during cocaine withdrawal in female relative to male rats. *Psychopharmacology*, *198*(1), 63–75. https://doi.org/10.1007/s00213-008-1089-8

Kerstetter, K. A., & Kippin, T. E. (2011). Impact of Sex and Gonadal Hormones on Cocaine and Food Reinforcement Paradigms. *Journal of Addiction Research & Therapy*, *Suppl 4*(2), 2963. https://doi.org/10.4172/2155-6105.s4-002

Kerstetter, K. A., Su, Z.-I., Ettenberg, A., & Kippin, T. E. (2013). Sex and estrous cycle differences in cocaine-induced approach-avoidance conflict. *Addiction Biology*, *18*(2), 222–229. https://doi.org/10.1111/j.1369-1600.2010.00292.x

Khatoon, R., Jahan, N., Khan, H. M., Rabbani, T., & Ahmad, S. (2014). Evaluation of Different Staining Techniques in the Diagnosis of Trichomonas vaginalis Infection in Females of Reproductive Age Group. *Journal of Clinical and Diagnostic Research : JCDR*, *8*(12), DC05. https://doi.org/10.7860/JCDR/2014/9765.5261

Kimoto, M., Yamashige, R., Matsunaga, K., Yokoyama, S., & Hirao, I. (2013). Generation of high-affinity DNA aptamers using an expanded genetic alphabet. *Nature Biotechnology*, *31*(5), 453–457. https://doi.org/10.1038/nbt.2556

Kippin, T. E., Fuchs, R. A., Mehta, R. H., Case, J. M., Parker, M. P., Bimonte-Nelson, H. A., & See, R. E. (2005). Potentiation of cocaine-primed reinstatement of drug seeking in female rats during estrus. *Psychopharmacology*, *182*(2), 245–252. https://doi.org/10.1007/s00213-005-0071-y

Knezevic, C. E., & Clarke, W. (2020). Cancer Chemotherapy: The Case for Therapeutic Drug Monitoring. *Therapeutic Drug Monitoring*, *42*(1), 6. https://doi.org/10.1097/FTD.0000000000000701

Koh, A., Kang, D., Xue, Y., Lee, S., Pielak, R. M., Kim, J., Hwang, T., Min, S., Banks, A., Bastien, P., Manco, M. C., Wang, L., Ammann, K. R., Jang, K.-I., Won, P., Han, S., Ghaffari, R., Paik, U., Slepian, M. J., … Rogers, J. A. (2016). A Soft, Wearable Microfluidic Device for the Capture, Storage, and Colorimetric Sensing of Sweat. *Science Translational Medicine*, *8*(366), 366ra165. https://doi.org/10.1126/scitranslmed.aaf2593

Kohlberger, M., & Gadermaier, G. (2022). SELEX: Critical factors and optimization strategies for successful aptamer selection. *Biotechnology and Applied Biochemistry*, *69*(5), 1771–1792. https://doi.org/10.1002/bab.2244

Kosten, T. A., Miserendino, M. J. D., Haile, C. N., DeCaprio, J. L., Jatlow, P. I., & Nestler, E. J. (1997). Acquisition and maintenance of intravenous cocaine self-administration in Lewis and Fischer inbred rat strains1. *Brain Research*, *778*(2), 418–429. https://doi.org/10.1016/S0006-8993(97)01205-5

Kovács, T., Szabó-Meleg, E., & Ábrahám, I. M. (2020). Estradiol-Induced Epigenetically Mediated Mechanisms and Regulation of Gene Expression. *International Journal of Molecular Sciences*, *21*(9), Article 9. https://doi.org/10.3390/ijms21093177

Lacy, R. T., Strickland, J. C., Feinstein, M. A., Robinson, A. M., & Smith, M. A. (2016). The Effects of Sex, Estrous Cycle, and Social Contact on Cocaine and Heroin Self-Administration in Rats. *Psychopharmacology*, *233*(17), 3201. https://doi.org/10.1007/s00213-016-4368-9

Lada, M. W., Vickroy, T. W., & Kennedy, R. T. (1997). High temporal resolution monitoring of glutamate and aspartate in vivo using microdialysis on-line with capillary electrophoresis with laser-induced fluorescence detection. *Analytical Chemistry*, *69*(22), 4560–4565. https://doi.org/10.1021/ac970518u

Lai, R. Y., Seferos, D. S., Heeger, A. J., Bazan, G. C., & Plaxco, K. W. (2006). Comparison of the Signaling and Stability of Electrochemical DNA Sensors Fabricated from 6- or 11-Carbon Self-Assembled Monolayers. *Langmuir*, *22*(25), 10796–10800. https://doi.org/10.1021/la0611817

Larson, E. B., Roth, M. E., Anker, J. J., & Carroll, M. E. (2005). Effect of short- vs. Long-term estrogen on reinstatement of cocaine-seeking behavior in female rats. *Pharmacology Biochemistry and Behavior*, *82*(1), 98–108. https://doi.org/10.1016/j.pbb.2005.07.015

Leung, K. K., Downs, A. M., Ortega, G., Kurnik, M., & Plaxco, K. W. (2021a). Elucidating the Mechanisms Underlying the Signal Drift of Electrochemical Aptamer-Based Sensors in Whole Blood. *ACS Sensors*, *6*(9), 3340–3347. https://doi.org/10.1021/acssensors.1c01183

Leung, K. K., Downs, A. M., Ortega, G., Kurnik, M., & Plaxco, K. W. (2021b). Elucidating the Mechanisms Underlying the Signal Drift of Electrochemical Aptamer-Based

Sensors in Whole Blood. *ACS Sensors*, *6*(9), 3340–3347. https://doi.org/10.1021/acssensors.1c01183

Leung, K. K., Gerson, J., Emmons, N., Heemstra, J. M., Kippin, T. E., & Plaxco, K. W. (2024). The Use of Xenonucleic Acids Significantly Reduces the In Vivo Drift of Electrochemical Aptamer-Based Sensors. *Angewandte Chemie (International Ed. in English)*, *63*(21), e202316678. https://doi.org/10.1002/anie.202316678

Leung, K. K., Gerson, J., Emmons, N., Roehrich, B., Verrinder, E., Fetter, L. C., Kippin, T. E., & Plaxco, K. W. (2023). A tight squeeze: Geometric effects on the performance of three-electrode electrochemical-aptamer based sensors in constrained, in vivo placements. *Analyst*, *148*(7), 1562–1569. https://doi.org/10.1039/D2AN02096C

Lex, B. W. (1991). Some gender differences in alcohol and polysubstance users. *Health Psychology: Official Journal of the Division of Health Psychology, American Psychological Association*, *10*(2), 121–132. https://doi.org/10.1037//0278-6133.10.2.121

Li, H., Dauphin-Ducharme, P., Arroyo-Currás, N., Tran, C. H., Vieira, P. A., Li, S., Shin, C., Somerson, J., Kippin, T. E., & Plaxco, K. W. (2017). A Biomimetic Phosphatidylcholine-Terminated Monolayer Greatly Improves the In Vivo Performance of Electrochemical Aptamer-Based Sensors. *Angewandte Chemie (International Ed. in English)*, *56*(26), 7492–7495. https://doi.org/10.1002/anie.201700748

Li, H., Dauphin-Ducharme, P., Ortega, G., & Plaxco, K. W. (2017). Calibration-Free Electrochemical Biosensors Supporting Accurate Molecular Measurements Directly

in Undiluted Whole Blood. *Journal of the American Chemical Society*, *139*(32), 11207–11213. https://doi.org/10.1021/jacs.7b05412

Li, H., Li, S., Dai, J., Li, C., Zhu, M., Li, H., Lou, X., Xia, F., & Plaxco, K. W. (n.d.). High frequency, calibration-free molecular measurements in situ in the living body. *Chemical Science*, *10*(47), 10843–10848. https://doi.org/10.1039/c9sc04434e

Li, S., Dai, J., Zhu, M., Arroyo-Currás, N., Li, H., Wang, Y., Wang, Q., Lou, X., Kippin, T. E., Wang, S., Plaxco, K. W., Li, H., & Xia, F. (2023). Implantable Hydrogel-Protective DNA Aptamer-Based Sensor Supports Accurate, Continuous Electrochemical Analysis of Drugs at Multiple Sites in Living Rats. *ACS Nano*, *17*(18), 18525–18538. https://doi.org/10.1021/acsnano.3c06520

Li, S., Ferrer-Ruiz, A., Dai, J., Ramos-Soriano, J., Du, X., Zhu, M., Zhang, W., Wang, Y., Ángeles Herranz, M., Jing, L., Zhang, Z., Li, H., Xia, F., & Martín, N. (2022). A pH-independent electrochemical aptamer-based biosensor supports quantitative, real-time measurement in vivo. *Chemical Science*, *13*(30), 8813–8820. https://doi.org/10.1039/D2SC02021A

Lin, S., Cheng, X., Zhu, J., Wang, B., Jelinek, D., Zhao, Y., Wu, T.-Y., Horrillo, A., Tan, J., Yeung, J., Yan, W., Forman, S., Coller, H. A., Milla, C., & Emaminejad, S. (2022). Wearable microneedle-based electrochemical aptamer biosensing for precision dosing of drugs with narrow therapeutic windows. *Science Advances*, *8*(38), eabq4539. https://doi.org/10.1126/sciadv.abq4539

Lin, Y.-L., Wu, M.-T., & Yang, F.-Y. (2018). Pharmacokinetics of doxorubicin in glioblastoma multiforme following ultrasound-Induced blood-brain barrier disruption

as determined by microdialysis. *Journal of Pharmaceutical and Biomedical Analysis*, *149*, 482–487. https://doi.org/10.1016/j.jpba.2017.11.047

Lippow, S. M., Wittrup, K. D., & Tidor, B. (2007). Computational design of antibody-affinity improvement beyond in vivo maturation. *Nature Biotechnology*, *25*(10), 1171–1176. https://doi.org/10.1038/nbt1336

Liu, H., & Yu, J. (2018). Challenges of SELEX and Demerits of Aptamer-Based Methods. In *Aptamers for Analytical Applications* (pp. 345–364). John Wiley & Sons, Ltd. https://doi.org/10.1002/9783527806799.ch12

Long, J. A. (Joseph A. (with U.S. National Library of Medicine). (1922). *The oestrous cycle in the rat and its associated phenomena*. Berkeley, Calif. : University of California Press. http://archive.org/details/06120800R.nlm.nih.gov

Lonsdale, D. O., Udy, A. A., Roberts, J. A., & Lipman, J. (2013). Antibacterial therapeutic drug monitoring in cerebrospinal fluid: Difficulty in achieving adequate drug concentrations. *Journal of Neurosurgery*, *118*(2), 297–301. https://doi.org/10.3171/2012.10.JNS12883

Lovallo, W. R. (2006). Cortisol secretion patterns in addiction and addiction risk. *International Journal of Psychophysiology : Official Journal of the International Organization of Psychophysiology*, *59*(3), 195. https://doi.org/10.1016/j.ijpsycho.2005.10.007

Luan, Y., & Yao, Y. (2018). The Clinical Significance and Potential Role of C-Reactive Protein in Chronic Inflammatory and Neurodegenerative Diseases. *Frontiers in Immunology*, *9*, 1302. https://doi.org/10.3389/fimmu.2018.01302

Lynch, W. J., Arizzi, M. N., & Carroll, M. E. (2000). Effects of sex and the estrous cycle on regulation of intravenously self-administered cocaine in rats. *Psychopharmacology*, *152*(2), 132–139. https://doi.org/10.1007/s002130000488

Lynch, W. J., & Carroll, M. E. (1999). Sex differences in the acquisition of intravenously self-administered cocaine and heroin in rats. *Psychopharmacology*, *144*(1), 77–82. https://doi.org/10.1007/s002130050979

Marken, F., Neudeck, A., & Bond, A. M. (2010). Cyclic Voltammetry. In F. Scholz, A. M. Bond, R. G. Compton, D. A. Fiedler, G. Inzelt, H. Kahlert, Š. Komorsky-Lovrić, H. Lohse, M. Lovrić, F. Marken, A. Neudeck, U. Retter, F. Scholz, & Z. Stojek (Eds.), *Electroanalytical Methods: Guide to Experiments and Applications* (pp. 57–106). Springer. https://doi.org/10.1007/978-3-642-02915-8_4

Martz, J. R., Vasquez, A., Gillette, R., Gore, A. C., & Dominguez, J. M. (2023). The medial preoptic area and acute cocaine's stimulant effects in rats: Potential influences of estradiol and biological sex. *Hormones and Behavior*, *148*, 105296. https://doi.org/10.1016/j.yhbeh.2022.105296

Mayer, M. D., & Lai, R. Y. (2018). Effects of redox label location on the performance of an electrochemical aptamer-based tumor necrosis factor-alpha sensor. *Talanta*, *189*, 585–591. https://doi.org/10.1016/j.talanta.2018.07.055

Mendelsohn, M. E. (2002). Genomic and nongenomic effects of estrogen in the vasculature1. *The American Journal of Cardiology*, *90*(1, Supplement 1), F3–F6. https://doi.org/10.1016/S0002-9149(02)02418-9

Mendelson, J. H., Mello, N. K., & Negus, S. S. (1999). Effects of luteinizing hormone-releasing hormone on plasma cocaine levels in rhesus monkeys. *The Journal of Pharmacology and Experimental Therapeutics*, *289*(2), 791–799.

Miller, D. S., Bauer, B., & Hartz, A. M. S. (2008). Modulation of P-glycoprotein at the Blood-Brain Barrier: Opportunities to Improve CNS Pharmacotherapy. *Pharmacological Reviews*, *60*(2), 196–209. https://doi.org/10.1124/pr.107.07109

Miller, P. R., Taylor, R. M., Tran, B. Q., Boyd, G., Glaros, T., Chavez, V. H., Krishnakumar, R., Sinha, A., Poorey, K., Williams, K. P., Branda, S. S., Baca, J. T., & Polsky, R. (2018). Extraction and biomolecular analysis of dermal interstitial fluid collected with hollow microneedles. *Communications Biology*, *1*(1), Article 1. https://doi.org/10.1038/s42003-018-0170-z

Misbin, R. I. (1977). Phenformin-associated lactic acidosis: Pathogenesis and treatment. *Annals of Internal Medicine*, *87*(5), 591–595. https://doi.org/10.7326/0003-4819-87-5-591

Mitusova, K., Peltek, O. O., Karpov, T. E., Muslimov, A. R., Zyuzin, M. V., & Timin, A. S. (2022). Overcoming the blood–brain barrier for the therapy of malignant brain tumor: Current status and prospects of drug delivery approaches. *Journal of Nanobiotechnology*, *20*(1), 412. https://doi.org/10.1186/s12951-022-01610-7

Miyakawa, Y., Meyer, J. S., Ishihara, N., Naritomi, H., Nakai, K., Hsu, M. C., & Deshmukh, V. D. (1977). Effect of cerebrospinal fluid removal on cerebral blood flow and metabolism in the baboon: Influence of tyrosine infusion and cerebral embolism on cerebrospinal fluid pressure autoregulation. *Stroke*, *8*(3), 346–351. https://doi.org/10.1161/01.str.8.3.346

Morikawa, G., Fukami, K., Moriiwa, Y., Okazawa, K., & Yanagida, A. (2023). Evaluation of the clinical and quantitative performance of a practical HPLC-UV platform for in-hospital routine therapeutic drug monitoring of multiple drugs. *Journal of Pharmaceutical Health Care and Sciences*, *9*, 29. https://doi.org/10.1186/s40780-023-00298-7

Movassaghi, C. S., Alcañiz Fillol, M., Kishida, K. T., McCarty, G., Sombers, L. A., Wassum, K. M., & Andrews, A. M. (2024). Maximizing Electrochemical Information: A Perspective on Background-Inclusive Fast Voltammetry. *Analytical Chemistry*, *96*(16), 6097–6105. https://doi.org/10.1021/acs.analchem.3c04938

Mruk, D. D., & Cheng, C. Y. (2015). The Mammalian Blood-Testis Barrier: Its Biology and Regulation. *Endocrine Reviews*, *36*(5), 564–591. https://doi.org/10.1210/er.2014-1101

Nakatsuka, N., Heard, K. J., Faillétaz, A., Momotenko, D., Vörös, J., Gage, F. H., & Vadodaria, K. C. (2021). Sensing serotonin secreted from human serotonergic neurons using aptamer-modified nanopipettes. *Molecular Psychiatry*, *26*(7), 2753–2763. https://doi.org/10.1038/s41380-021-01066-5

Nandi, T. (2023). IMPORTANCE OF SUFFICIENT TIME-POINTS FOR EFFICIENT PHARMACOKINETIC (PK) COMPARTMENTAL MODELING. *International Journal of Applied Pharmaceutics*, *15*, 87–92. https://doi.org/10.22159/ijap.2023v15i1.46553

Ngernsutivorakul, T., White, T. S., & Kennedy, R. T. (2018). Microfabricated Probes for Studying Brain Chemistry: A Review. *ChemPhysChem*, *19*(10), 1128–1142. https://doi.org/10.1002/cphc.201701180

Ni, X., Castanares, M., Mukherjee, A., & Lupold, S. E. (2011). Nucleic acid aptamers: Clinical applications and promising new horizons. *Current Medicinal Chemistry*, *18*(27), 4206. https://doi.org/10.2174/092986711797189600

Niedzwiecki, M. M., Samant, P., Walker, D. I., Tran, V., Jones, D. P., Prausnitz, M. R., & Miller, G. W. (2018). Human Suction Blister Fluid Composition Determined Using High-Resolution Metabolomics. *Analytical Chemistry*, *90*(6), 3786–3792. https://doi.org/10.1021/acs.analchem.7b04073

Nikolin, B., Imamović, B., Medanhodžić-Vuk, S., & Sober, M. (2004). HIGH PERFOMANCE LIQUID CHROMATOGRAPHY IN PHARMACEUTICAL ANALYSES. *Bosnian Journal of Basic Medical Sciences*, *4*(2), 5–9.

Niyomchai, T., Akhavan, A., Festa, E. D., Lin, S.-N., Lamm, L., Foltz, R., & Quiñones-Jenab, V. (2006). Estrogen and progesterone affect cocaine pharmacokinetics in female rats. *Brain Research Bulletin*, *68*(5), 310–314. https://doi.org/10.1016/j.brainresbull.2005.09.001

Noh, S., Kim, J., Kim, G., Park, C., Jang, H., Lee, M., & Lee, T. (2021). Recent Advances in CRP Biosensor Based on Electrical, Electrochemical and Optical Methods. *Sensors*, *21*(9), Article 9. https://doi.org/10.3390/s21093024

Oliveira, R., Pinho, E., Azevedo, N. F., & Almeida, C. (2024). Post-SELEX modifications with locked nucleic acids (LNA) of a SEA-specific DNA aptamer assisted by in silico modelling. *Molecular Systems Design & Engineering*, *9*(8), 847–855. https://doi.org/10.1039/D4ME00043A

Paci, A., Veal, G., Bardin, C., Levêque, D., Widmer, N., Beijnen, J., Astier, A., & Chatelut, E. (2014). Review of therapeutic drug monitoring of anticancer drugs part 1 –

Cytotoxics. *European Journal of Cancer*, *50*(12), 2010–2019. https://doi.org/10.1016/j.ejca.2014.04.014

Pan, Y., Feng, J., Cheng, Q., & Li, F. (2007). Intracerebral microdialysis technique and its application on brain pharmacokinetic-pharmacodynamic study. *Archives of Pharmacal Research*, *30*(12), 1635–1645. https://doi.org/10.1007/BF02977335

Park, J., Zhang, Y., Vykhodtseva, N., Jolesz, F. A., & McDannold, N. J. (2012). The kinetics of blood brain barrier permeability and targeted doxorubicin delivery into brain induced by focused ultrasound. *Journal of Controlled Release*, *162*(1), 134–142. https://doi.org/10.1016/j.jconrel.2012.06.012

Pasarin, D., Ghizdareanu, A.-I., Enascuta, C. E., Matei, C. B., Bilbie, C., Paraschiv-Palada, L., & Veres, P.-A. (2023). Coating Materials to Increase the Stability of Liposomes. *Polymers*, *15*(3), 782. https://doi.org/10.3390/polym15030782

Pellitero, M. A., Curtis, S. D., & Arroyo-Currás, N. (2021). Interrogation of Electrochemical Aptamer-Based Sensors via Peak-to-Peak Separation in Cyclic Voltammetry Improves the Temporal Stability and Batch-to-Batch Variability in Biological Fluids. *ACS Sensors*, *6*(3), 1199–1207. https://doi.org/10.1021/acssensors.0c02455

Phillips, P. E. M., Robinson, D. L., Stuber, G. D., Carelli, R. M., & Wightman, R. M. (2003). Real-Time Measurements of Phasic Changes in Extracellular Dopamine Concentration in Freely Moving Rats by Fast-Scan Cyclic Voltammetry. In J. Q. Wang (Ed.), *Drugs of Abuse: Neurological Reviews and Protocols* (pp. 443–464). Humana Press. https://doi.org/10.1385/1-59259-358-5:443

Poovaiah, N., Davoudi, Z., Peng, H., Schlichtmann, B., Mallapragada, S., Narasimhan, B., & Wang, Q. (2018). Treatment of neurodegenerative disorders through the blood–brain

barrier using nanocarriers. *Nanoscale*, *10*(36), 16962–16983. https://doi.org/10.1039/C8NR04073G

Potter, S., El Hady, A., & Fetz, E. (2014). Closed-Loop Neuroscience and Neuroengineering. *Frontiers in Neural Circuits*, *8*. https://doi.org/10.3389/fncir.2014.00115

Powers, J. B. (1970). Hormonal control of sexual receptivity during the estrous cycle of the rat. *Physiology & Behavior*, *5*(8), 831–835. https://doi.org/10.1016/0031-9384(70)90167-8

Quiñones-Jenab, V., Ho, A., Schlussman, S. D., Franck, J., & Kreek, M. J. (1999). Estrous cycle differences in cocaine-induced stereotypic and locomotor behaviors in Fischer rats. *Behavioural Brain Research*, *101*(1), 15–20. https://doi.org/10.1016/s0166-4328(98)00073-4

Rafi, H., & Zestos, A. G. (2021). Review—Recent Advances in FSCV Detection of Neurochemicals via Waveform and Carbon Microelectrode Modification. *Journal of the Electrochemical Society*, *168*(5), 057520. https://doi.org/10.1149/1945-7111/ac0064

Rebollo, J., Valenzuela, B., Duart-Duart, M., Escudero-Ortiz, V., Gonzalez, M. S., & Brugarolas, A. (2010). Use of therapeutic drug monitoring of cancer chemotherapy to modify initial per-protocol doses. *Journal of Clinical Oncology*, *28*(15_suppl), e13015–e13015. https://doi.org/10.1200/jco.2010.28.15_suppl.e13015

Redlarski, G., Palkowski, A., & Krawczuk, M. (2016). Body surface area formulae: An alarming ambiguity. *Scientific Reports*, *6*, 27966. https://doi.org/10.1038/srep27966

Ribet, F., Dobielewski, M., Böttcher, M., Beck, O., Stemme, G., & Roxhed, N. (2020). *Minimally invasive and volume-metered extraction of interstitial fluid:bloodless*

point-of-care sampling for bioanalyte detection. https://urn.kb.se/resolve?urn=urn:nbn:se:kth:diva-266802

Roberts, D. C., Bennett, S. A., & Vickers, G. J. (1989). The estrous cycle affects cocaine self-administration on a progressive ratio schedule in rats. *Psychopharmacology*, *98*(3), 408–411. https://doi.org/10.1007/BF00451696

Roberts, J. G., & Sombers, L. A. (2017). Fast Scan Cyclic Voltammetry: Chemical Sensing in the Brain and Beyond. *Analytical Chemistry*, *90*(1), 490. https://doi.org/10.1021/acs.analchem.7b04732

Rodbard, D. (2016). Continuous Glucose Monitoring: A Review of Successes, Challenges, and Opportunities. *Diabetes Technology & Therapeutics*, *18 Suppl 2*(Suppl 2), S3–S13. https://doi.org/10.1089/dia.2015.0417

Roney, J. R., & Simmons, Z. L. (2013). Hormonal predictors of sexual motivation in natural menstrual cycles. *Hormones and Behavior*, *63*(4), 636–645. https://doi.org/10.1016/j.yhbeh.2013.02.013

Roth, M. E., Cosgrove, K. P., & Carroll, M. E. (2004). Sex differences in the vulnerability to drug abuse: A review of preclinical studies. *Neuroscience & Biobehavioral Reviews*, *28*(6), 533–546. https://doi.org/10.1016/j.neubiorev.2004.08.001

RStudio, Rs. (2020). *RStudio: Integrated Development for R. RStudio* [Computer software].

Rudenko, N., Fursova, K., Shepelyakovskaya, A., Karatovskaya, A., & Brovko, F. (2021). Antibodies as Biosensors' Key Components: State-of-the-Art in Russia 2020–2021. *Sensors (Basel, Switzerland)*, *21*(22), 7614. https://doi.org/10.3390/s21227614

Saddique, Z., Faheem, M., Habib, A., UlHasan, I., Mujahid, A., & Afzal, A. (2023). Electrochemical Creatinine (Bio)Sensors for Point-of-Care Diagnosis of Renal

Malfunction and Chronic Kidney Disorders. *Diagnostics*, *13*(10), 1737. https://doi.org/10.3390/diagnostics13101737

Samant, P. P., Niedzwiecki, M. M., Raviele, N., Tran, V., Mena-Lapaix, J., Walker, D. I., Felner, E. I., Jones, D. P., Miller, G. W., & Prausnitz, M. R. (2020). Sampling interstitial fluid from human skin using a microneedle patch. *Science Translational Medicine*, *12*(571), eaaw0285. https://doi.org/10.1126/scitranslmed.aaw0285

Samant, P. P., & Prausnitz, M. R. (2018). Mechanisms of sampling interstitial fluid from skin using a microneedle patch. *Proceedings of the National Academy of Sciences*, *115*(18), 4583–4588. https://doi.org/10.1073/pnas.1716772115

Sampson, T. (2003). Aptamers and SELEX: The technology. *World Patent Information*, *25*(2), 123–129. https://doi.org/10.1016/S0172-2190(03)00035-8

Santos-Cancel, M., Simpson, L. W., Leach, J. B., & White, R. J. (2019). Direct, Real-Time Detection of Adenosine Triphosphate Release from Astrocytes in 3-Dimensional Culture Using an Integrated Electrochemical, Aptamer-Based Sensor. *ACS Chemical Neuroscience*, *10*(4), 2070–2079. https://doi.org/10.1021/acschemneuro.9b00033

Sardi, I., la Marca, G., Cardellicchio, S., Giunti, L., Malvagia, S., Genitori, L., Massimino, M., de Martino, M., & Giovannini, M. G. (2013). Pharmacological modulation of blood-brain barrier increases permeability of doxorubicin into the rat brain. *American Journal of Cancer Research*, *3*(4), 424–432.

Sarter, M., & Kim, Y. (2015). Interpreting chemical neurotransmission in vivo: Techniques, time scales, and theories. *ACS Chemical Neuroscience*, *6*(1), 8–10. https://doi.org/10.1021/cn500319m

Saxena, S., Lu, Y., Zhang, Z., Li, Y., Soleymani, L., & Hoare, T. (2024). Zwitter-repel: An anti-fouling coating promoting electrochemical biosensing in biological fluids. *Chemical Engineering Journal*, *495*, 153522. https://doi.org/10.1016/j.cej.2024.153522

Schultz, K. N., & Kennedy, R. T. (2008). Time-Resolved Microdialysis for In Vivo Neurochemical Measurements and Other Applications. *Annual Review of Analytical Chemistry*, *1*(Volume 1, 2008), 627–661. https://doi.org/10.1146/annurev.anchem.1.031207.113047

Schwarz, G. (1978). Estimating the Dimension of a Model. *The Annals of Statistics*, *6*(2), 461–464. https://doi.org/10.1214/aos/1176344136

Seo, J.-W., Fu, K., Correa, S., Eisenstein, M., Appel, E. A., & Soh, H. T. (2021). *Real-time monitoring of drug pharmacokinetics within tumor tissue in live animals* (p. 2021.07.03.451023). bioRxiv. https://doi.org/10.1101/2021.07.03.451023

Serber, G. A. F., & Wild, C. J. (2003). *Nonlinear Regression | Wiley Series in Probability and Statistics*. Wiley-Interscience. https://onlinelibrary.wiley.com/doi/book/10.1002/0471725315

Sertkaya, A., Beleche, T., Jessup, A., & Sommers, B. D. (2024). Costs of Drug Development and Research and Development Intensity in the US, 2000-2018. *JAMA Network Open*, *7*(6), e2415445. https://doi.org/10.1001/jamanetworkopen.2024.15445

Seymour, J. P., Wu, F., Wise, K. D., & Yoon, E. (2017). State-of-the-art MEMS and microsystem tools for brain research. *Microsystems & Nanoengineering*, *3*(1), 1–16. https://doi.org/10.1038/micronano.2016.66

Shannon, R. J., Carpenter, K. L. H., Guilfoyle, M. R., Helmy, A., & Hutchinson, P. J. (2013). Cerebral microdialysis in clinical studies of drugs: Pharmacokinetic applications. *Journal of Pharmacokinetics and Pharmacodynamics*, *40*(3), 343–358. https://doi.org/10.1007/s10928-013-9306-4

Sharma, S., Byrne, H., & O'Kennedy, R. J. (2016). Antibodies and antibody-derived analytical biosensors. *Essays in Biochemistry*, *60*(1), 9–18. https://doi.org/10.1042/EBC20150002

Shaver, A., Curtis, S. D., & Arroyo-Currás, N. (2020). Alkanethiol Monolayer End Groups Affect the Long-Term Operational Stability and Signaling of Electrochemical, Aptamer-Based Sensors in Biological Fluids. *ACS Applied Materials & Interfaces*, *12*(9), 11214–11223. https://doi.org/10.1021/acsami.9b22385

Shaver, A., Mahlum, J. D., Scida, K., Johnston, M. L., Aller Pellitero, M., Wu, Y., Carr, G. V., & Arroyo-Currás, N. (2022). Optimization of Vancomycin Aptamer Sequence Length Increases the Sensitivity of Electrochemical, Aptamer-Based Sensors In Vivo. *ACS Sensors*, *7*(12), 3895–3905. https://doi.org/10.1021/acssensors.2c01910

Sloan, C. D. K., Nandi, P., Linz, T. H., Aldrich, J. V., Audus, K. L., & Lunte, S. M. (2012). Analytical and Biological Methods for Probing the Blood-Brain Barrier. *Annual Review of Analytical Chemistry (Palo Alto, Calif.)*, *5*, 505–531. https://doi.org/10.1146/annurev-anchem-062011-143002

Smita, P., Narayan, P. A., J, K., & Gaurav, P. (2022). Therapeutic drug monitoring for cytotoxic anticancer drugs: Principles and evidence-based practices. *Frontiers in Oncology*, *12*, 1015200. https://doi.org/10.3389/fonc.2022.1015200

Ström, J. O., Theodorsson, A., Ingberg, E., Isaksson, I.-M., & Theodorsson, E. (2012). Ovariectomy and 17β-estradiol Replacement in Rats and Mice: A Visual Demonstration. *Journal of Visualized Experiments : JoVE*, *64*, 4013. https://doi.org/10.3791/4013

Swenson, H., & Stadie, N. P. (2019). Langmuir's Theory of Adsorption: A Centennial Review. *Langmuir*, *35*(16), 5409–5426. https://doi.org/10.1021/acs.langmuir.9b00154

Timmerman, P., Mokrzycki, N., Delrat, P., Meulder, M. D., Erbach, E., Lentheric, I., McIntosh, M., & Dzygiel, P. (2014). Recommendations from The European Bioanalysis Forum on Method Establishment for Tissue Homogenates. *Bioanalysis*, *6*(12), 1647–1656. https://doi.org/10.4155/bio.14.34

Tran, B. Q., Miller, P. R., Taylor, R. M., Boyd, G., Mach, P. M., Rosenzweig, C. N., Baca, J. T., Polsky, R., & Glaros, T. (2018). Proteomic Characterization of Dermal Interstitial Fluid Extracted Using a Novel Microneedle-Assisted Technique. *Journal of Proteome Research*, *17*(1), 479–485. https://doi.org/10.1021/acs.jproteome.7b00642

Umpleby, R. J., Baxter, S. C., Rampey, A. M., Rushton, G. T., Chen, Y., & Shimizu, K. D. (2004). Characterization of the heterogeneous binding site affinity distributions in molecularly imprinted polymers. *Journal of Chromatography B*, *804*(1), 141–149. https://doi.org/10.1016/j.jchromb.2004.01.064

Vallée-Bélisle, A., Ricci, F., & Plaxco, K. W. (2009). Thermodynamic basis for the optimization of binding-induced biomolecular switches and structure-switching biosensors. *Proceedings of the National Academy of Sciences*, *106*(33), 13802–13807. https://doi.org/10.1073/pnas.0904005106

van Haaren, F., & Meyer, M. E. (1991). Sex differences in locomotor activity after acute and chronic cocaine administration. *Pharmacology, Biochemistry, and Behavior*, *39*(4), 923–927. https://doi.org/10.1016/0091-3057(91)90054-6

Vanholder, R., Gryp, T., & Glorieux, G. (2018). Urea and chronic kidney disease: The comeback of the century? (in uraemia research). *Nephrology, Dialysis, Transplantation: Official Publication of the European Dialysis and Transplant Association - European Renal Association*, *33*(1), 4–12. https://doi.org/10.1093/ndt/gfx039

Vasudevan, N., & Pfaff, D. W. (2008). Non-genomic actions of estrogens and their interaction with genomic actions in the brain. *Frontiers in Neuroendocrinology*, *29*(2), 238–257. https://doi.org/10.1016/j.yfrne.2007.08.003

Vermeer, B. J., Reman, F. C., & van Gent, C. M. (1979). The determination of lipids and proteins in suction blister fluid. *The Journal of Investigative Dermatology*, *73*(4), 303–305. https://doi.org/10.1111/1523-1747.ep12531833

Vieira, P. A., Shin, C. B., Arroyo-Currás, N., Ortega, G., Li, W., Keller, A. A., Plaxco, K. W., & Kippin, T. E. (2019). Ultra-High-Precision, in-vivo Pharmacokinetic Measurements Highlight the Need for and a Route Toward More Highly Personalized Medicine. *Frontiers in Molecular Biosciences*, *6*, 69. https://doi.org/10.3389/fmolb.2019.00069

Vijayan, A. L., Vanimaya, Ravindran, S., Saikant, R., Lakshmi, S., Kartik, R., & G, Manoj. (2017). Procalcitonin: A promising diagnostic marker for sepsis and antibiotic therapy. *Journal of Intensive Care*, *5*(1), 51. https://doi.org/10.1186/s40560-017-0246-8

Visalli, T., Turkall, R., & Abdel-Rahman, M. S. (2005). Gender differences in cocaine pharmacokinetics in CF-1 mice. *Toxicology Letters*, *155*(1), 35–40. https://doi.org/10.1016/j.toxlet.2004.08.008

Wade, G. N., & Gray, J. M. (1979). Gonadal effects on food intake and adiposity: A metabolic hypothesis. *Physiology & Behavior*, *22*(3), 583–593. https://doi.org/10.1016/0031-9384(79)90028-3

Wang, Y.-P., Eriksson, L. A., & Zhang, R.-B. (2024). Mechanism of Dual-Site Recognition in a Classic DNA Aptamer. *Journal of Chemical Information and Modeling*, *64*(19), 7698–7708. https://doi.org/10.1021/acs.jcim.4c01389

Westermeyer, J., & Boedicker, A. E. (2000). Course, Severity, and Treatment of Substance Abuse Among Women Versus Men. *The American Journal of Drug and Alcohol Abuse*, *26*(4), 523–535. https://doi.org/10.1081/ADA-100101893

Whalen, R. E. (1974). Estrogen-progesterone induction of mating in female rats. *Hormones and Behavior*, *5*(2), 157–162. https://doi.org/10.1016/0018-506X(74)90040-3

White, R. J., Rowe, A. A., & Plaxco, K. W. (2010). Re-engineering aptamers to support reagentless, self-reporting electrochemical sensors. *The Analyst*, *135*(3), 589–594. https://doi.org/10.1039/b921253a

Wilson, D. S., & Szostak, J. W. (1999). In vitro selection of functional nucleic acids. *Annual Review of Biochemistry*, *68*, 611–647. https://doi.org/10.1146/annurev.biochem.68.1.611

Wu, Y., Ranallo, S., Del Grosso, E., Chamoro-Garcia, A., Ennis, H. L., Milosavić, N., Yang, K., Kippin, T., Ricci, F., Stojanovic, M., & Plaxco, K. W. (2023). Using Spectroscopy to Guide the Adaptation of Aptamers into Electrochemical Aptamer-Based Sensors.

Bioconjugate Chemistry, *34*(1), 124–132. https://doi.org/10.1021/acs.bioconjchem.2c00275

Wu, Y., Shi, J., Kippin, T. E., & Plaxco, K. W. (2024). Codeposition Enhances the Performance of Electrochemical Aptamer-Based Sensors. *Langmuir*, *40*(16), 8703–8710. https://doi.org/10.1021/acs.langmuir.4c00585

Wu, Y., Tehrani, F., Teymourian, H., Mack, J., Shaver, A., Reynoso, M., Kavner, J., Huang, N., Furmidge, A., Duvvuri, A., Nie, Y., Laffel, L. M., Doyle, F. J. I., Patti, M.-E., Dassau, E., Wang, J., & Arroyo-Currás, N. (2022). Microneedle Aptamer-Based Sensors for Continuous, Real-Time Therapeutic Drug Monitoring. *Analytical Chemistry*, *94*(23), 8335–8345. https://doi.org/10.1021/acs.analchem.2c00829

Wu, Y. X., & Kwon, Y. J. (2016). Aptamers: The "evolution" of SELEX. *Methods*, *106*, 21–28. https://doi.org/10.1016/j.ymeth.2016.04.020

Xing, M., Yan, F., Yu, S., & Shen, P. (2015). Efficacy and Cardiotoxicity of Liposomal Doxorubicin-Based Chemotherapy in Advanced Breast Cancer: A Meta-Analysis of Ten Randomized Controlled Trials. *PLoS ONE*, *10*(7), e0133569. https://doi.org/10.1371/journal.pone.0133569

Yang, H., Thompson, A. B., McIntosh, B. J., Altieri, S. C., & Andrews, A. M. (2013). Physiologically Relevant Changes in Serotonin Resolved by Fast Microdialysis. *ACS Chemical Neuroscience*, *4*(5), 790–798. https://doi.org/10.1021/cn400072f

Zhou, L., Li, X., Zhu, B., & Su, B. (2022). An Overview of Antifouling Strategies for Electrochemical Analysis. *Electroanalysis*, *34*(6), 966–975. https://doi.org/10.1002/elan.202100406

Zhu, Q., Liu, G., & Kai, M. (2015). DNA Aptamers in the Diagnosis and Treatment of Human Diseases. *Molecules*, *20*(12), Article 12. https://doi.org/10.3390/molecules201219739

Zhu, Q., Shibata, T., Kabashima, T., & Kai, M. (2012). Inhibition of HIV-1 protease expression in T cells owing to DNA aptamer-mediated specific delivery of siRNA. *European Journal of Medicinal Chemistry*, *56*, 396–399. https://doi.org/10.1016/j.ejmech.2012.07.045

Zhuo, Z., Yu, Y., Wang, M., Li, J., Zhang, Z., Liu, J., Wu, X., Lu, A., Zhang, G., & Zhang, B. (2017). Recent Advances in SELEX Technology and Aptamer Applications in Biomedicine. *International Journal of Molecular Sciences*, *18*(10), 2142. https://doi.org/10.3390/ijms18102142